PhD Dissertation

COORDINATION OF ACTIN AND MICROTUBULE DYNAMICS BY THE FORMIN PROTEIN DISHEVELLED-ASSOCIATED ACTIVATOR OF MORPHOGENESIS

Andrea Vig

2018

Supervisor: Dr. Beáta Bugyi

Interdisciplinary Medical Sciences D93 Doctoral School

Leader of the Doctoral School: Prof. Dr. Balázs Sümegi

Program: Investigating functional protein dynamics using biophysical methods (B-130/199)

Leader of the Program: Prof. Dr. Miklós Nyitrai

UNIVERSITY OF PÉCS
MEDICAL SCHOOL

TABLE OF CONTENT

ABBREVIATIONS

ADF: Actin-depolymerizing factor
AF: Actin filaments
Arp2/3 complex: Actin-related protein 2/3 complex
BSA: bovine serum albumin
CC: Coiled-coil region
CNS: Central nervous system
CP: Capping protein
CT: C-terminus
DAAM: Dishevelled-associated activator of morphogenesis
DAD: Diaphanous autoregulatory domain
DABCO: 1,4-diazabicyclo-[2,2,2]octane
DD: Dimerization domain
Dia: Diaphanous-related formin
DID: Diaphanous inhibitory domain
DRF: Diaphanous-related formin family
FH: Formin homology
FHOD: FH1/FH2 domain-containing protein
FHOS: Formin homology 2 domain-containing
FMN: Formin
FMNL/FRL: Formin-like protein
GBD: GTPase-binding domain
GST: Glutathione S-transferase
IDR: Intrinsically disordered region
IF: Intermediate filaments
INF: Inverted formin
IPTG: Isopropyl-β-D-thiogalactopyranoside
LatA: LatrunculinA
MAP: Microtubule-associated protein
MEA: β-mercaptoethanol
MT: Microtubules
MTOC: Microtubule organizing center
NEM: N-ethylmaleimide
PCP: Planar cell polarity
Pyrene: N-(1-pyrene)-iodoacetamide
SALS: Sarcomere length short
TIP: Microtubule end-tracking protein
TIRFM: Total internal reflection fluorescence microscopy
WH2: Wiskott-Aldrich syndrome homology 2

1. INTRODUCTION

1. 1. Cytoskeletal polymer networks

Essential components of the eukaryotic cells are the polymer networks built from protein subunits; including microfilaments (or actin filaments, AF), intermediate filaments (IF) and microtubules (MT). These cytoskeletal protein arrays have fundamental roles in virtually all cellular functions; including but not limited to cell division, motility, adhesion, signaling, endocytic trafficking and transport. Health relies on proper cellular functionality governed by the spatiotemporal regulation of the morphology and dynamics of these polymer networks, which is orchestrated by a large repertoire of associated proteins. Therefore, understanding the functional and structural principles of the regulation of these cytoskeletal polymers is basic for medicine and life sciences.

1. 2. Biochemical aspects of cytoskeletal polymer dynamics

Cytoskeletal filament networks are composed of biopolymers that share common characteristics with respect to their assembly. An inherent property of these arrays is that they are built from subunits upon polymerization (*Figure 1-3*). The subunit of the AF system is the actin monomer, while MTs are built from α-β tubulin heterodimers. Intermediate filaments do not share a common protein subunit; more than 50 different IF proteins are known, which are categorized into six different types (Type I-VI). The polymerization is an intrinsic property of these biopolymers; subunits can spontaneously self-assemble into polymers under appropriate conditions (e.g. salt concentration, temperature) even in the absence of any associated proteins. In cells, the polymers are organized into higher order structural arrays by regulatory proteins, which also fine tune their functionality to generate diverse subcompartments optimized for specific cellular processes.

1. 2. 1. Structural and kinetic features of actin (micro-) filaments

Actin was discovered and first extracted from skeletal muscle in the beginning of 1940's in Albert Szent-Györgyi's lab (Institute of Medical Chemistry, University of Szeged) by Ilona Banga and Brúnó F. Straub (1). Since this seminal discovery, actin has been attracting and astonishing researchers for more than 70 years now. The basic

building block of the actin filament system is the globular actin molecule (monomeric, or G-actin) (*Figure 1, A*). The actin monomer is composed of two main domains (inner and outer domains, named after their orientation in the polymer), which can be further divided into four subdomains (S1-4). G-actin possesses structural polarity with a barbed (or plus) face and a pointed (or minus) face defined by S1-3 and S2-4, respectively. Actin binds a molecule of adenosine nucleotide (ATP, ADP) in the nucleotide-binding cleft in complex with a divalent cation (Ca^{2+} *in vitro* and Mg^{2+} *in vivo*). Upon polymerization, which can be initiated by increased ionic strength in cell-free environments (e.g. by adding 100 mM KCl and/or 2 mM $MgCl_2$), the monomers assemble into a helical fiber-like structure (filamentous or F-actin) (*Figure 1, A*). Due to the ordered arrangement of the subunits within the filament, the structure of F-actin is polarized; one end is called barbed (or plus) end, while the opposite end is the pointed (or minus) end. Polymerization starts with the formation of actin dimers and trimers, containing two and three actin subunits, respectively (*Figure 1, B*). This, so called nucleation phase is thermodynamically extremely unfavorable, as revealed by Brownian dynamics simulations and binding free energy calculations for the nucleation intermediates (2). Once the kinetic barrier of nucleation is overcome the diffusion-limited association of actin monomers to the filament results in growth during the elongation phase. In this regime, the kinetic parameters favor monomer incorporation and the binding free energy is negative (2). The association and dissociation of subunits are characterized by different rate constants at the two ends of the filament due to structural compatibilities, which give rise to the kinetic polarity of the actin polymer (3,4). Due to the kinetic differences, the lengthening of the filament is ~ 10fold faster at barbed ends as compared to pointed ends. At steady-state a dynamic equilibrium is established by the net assembly of subunits at the barbed ends, which is balanced by their net disassembly at the pointed ends. In this regime actin filaments coexist with monomers. The steady-state amount of free G-actin is called the critical concentration (c_c). Its value can be derived as the ratio of the dissociation (k_-) and association (k_+) rate constants ($c_c \sim 0.1\ \mu M$ and $0.6\ \mu M$ for the barbed and pointed end, respectively, in the ATP regime). Thus, biochemically it is a dissociation equilibrium constant for monomer:filament end interaction. However, due the different nucleotide states of the associating and dissociating actin subunits (as discussed below) the critical concentration is not considered as a true dissociation equilibrium constant.

Actin is an ATPase (*Figure 1, B*). The ATPase activity of G-actin is extremely low ($0.6\,h^{-1}$), which is substantially increased upon the structural changes accompanying the incorporation of the monomer into the filament (5-8). During polymerization, ATP is hydrolyzed into ADP-Pi ($t_{1/2} = 2\,s$) and subsequently the inorganic γ-phosphate is released ($t_{1/2} = 350\,s$), which results in inhomogeneous nucleotide distribution along the filament. The ATPase activity of actin is not essential for polymerization, ADP-G-actin can form filaments, as well.

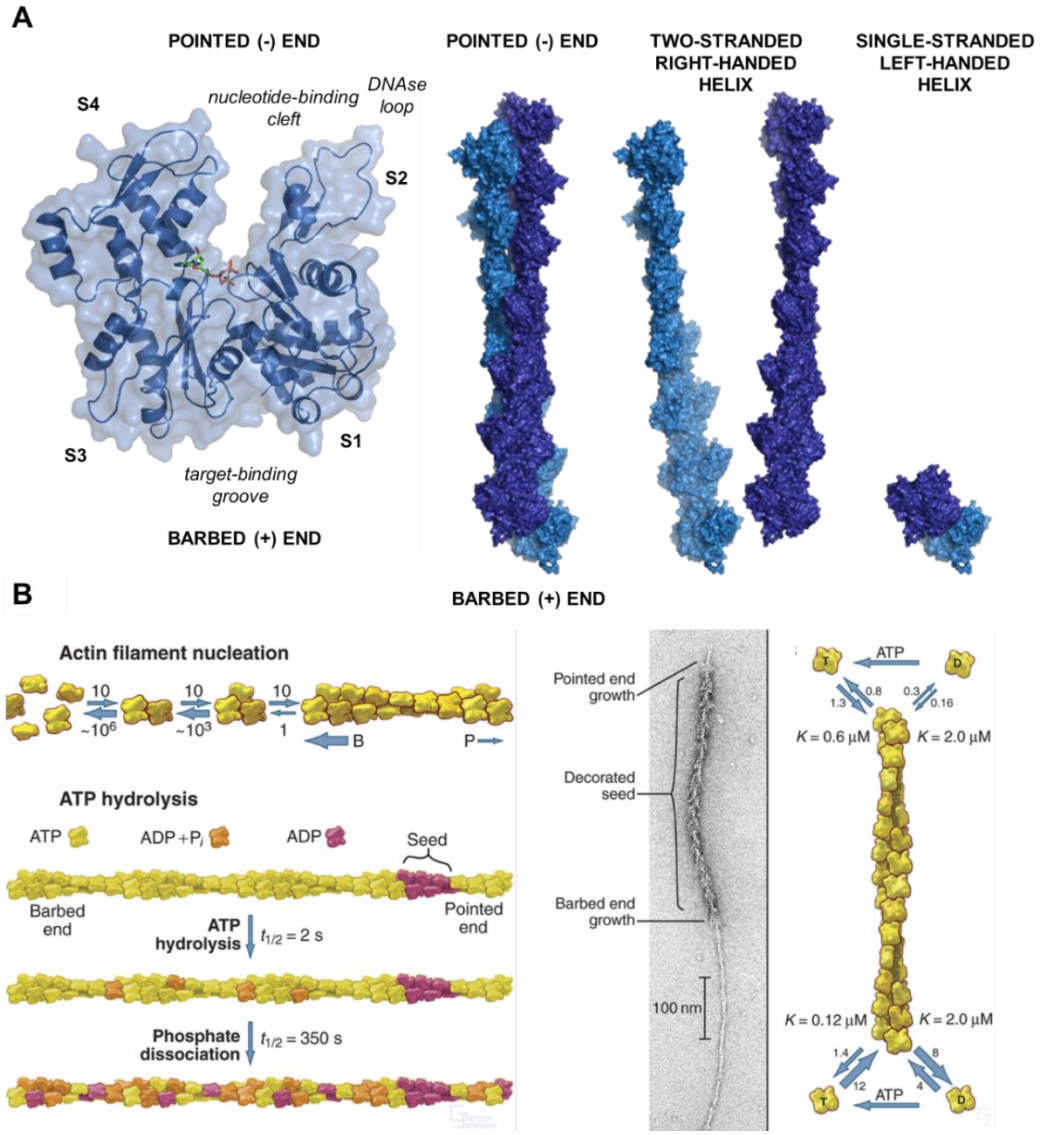

Figure 1. Structural and kinetic features of actin dynamics.

(A) X-ray structure of monomeric, and structural model of filamentous actin (5,9). Ribbon representation of the actin monomer with the bound nucleotide, subdomains are labeled as S1-4 (PDB 1HLU). Structural model of the actin filament. The two-stranded, right-handed helix and the single-stranded, left-handed helices are shown. Image credit: Beáta Bugyi. (B) Actin polymer dynamics and structural and kinetic polarity of F-actin (3,10).

1. 2. 2. Structural and kinetic features of intermediate filaments

Intermediate filament proteins form a large family and show cell and tissue specific distribution (*Figure 2, A*) (11). Despite varying in size and primary amino acid sequence, IF protein subunits share a common tripartite domain structure (11-13) (*Figure 2, B*). They consist of a conserved central α–helical rod region, which is surrounded by N-, and C-terminal domains (head and tail, respectively) varying considerably in size and secondary structure. Assembly of IFs starts upon the association of two subunits by wounding around the two rod domains, which results in a coiled-coil dimer (*Figure 2, C*). These dimers can be homodimers in case of for example lamins and class III IFs. Whereas keratins found in epithelial cells are obligate heterodimers consisting of one acidic and one basic keratin polypeptide. Subsequently, two dimers bind in an antiparallel fashion and form a tetramer. The end-to-end association of tetramers results in the formation of protofilaments, finally eight protofilaments assemble to an intermediate filament. In contrast to the two other cytoskeletal polymers IFs have no structural polarity due to the antiparallel structure of the tetramers. IFs do not undergo dynamic assembly or disassembly, either; their dynamics is regulated by phosphorylation.

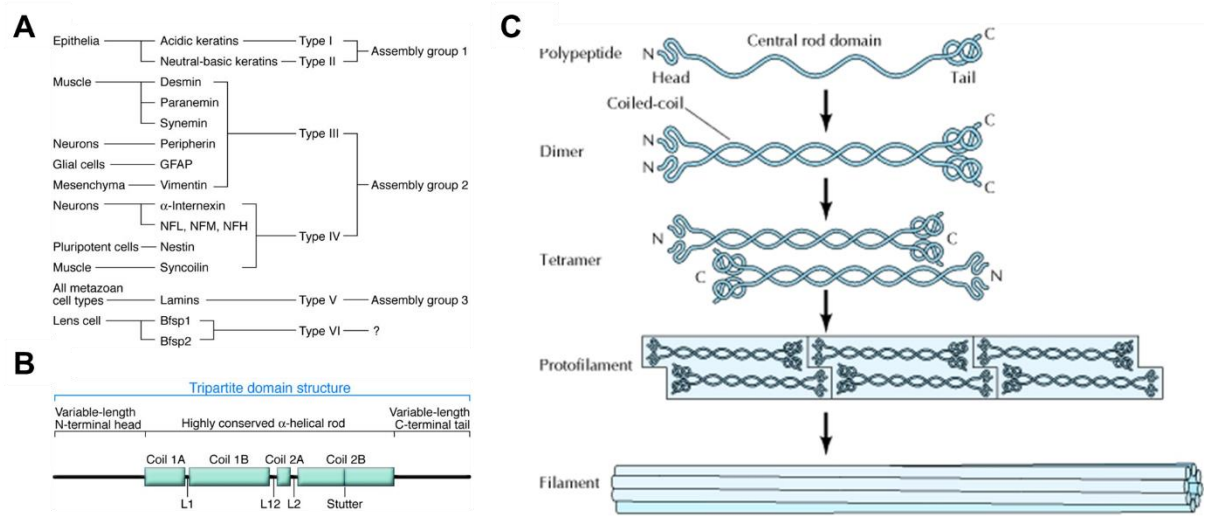

Figure 2. Structural and kinetic features of intermediate filaments.

(A) Different types of IF proteins. (B) Schematic representation of the characteristic tripartite domain structure of IF proteins. (C) Schematic representation of the sequential assembly of IF protein subunits to filaments (11,14).

1. 2. 3. Structural and kinetic features of microtubules

Microtubules are the largest cytoskeletal polymers, they are stiff hollow tubes with a diameter of ~ 25 nm that grow and shrink primarily at their plus ends. Their subunit is composed of α- and β-tubulins that bind tightly by non-covalent bonds forming heterodimers (*Figure 3, A*) (15). A third type of tubulin, the γ-tubulin exists also in cells, which localizes to the centrosome where it functions in the initiation of microtubule assembly. The α- and β-tubulins share ~ 40 % amino acid sequence identity, both have different isoforms and undergo posttranslational modifications (16). Most microtubules are composed of 13 protofilaments built from tubulin heterodimers bound together in a head-to-tail manner folding together into a tube (*Figure 3, B*). The assembly of tubulin heterodimers can occur in cell-free environment by e.g. increasing the temperature above ~ 30^{o}C and the viscosity. Microtubules are polarized structures orienting the β-tubulin and α-tubulin of the heterodimer towards the plus and minus end, respectively. In the parallel-aligned protofilaments the neighboring heterodimers bind each other by α-α and β-β connections giving a robust and stiff structure with persistence length of millimeters. Both tubulins bind GTP in their nucleotide-binding N-terminal part, but GTP that is bound to α-tubulin is physically trapped at the heterodimer interface and never hydrolyzed or exchanged. During polymerization, the β-tubulin bound GTP is hydrolyzed and its energy, as elastic strain is stored in the microtubule lattice. Microtubules exhibit dynamic instability by alternating of rapid shortening (catastrophe) and growing (rescue) phases (*Figure 3, B*) (17). These transitions are controlled by the association and dissociation rates of tubulin to and from plus end and the rate of GTP hydrolysis. If the hydrolysis is slower than subunit addition a GTP-cap is realized and assembly takes place. However, if the hydrolysis is faster than addition of the subunits GDP-tubulin accumulates at the plus end that becomes unstable and starts to fall apart.

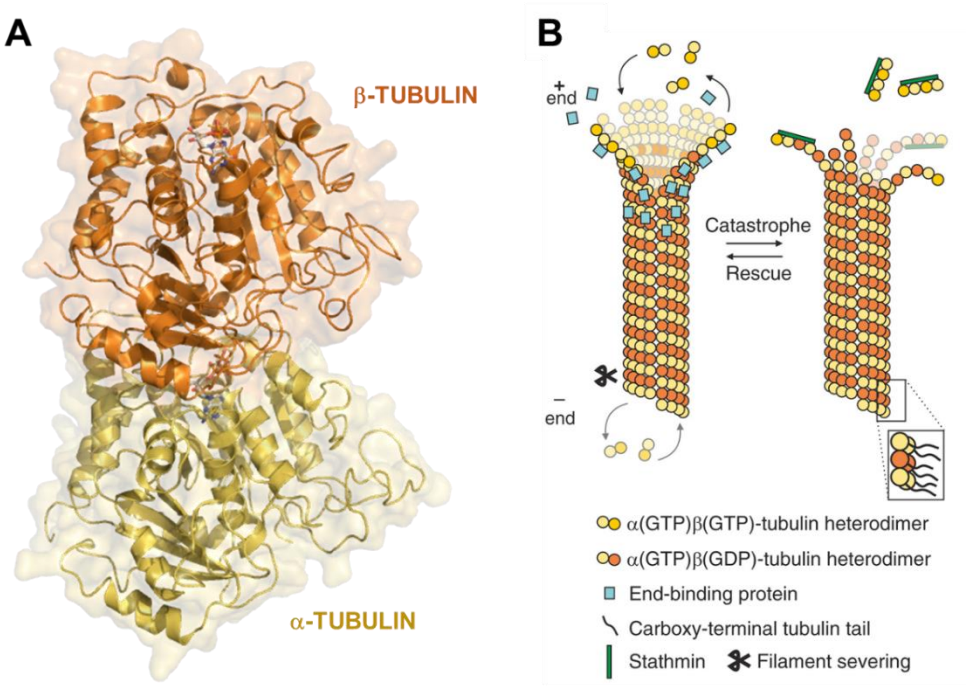

Figure 3. Structural and kinetic features of microtubule dynamics.

(A) Ribbon representation of the α-β tubulin heterodimer with bound GTP (PDB 1TUB). (B) Schematic representation of the structural and dynamic features of microtubules (18).

1. 3. Cellular aspects of microfilament and microtubule dynamics

As mentioned above, subunits of the cytoskeletal polymers can spontaneously self-assemble under appropriate conditions. However, this would result in uncontrolled and anarchic polymer formation in cells, which would not be compatible with life. Therefore, to control the proper functionality of cytoskeletal polymers, regulatory modules were evolved. According to current views, the fine-tuning of the structural and dynamic features of the cytoskeletal polymers is manifested by geometrical constrains, as well as by the diverse palette of associated proteins and their versatile activities (3,10,19,20). The coordinated action of actin-, and microtubule-binding proteins is key in the regulation of the proper functionality of cytoskeletal polymer systems. Cells use these proteins designed in various ways to affect the polymer-subunit equilibrium and to influence cytoskeletal filament structure and dynamics according to biological needs.

1. 3. 1. Basic activities of actin-, and microtubule-associated proteins

The basic activities of the individual associated proteins are relatively simple. It is however exceptional, how the simple addition or the synergic and antagonistic combination of these activities results in remarkable functional versatility of the

cytoskeleton. For the current understanding of how the members of each protein family contribute to this complex cytoskeletal regulation I direct the Readers to excellent reviews: (3,10,15,19,21-28).

The simplest view to start the classification of associated proteins may be to consider that they can interact with subunits and/or polymers. Upon interacting with subunits associated proteins can render them into a polymerization incompetent form by sequestration. In the sequestered complex subunits cannot assemble to polymers. Thus, this activity results in the inhibition of polymer assembly, and it also provides a way for the indirect regulation of end dynamics. Actin sequestrators are the members of the Wiskott-Aldrich syndrome homology 2 (WH2) domain-containing protein family (its canonical member is thymosin β4), while tubulins are sequestered by stathmin. Inversely, subunit binding can facilitate their assembly into polymers by either catalyzing nucleation and/or polymer elongation. The firstly identified actin nucleation catalyzing factor is the actin-related protein (Arp) 2/3 complex (29). The two actin-related subunits of the complex (Arp2 and Arp3) mimic a dimer to which a third actin monomer can bind. To provide spatiotemporal control for the Arp2/3-catalyzed assembly the complex has to be activated, which in part, requires its binding to the side of a pre-existing actin filament. Thus, the new filament (daughter filament) branches off from the side of an existing one (mother filament). Due to this special geometry branched filaments are created, such as found in lamellipodial structures (30). The actin-associated formin proteins can also act as nucleation factors by stabilizing nucleation intermediates. However, this activity is demonstrated only *in vitro*, the *in vivo* significance awaits further investigations. Microtubule nucleation is catalyzed in the microtubule organizing centers (MTOC) with the help of γ-tubulin (31). γ-tubulin and other associated proteins build the γ-tubulin-ring complex, which acts as a template for the subsequent association of α-β tubulin heterodimers. Subunit binding can result in directed filament growth, such as mediated by the small G-actin binding protein profilin; profilin:actin can incorporate only at filament barbed ends, while it does not associate to pointed ends due to structural incompatibilities. Polymer binding can also result in different functional consequences. Formins, as actin polymerases associate to actin filament plus ends and processively catalyze their growth in concert with profilin. Remarkably, some formins can increase the rate of profilin:actin incorporation above the diffusion-limited rate (32). Oppositely, end-binding capping

proteins can bind permanently to polymer ends and prevent both subunit addition and dissociation. Capping proteins include the actin filament barbed end capping heterodimeric CapG and gelsolin, the pointed end capper tropomodulin or the MT end binding TIPs (end-tracking proteins). Side-binding proteins by stabilizing or destabilizing polymers provide further regulation of polymer dynamics. As examples, tropomyosins bind in the groove of the two-stranded helix and stabilize actin filaments. The members of the microtubule-associated protein family (MAPs) are able to stabilize microtubules in a tissue specific manner. Rapid polymer depolymerization is a necessity in cell functioning, in which destabilizing and severing proteins play crucial role. The members of actin-depolymerizing factor (ADF)/cofilin protein family bind to subunits along the sides of actin filaments, distort the helical twist of F-actin, which results in polymer destabilization and breakage (severing). Gelsolin also severs actin filaments and remains at the barbed end. Katanin and spastin are microtubule severing ATPase enzymes, which recognize the posttranslational changes of α-tubulin. The cytoskeleton displays various structures for various functions. To build robust and stable structures for sufficient mechanical support, cells need not only single filaments but also bundled/cross-linked polymers. Bundles of filaments are created with the help of bundling proteins. Fascin creates parallel F-actin bundles, whereas filamin crosslinks actin filaments and tether them into a meshed structure. The larger MAP complexes and the smaller protein tau bundle microtubules, thereby regulating the spacing between the polymers in the bundle due to their size differences. Polarization of the polymers allow plus-, or minus-end directed motor proteins – including the actin-associated myosin family and the microtubule-associated kinesin, dynein proteins – to mediate force generation in contractile structures or cargo transport along the polymers.

Further level of cytoskeletal complexity can arise from the simultaneous interaction and regulation by proteins that bind both cytoskeletal polymer types giving an opportunity to structurally and functionally crosslink the actin and microtubule systems. Emerging evidences – mostly coming from studies related to the neuronal cytoskeleton – emphasize that the actin and microtubule cytoskeleton do not act individually, but their functions and dynamics are co-regulated by proteins, which can interact simultaneously with the two polymer networks (18).

1. 3. 2. Microfilament and microtubule networks and their crosstalk in neurons

My research focuses on the regulation of actin-microtubule cytoskeleton by associated proteins in the nervous system. In the section below, I summarize our current understanding of how the dynamics of the neuronal cytoskeleton, particularly the formation of axonal protrusions and growth is regulated.

The dynamic regulation of neuronal cytoskeleton is dominated by the actin and microtubule systems, particularly in highly motile regions, such as in axonal growth cones at the tip of growing neurons (*Figure 4*). Neurons are highly complex, dynamic and morphologically polarized cells in which the cytoskeleton takes prominent role in regulating the development, function, regeneration and degeneration (18,33).

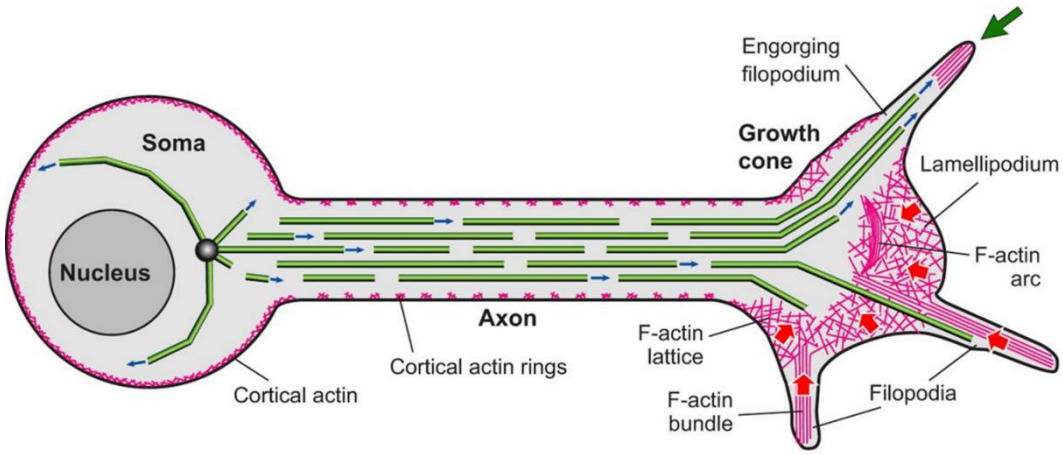

Figure 4. Schematic representation of the neuronal cytoskeleton.
Actin filaments and microtubules are colored in magenta and green, respectively (34).

Axons are slender neuronal extensions providing information tracks between neurons. These structures must grow and wire up correctly during development and serve the communication role between neurons for decades. Protrusions on the surface of neurons are fundamental for the formation of axons and dendrites and their collateral branch formation. The actin cytoskeleton generates protrusions, which allow the cell to extend and change its shape. Cellular structures of lamellipodia and filopodia are the basic forms of protrusive structures. Lamellipodia are flat membrane projections giving a robust ground for the motile machinery, while filopodia are finger-like projections – 'antenna' – extending into the extracellular environment for sampling

it (3,23,34,35). Both structures show similar dynamic behavior in extending and retracting; however, the organization of the microfilament system is different. The elongating leading edges of lamellipodia are supported by a complicated geometric arrangement – branched meshwork – of actin filaments (30). In filopodia, most of the actin filaments are organized into parallel bundles and their fast-growing barbed end is directed towards the tip where they generate protrusive force (36). Recently, it has been demonstrated that the cortex of axon shafts is underlined by short actin filaments, which are organized into repetitive rings by spectrin and linked to the cell membrane through ankyrins (37). Naturally, these neurites not only consist of actin polymers, but depend on their prominent function the microtubule cytoskeleton, as well. In axons, microtubules are uniformly oriented with their plus ends distal to the cell body, whereas in dendrites microtubules are typically of mixed orientations providing structural rigidity to support the outgrowth of these protrusions. Apart from stabilizing, they also facilitate intracellular transport and cargo trafficking by building paths for molecular motors such as dynein and kinesin (38). Other regions of neurons such as growth cones and branch points display characteristic microtubule orientation patterns and play essential role in outgrowth and guidance of axons.

Multiple interactions between actin and microtubules and their coordinated dynamics in neurons has been proposed (18,33,39). Actin tracks were demonstrated to be the guideline for growing microtubules, and vice-versa; MTs are able to influence the dynamics of F-actin meshwork. Some proteins that can orchestrate this coordinated dynamics have been identified, including tau and formins (40,41).

1. 4. The formin protein family

1. 4. 1. Identification of the proteins and the novel formin homology domains

Formin proteins were identified in the beginning of 1990's, as actin-associated proteins. The name of the protein originates from the verb *form*, since the first identified formin in mouse was thought to be a protein product of the *limb deformity* gene (42). However, it turned out that limb malformation is not caused by the formin protein, but the product of the structurally and functionally unrelated neighboring *gremlin* gene (43). In these years, the *Drosophila* Diaphanous and the *S. cerevisiae* Bni1 proteins were found to be homologous to the mouse formin protein. Based on sequence homology

two novel protein regions, the formin homology (FH) 1 and 2 domains were defined. These highly conserved domains amongst formins became the defining elements of this protein family. The FH domains were identified in increasing number of proteins, which broadly distribute from yeast to man. To date 15 human formin proteins are known, which can be clustered into 7 families (*Table 1*) (44).

formin class	proteins	gene locus	isoform
Diaphanous-related formin (Dia)	Dia1	5q31.3	2
	Dia2	Xq21.33	3
	Dia3	13q21.2	7
Dishevelled-associated activator of morphogenesis (DAAM)	DAAM1	14q23.1	3
	DAAM2	6p21.2	1
Formin-like protein (FMNL)	FMNL1	17q21.31	2
	FMNL2	2q23.3	2
	FMNL3	12q13.12	3
Inverted formin (INF)	INF1	14q32.33	2
	INF2	4q31.3	1
FH1/FH2 domain-containing protein (FHOD)	FHOD1	16q22.1	1
	FHOD3	18q12.2	2
Delphilin	Delphilin	7p22.1	1
Formin (FMN)	FMN1	15q13.3	4
	FMN2	1q43	1

Table 1. Name, gene locus and isoform number of human formin proteins.

1. 4. 1. 1. The FH2 domain

As introduced above, all formins contain a core FH2 domain, a ~ 300 – 400 amino acid central element that on average shows 24.8% sequence identity amongst human formins. High resolution X-ray structures of FH2 to date are from yeast Bni1 (1UX5), mouse Dia1 (1V9D), human Daam1 (2J1D, 2Z6E) and mouse FMNL3 (*Figure 5*) (45-48). The FH2 domain adopts almost completely α-helical fold. The N-terminus of the FH2 domain is composed of a lasso, an extended linker and a knob region with around 120 residues, followed by a coiled-coil and the C-terminal post region that contains a highly conserved GN(Y/F)MN sequence motif. Structural and functional

studies revealed that the proper functional form requires the dimerization of two FH2 domains (45,46). In the dimer the FH2 domains are head-to-tail oriented forming a donut shape. The N-terminal lasso of one FH2 envelops the post region of the other FH2 forming a hydrophobic inner dimerization interface established by highly conserved residues. Point mutations of highly conserved amino acids have been demonstrated to result in significant functional failures. Mutations of the Ile^{1432} and Lys^{1601} residues in yeast Bni1 or the corresponding residues in human Daam1 (Ile^{698} and Lys^{847}, respectively) results in a complete functional loss for actin nucleation and capping activities (46,49). Mutations in Ile^{845} or Met^{970} in mouse Dia1 result in inhibition of actin polymerization (45). Ile643Ala or Lys792Ala substitutions in INF2 result in reduced nucleation efficiency (50).

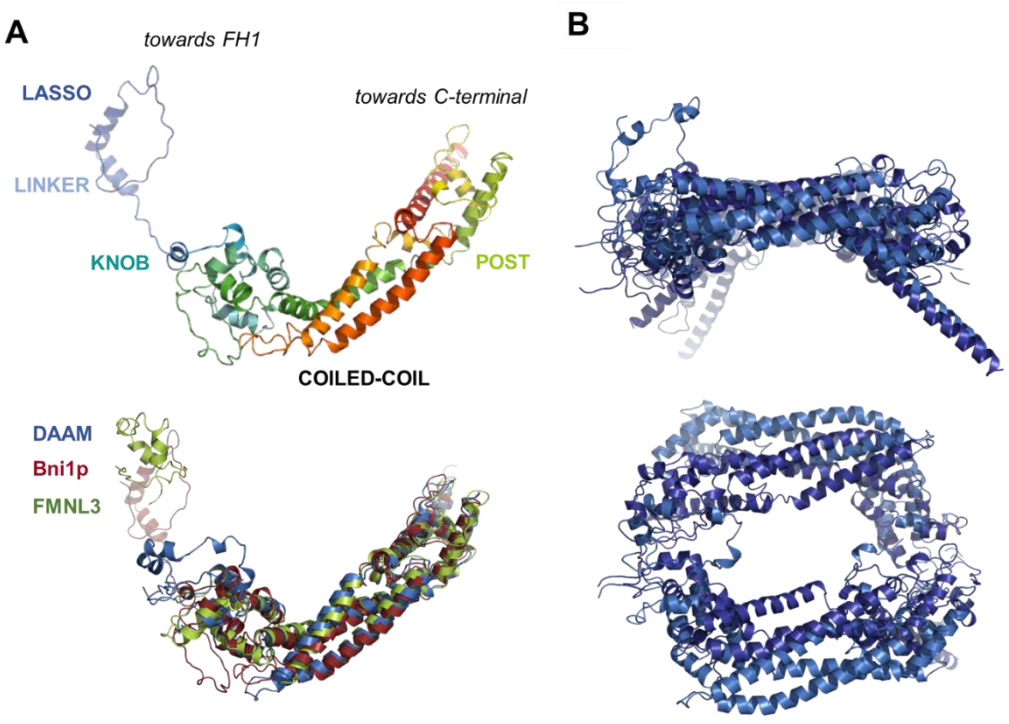

Figure 5. Structural characteristics of the FH2 domain of formins.

(A) *Top*: Rainbow representation of the structure of the FH2 domain of yeast Bni1p (PDB 1UX5). The lasso, linker, knob, coiled-coil and post regions are indicated. *Bottom*: Alignment of FH2 domains from Bni1p, Daam1 and FMNL3 (PDB 1UX5, 2Z6E, 4EAH). (B) Structural differences in Daam1 between its free (dark blue) and actin-bound states (light blue). Image credit: Beáta Bugyi.

Functional studies identified the FH2 domain of formins as the main actin-interacting element (3,4,23). A general feature of this region is that it can bind

monomeric actin and catalyze actin nucleation *in vitro* by stabilizing nucleation intermediates, thus it helps overcoming the kinetic barrier of actin assembly (*Figure 6*). Formin nucleation results in linear actin filaments unlike the branched structure created by the Arp2/3 complex machinery. Based on single molecule observations of mouse Dia1 in XTC fibroblasts treated with actin cytoskeleton disrupting agents, it was proposed that formins are actin filament nucleators in the cellular context (51). Also, FHOD3 formin was thought to be responsible for filament initiation in muscle cells, however later studies revealed that it rather seems to be required for the maintenance of assembled myofibrils (52,53). Thus, whether the nucleation activity of formins has relevance *in vivo* awaits further investigations.

Besides monomer binding, the FH2 domain can interact with filament ends, as well (*Figure 6*). A remarkable feature of the FH2 domain is that it can remain associated to barbed ends simultaneously with monomer incorporation during filament elongation (54,55). This mechanism is called processive elongation. By binding to filament ends different formins can affect filament elongation differently. As examples, mouse Dia1 does not significantly affect barbed end association rate constant of free G-actin. In contrast, *Drosophila* DAAM or the yeast Cdc12 almost completely prevents subunit addition to filament ends in the absence of profilin, thus these formins possess a capping-like activity (32,56,57). Based on single molecule visualization of EGFP-tagged mouse Dia1 in XTC fibroblasts the processive end tracking of formins was demonstrated in the cellular environment (58,59) and it is considered to be functionally important for the maintenance of filopodial actin elongation (60-62). By binding to the filament side FH2 domains of some formins are able to organize actin filaments into higher-order bundled structures, this activity may have relevance in the stabilization of cellular actin structures (63).

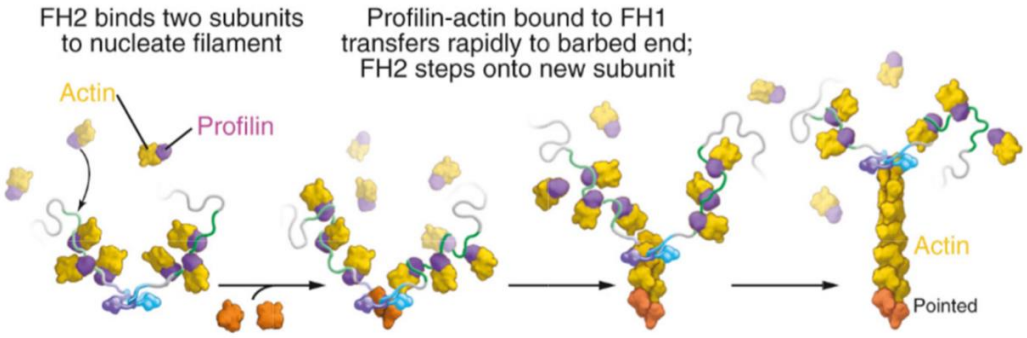

Figure 6. Schematic representation of the actin activities of formin proteins. (64)

1. 4. 1. 2. FH1 domain

FH1 positioned N-terminally to the core FH2 is composed of regions rich in proline amino acids. The poly-proline tracks vary in number and length for different formins. Crystal structure (65,66) and solution studies (67) showed that poly-proline regions that contain at least six prolines within a stretch of eight residues cover the full binding site of the small G-actin binding protein profilin. Consistently, these regions of the FH1 domain interact with profilin in a profilin-isoform dependent manner (68,69). The profilin binding proline-rich parts of the FH1 are intercalated by flexible unstructured linker regions. These regions are attributed to endow the relatively rigid structure of the proline rich region with flexibility, as well as to serve as spacers to allow simultaneous binding of many profilin-actin units (69-71). In cells a large pool of monomeric actin is bound to profilin, which is expected to have a strong influence on actin dynamics, since profilin suppresses actin nucleation and directs monomer incorporation to the barbed ends (7,9,23). Profilin is an important cofactor of formins, since it tunes the kinetic features of formin-assisted actin assembly. First, it suppresses actin nucleation catalyzed by the FH1-FH2 domain. On the other hand, it can facilitate barbed end growth mediated by FH1-FH2. As the result of the concerted action of profilin-FH1-FH2, the barbed end association rate constant can be increased by ~ 1-15fold as compared to the rate characteristic to spontaneous elongation, in a formin type- dependent manner. Thus, the profilin:FH1 interaction renders some formins to unique actin assembly machineries, which can accelerate filament elongation from profilin:actin at the barbed end over the rate of diffusion-limited growth (10,32).

1. 4. 2. Diaphanous-related formins

In addition to the FH1 and FH2 domains sequence analysis revealed that formins consist of less well conserved domains flanking the formin homology regions. Certain formin proteins were recognized as effectors of RhoGTPases, which provides a spatiotemporal control to regulate the activities of formins in the cellular context (72). While not all formins interact with RhoGTPases a subgroup of formins were identified as Diaphanous-related formins (DRFs) based on N-, and C-terminal sequence similarities (*Figure 7*). This subgroup includes Dia, FRL/FMNL, FHOD and Daam proteins in mammals and Bni1, Bnr1 and SepA in yeast. DRFs possess an N-terminal

GTP-binding (GBD) domain followed by the Diaphanous inhibitory domain (DID), while at the C-terminus the Diaphanous autoregulatory domain (DAD) is located (*Figure 7*). The structural basis and functional consequences of the regulation of DRFs by the Rho superfamily were investigated contributing to the better mechanistic understanding of formin proteins (73-78). In the absence of RhoGTPases the DAD binds to the DID region forming an intramolecular autoinhibitory complex, which inhibits the interaction of the FH2 domain with actin, thus renders formins in an inactive state. Activation of the FH2 requires the binding of a RhoGTPase to the GBD, which results in the displacement of the C-terminal DAD from its N-terminal DID recognition site and the FH domains are freed to access their interaction partners; actin and profilin (*Figure 7*).

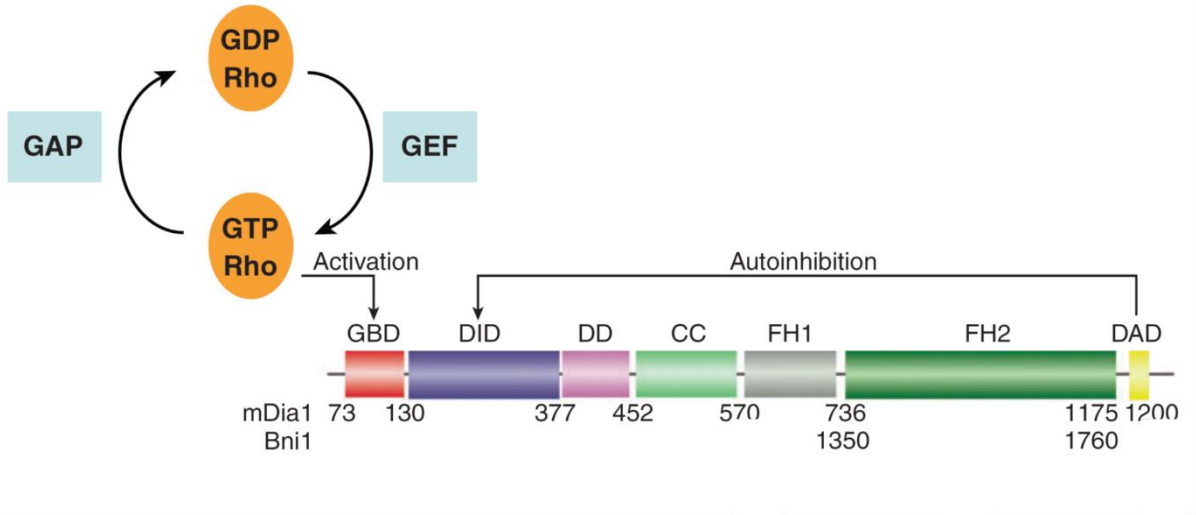

Figure 7. Schematic representation of the regulation of the actin activities of the FH1-FH2 domain of DRFs by N and C terminal regions. (79)

1. 4. 2. 1. Dishevelled-associated activator of morphogenesis (DAAM) formins

In my PhD work I was particularly interested in a formin belonging to the DRF family; Dishevelled-associated activator of morphogenesis (DAAM) formin. Therefore, this paragraph is dedicated to introduce this formin protein.

DAAM proteins of the formin family were first identified in 2001 and named after their binding to the cytoplasmic phosphoprotein Dishevelled, which is part of the β-catenin-independent non-canonical Wnt/PCP signaling pathway regulating cell movements and polarity during development through the modification of the actin

cytoskeleton (80). However, later studies questioned the role of DAAM in planar cell polarity signaling (81).

Analysis of model animals (mouse, chicken, *Xenopus, Drosophila*) revealed that DAAM is expressed in different tissues during embryogenesis and adults, and it is important for developmental and morphogenetic processes through the regulation of the actin cytoskeleton (82). As examples, *Drosophila* DAAM is required to the regulation of the actin cytoskeleton in tracheal tissues by organizing apical actin cables that define the taenidial fold pattern of the tracheal cuticle (81). The mouse and *Drosophila* DAAM proteins are expressed in skeletal and cardiac muscles, where they are associated to sarcomeric thin filaments and are essential for proper sarcomerogenesis and skeletal and heart muscle functioning (83). The absence of *Drosophila* DAAM reduces larval motility and causes a flightless phenotype in adult animals. Complex sarcomeric defects result from shorter and thinner sarcomeres, decreased actin filament levels and the absence of regular Z-disc and M-band phenotypes. Interestingly, despite of its barbed end association demonstrated *in vitro* DAAM is located at the pointed end in both mouse and *Drosophila* muscle cells (56,83). Consistently with animal studies, deletion of the human *DAAM1* gene is implicated in congenital heart defects, suggesting an evolutionary conserved function of DAAM in muscles (84).

DAAM proteins are abundant in the nervous system (82,85,86) where they are critical for axonal morphogenesis (87). DAAM has been shown to localize to neurite and growth cones and promotes neuronal growth, filopodia formation and axonal pathfinding. In primary neuronal cultures of *Drosophila* DAAM$^{mat/zyg}$ mutant embryos (maternal and zygotic dDAAM functions are both impaired) both the number and length of filopodia were markedly reduced, as compared to wild-type embryos (87). In *Drosophila* CNS the expression of N-, or C-terminally truncated versions of DAAM lacking either the GBD and DID regions or the DAD, respectively, revealed similar localization as the wild-type protein. The truncated proteins enhanced neuronal growth and increased filopodia number as compared to wild-type flies, which suggests that these proteins are constitutively active (87). Similar observation was made in the tracheal system in *Drosophila* (81). Our lab previously showed that *in vitro* DAAM from *Drosophila* behaves as a *bona fide* formin based on the nucleation promoting activity of the FH2 (56). Similarly, human Daam1 is also an actin nucleation factor, suggesting

that this activity is conserved between species (49,88). DAAM FH1 has been demonstrated to bind profilin1 and 2 (89). *Drosophila* DAAM is an unusual formin regarding its effects on elongation. In the absence of profilin both DAAM FH2 and FH1-FH2 almost completely block filament elongation by their capping-like activity (56). In contrast, DAAM FH1-FH2 can maintain actin assembly in the presence of profilin, although it cannot increase the rate of elongation above the diffusion-limited rate (56). The strong requirement of profilin for efficient maintenance of DAAM-mediated actin assembly is further corroborated by cellular studies. In *Drosophila* S2 cells DAAM overexpression results in cell shape changes and robust filopodia formation, which is counteracted by the depletion of profilin, suggesting functional interaction between the two proteins (56).

2. MOTIVATION TO MY PhD WORK

In the sections below, I summarize some recent observations on formins, which are central to my research and serve as the motivation to my PhD work.

2. 1. Emerging novel activities of the C-terminal regions of formins

Recent studies showed that – besides functioning as an autoregulatory element – the C-terminal regions of some formins from yeast to mammals (such as mouse Dia1, FMNL3, INF2, *Drosophila* Capuccino, human Daam, yeast Bni1 and Bnr1) can influence actin assembly mediated by the active FH2 domain (90-93). Biochemical studies indicate that a common feature of the C-terminal regions studied so far is that they can increase the efficiency of the FH2-catalyzed nucleation. Additionally, isolated C-terminal regions can directly interact with actin even in the absence of the FH2 domain. However, this interaction can have different functional consequences. The C-terminus of INF2 contains a WH2/DAD-like motif, which in its isolated form sequesters monomeric actin and severs actin filaments (90). While the WH2-DAD-CT region of FMNL3 in its dimeric form nucleates actin and slows elongation (92). Similarly, the isolated dimeric DAD from Dia1 seems to be sufficient to promote actin nucleation (91). In contrast, the tail region of Capuccino, even if in its dimeric form, does not influence nucleation or elongation in the absence of FH2 (93). These observations support that the activities of the C-terminal regions related to monomer binding and filament end interactions vary amongst formins, and raise the question how and which of the activities of the isolated C-terminal regions are transmitted to the functionality of each formin in the context of the FH1-FH2 domains.

2. 2. Emerging novel activities of formins in the coordination of actin-microtubule cytoskeleton

According to the classical views, formins are key regulators of the actin cytoskeleton. Recent evidences, however, emphasize that the members of this protein family including mouse Dia1/2, INF1/2 and *Drosophila* Capuccino can interact with microtubules as well, and stabilize microtubule-based structures during cell migration, division and virus infection (94-100). *In vitro* studies on mouse Dia1/2, INF2 and *Drosophila* Capuccino suggest that the microtubule-binding region comprises the FH2

domain, the same portion of the protein that is essential for proper actin interaction. In contrast, isolated FH2 of INF1 does not bind microtubules, instead a novel C-terminal microtubule-binding domain is required for the interaction (97). The stoichiometry of the interaction and direct visualization of EGFP-mouse Dia2 FH1-FH2 suggests that formins bind along the microtubule lattice (95). The consequences of formin-microtubule interaction on microtubule dynamics have started to be described. The mouse Dia1/2 can stabilize microtubules against cold-, and dilution-induced depolymerization, presumably by reducing subunit dissociation from the polymer (95). The mouse Dia2, INF2 and *Drosophila* Capuccino can bundle microtubules (95,96,99). Interestingly, INF2 can co-align microtubules with actin filaments (96).

The biochemical details and the functional consequences of the formin-microtubule interaction have just started to be investigated. The observations raise the question which regions of formins are required for microtubule interaction and actin-microtubule co-alignment. Moreover, the intriguing possibility is raised that formins can interact simultaneously with the actin and microtubule cytoskeleton and can coordinate their dynamics.

3. OBJECTIVES AND QUESTIONS

According to the above discussion the C-terminal regions of formins can have a role in FH1-FH2-assisted actin assembly, on the other hand formins emerge as regulators of the microtubule cytoskeleton, as well as novel coordinators of the actin-microtubule cytoskeleton.

In my PhD work I aimed to investigate the activities of the C-terminal regions of *Drosophila* DAAM (dDAAM) in actin assembly and the role of its FH2 and C-terminal regions in microtubule and actin-microtubule interactions. For this purpose, I planned to study the interactions of recombinantly produced proteins with actin and microtubules by using *in vitro* protein biochemical and biophysical approaches.

I addressed the following questions:

1. Is dDAAM autoregulated by its N-terminal and C-terminal domains, similarly to other DRFs, as predicted from comparative sequence analysis?
2. Does the C-terminus of dDAAM influence the FH1-FH2-mediated actin assembly? If it does so, which regions are important for this activity?
3. Does the isolated C-terminal region of dDAAM can bind directly to actin?
4. Does dDAAM bind microtubules? If it does so, which regions are important for this interaction and what are the functional consequences?
5. Does dDAAM bind simultaneously to actin and microtubules? If it does so, which regions are important for this interaction?

4. EXPERIMENTAL PROCEDURES

4. 1. Protein purifications

Actin (rabbit skeletal muscle actin, gene: *Acta1*): Acetone-dried muscle powder was extracted from skeletal rabbit muscle as described by Feuer et al. (101). Ca^{2+}-bound G-actin was purified according to the method developed by Spudich and Watt (102) and subsequently gel filtered on Superdex200 resin (GE Healthcare). Ca^{2+}-G-actin was stored in G buffer (4 mM Tris-HCl pH7.8, 0.2 mM ATP, 0.1 mM $CaCl_2$, 0.5 mM β-mercaptoethanol (MEA), 0.005% NaN_3) on ice. The actin concentration was determined spectrophotometrically (*Table 2*).

Fluorescent labeling of actin: Actin was labeled at Cys^{374} with N-(1-pyrene)iodoacetamide (pyrene, Sigma-Aldrich) and with the primary amine specific Alexa Fluor® 488 carboxylic acid succinimidyl ester (Alexa488NHS, Invitrogen) at Lys^{328} according to standard protocols (56,103-105). Labeling ratios were derived spectrophotometrically (*Table 2*). Typical labeling ratios of ~ 80 % and ~ 40 % were obtained for pyrene and Alexa488NHS, respectively.

Tubulin: Unlabeled and Hylite Fluor™ 488 tubulin was purchased from Cytoskeleton. The lyophilized proteins were dissolved in BRB buffer (80 mM PIPES pH6.9, 1 mM $MgCl_2$, 1 mM EGTA, 2 mM GTP, 1 mM DTT) according to the manufacturer's instructions. Taxol-stabilized microtubules (10 μM) were prepared by adding 6 % glycerol to the tubulin solution and incubating the samples in a 35°C water bath for 20 min, then 20 μM taxol was added.

Profilin (mouse profilin 1): Recombinant profilin was purified as described previously (106). Profilin was labeled by Alexa Fluor® C_5 568 maleimide (Alexa568C, Invitrogen) according to standard thiol-reactive probe labeling protocols. Protein concentration and labeling ratio was determined spectrophotometrically (*Table 2*). Freshly purified profilin was flash frozen in liquid N_2 and stored at – 80°C until use. Control experiments were performed to justify that the fluorescent label does not affect the interaction of profilin with monomeric actin (*data not shown*).

Capping Protein (CP, mouse heterodimeric α1β2): Recombinant CP was purified as described previously (103). Freshly purified CP was flash frozen in liquid N_2 and stored at – 80°C until use.

molecule	molecular weight (Da)	ε_{280nm} (mg×ml^{-1}×cm^{-1})	ε_{290nm} (mg×ml^{-1}×cm^{-1})	λ_{max} (nm) $\varepsilon_{\lambda max}$ (M^{-1}cm^{-1})	correction factor ($CF_{280\ nm}$)*
Actin	42300	0.63	1.11	-	-
Tubulin	55000	1.15	-	-	-
Profilin	14800	1.13	-	-	-
Capping protein	64267	1.12	-	-	-
Alexa488NHS	643	-	-	495 71000	0.11
pyrene	297	-	-	344 22000	0.127
Alexa568	880.92	-	-	577 91300	0.46

Table 2. Properties of purified proteins and fluorescent dyes used in this study.

*The contribution of the fluorescent dye to the absorption of the protein measured at 280 nm was corrected as follows: $A_{280\,nm,\ corrected} = A_{280\,nm,\ measured} - CF_{280\,nm} \times \varepsilon_{\lambda max}$.

dDAAM proteins: For bacterial protein expression cDNAs of native and truncated *Drosophila melanogaster* DAAM subfragments (DID: 115-356 aa cDAAM: 568-1153 aa, FH1-FH2: 568-1054 aa, cDAAMΔCT: 568-1116, DAD-CT: 1083-1153 aa, DAD: 1083-1119 aa) and their mutated version (FH1-FH2^{I732A}, cDAAM^{I732A}, cDAAM$^{R\text{-}A}$, DAD-CT$^{R\text{-}A}$) were inserted into pGEX-2T vector (Amersham Biosciences) (*Figure 8*). The molecular cloning was performed by our collaborator (József Mihály, Hungarian Academy of Sciences, Biological Research Centre, Szeged, Hungary).

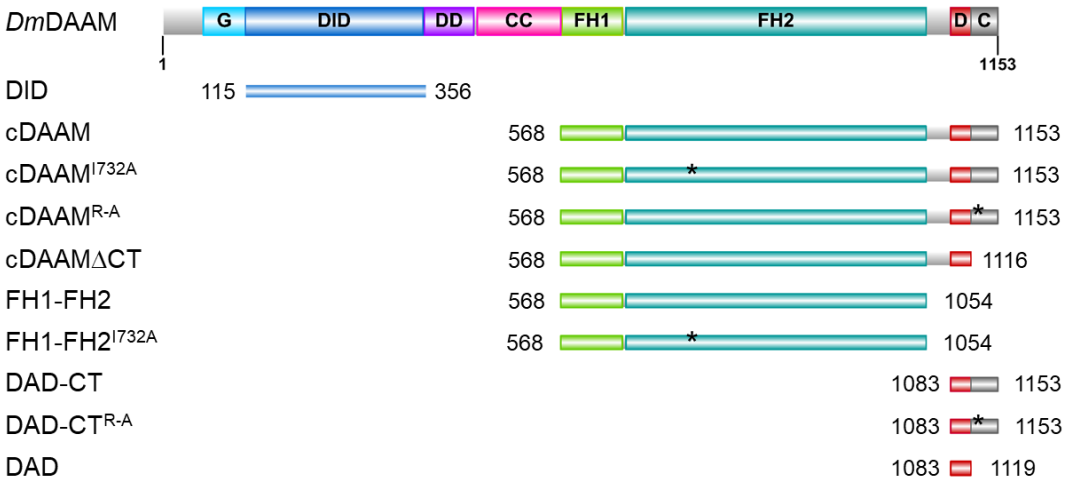

Figure 8. Domain organizations of full-length *Drosophila melanogaster* DAAM formin (*Dm*DAAM) and of the constructs used in this study.

G: GTP binding domain, DID: diaphanous inhibitory domain, DD: dimerization domain, CC: coiled coil, FH: fomin homology, D: diaphanous autoregulatory domain, CT: C-terminal sequence element. Numbers indicate of the first and the last residue in each construct. Asterisks highlight the positions of the mutated amino acids. The figure was made with Illustrator for Biological Sciences.

dDAAM constructs were expressed as Gluthation S-Transferase (GST) fusion proteins in *Escherichia coli* BL21(DE3)pLysS strain (Novagen). Transformed bacteria were grown at 37°C in Luria Broth powder microbial growth medium (Sigma-Aldrich). Protein expression was induced by addition of 1 mM isopropyl β-D-1-thiogalactopyranoside (IPTG) at OD_{600} ~ 0.6 - 0.8. After overnight expression at 20°C, the bacterial extracts were collected by centrifugation (10.000 g, 15 min, 4°C) and stored at – 80°C until use. For protein purification the bacterial pellet was lysed by sonication in Lysis buffer (50 mM Tris-HCl pH7.6, 5 mM DTT, 50 mM NaCl, 5 mM EDTA, 1 % sucrose, 10 % glycerol supplemented with 1 mM PMSF, 5 mM $MgCl_2$, 0.1 mg/ml DNase and Protease Inhibitor Cocktail (Sigma-Aldrich P8465)). The cell lysate was ultracentrifuged (110.000 g, 1 h, 4°C). The supernatant was slowly loaded onto Gluthatione Sepharose 4B resin (Amersham Biosciences) and incubated overnight in batch. For Formin Homology (FH) domain-containing constructs, the column was sequentially washed with Lysis buffer, Wash1 buffer (50 mM Tris-HCl pH7.6, 5 mM DTT, 400 mM NaCl, 10 % glycerol, 1% sucrose), ATP buffer (50 mM Tris-HCl pH7.6, 5 mM DTT, 100 mM KCl, 10 mM $MgCl_2$, 0.25 mM ATP, 5 % glycerol, 1% sucrose) and Wash2 buffer (50 mM Tris-HCl pH7.6, 5 mM DTT, 50 mM NaCl, 5 mM $MgCl_2$, 10 mM KCl, 5 % glycerol, 1% sucrose). For the constructs lacking the FH domains, the column was washed with Lysis buffer followed by Wash2 buffer. The proteins were eluted by Wash2 buffer supplemented with 50 mM Gluthation Reduced (Sigma-Aldrich), concentrated (Vivaspin 30000 Da cut-off) and loaded onto a PD10 column (GE Healthcare) for buffer exchange to Storing buffer (50 mM Hepes pH7.6, 5 mM DTT, 50 mM NaCl, 5 % glycerol, 1 % sucrose). The protein samples were clarified by ultracentrifugation (100.000g, 30 min, 4°C), flash frozen in liquid nitrogen and stored at – 80°C until use. Typically, 5 – 6 g bacterial pellet yielded 2 – 2.5 mg protein. The protein concentrations were measured spectrophotometrically, the extinction coefficients at 280 nm and molecular weights were derived from the amino acid sequences (ExPAsy ProtParam, http://web.expasy.org/protparam/, *Table 3*). Control

experiments showed that a freeze/thaw cycle does not affect the functionality of the DAAM constructs (*data not shown*).

construct	amino acids	number of amino acids	molecular weight (Da)	extinction coefficient ($M^{-1}cm^{-1}$)	isoelectric point
FH1-FH2	568-1054	486	81397.8	65780	7.61
cDAAM	568-1153	585	92395.8	65780	8.66
cDAAMΔCT	568-1119	551	88214.36	65780	8.19
$cDAAM^{R-A}$	568-1153	585	91572.81	65780	6.67
DAD-CT	1083-1153	71	34810.8	42860	7.68
$DAD\text{-}CT^{R-A}$	1083-1153	71	33716.5	42860	5.53
DAD	1083-1119	36	30955.7	42860	6.40
$FH1\text{-}FH2^{I732A}$	568-1054	486	81397.8	65780	7.61
$cDAAM^{I732A}$	568-1153	585	92395.8	65780	8.66
DID	115-356	241	53813.2	48820	6.35

Table 3. Properties of GST-tagged DAAM constructs used in this study.

4. 2. General experimental considerations

Samples at each protein concentration were prepared individually for the experiments. All measurements were performed at 20°C. The sum of the volume of the proteins and the volume of their storing buffer was constant in the samples and represented maximum 50 % of the total volume of the sample. The concentrations given in the text are final concentrations. In all experiments Mg^{2+}-ATP-actin was used. The actin monomer bound Ca^{2+} was replaced by Mg^{2+} by adding 200 μM EGTA and 50 μM $MgCl_2$ and incubating the samples for 5 – 10 min at room temperature.

4. 3. Fluorescence spectroscopy

4. 3. 1. Steady-state anisotropy measurements

Steady-state fluorescence anisotropy (anisotropy), as a fluorescence parameter is a valuable tool to investigate protein-protein interactions. Anisotropy measurements allow to obtain information about the average angular displacement of the fluorophore between photon absorption and emission, which depends on the rotational diffusion of

the fluorophore (107). The binding of a partner molecule to the fluorescently labeled protein results in the formation of a larger complex, characterized by slower rotational diffusion, which can result in an increase in the value of fluorescence anisotropy. Conversely, the dissociation of a molecule from the fluorescently labeled protein can result in a decrease in anisotropy. To measure steady-state anisotropy, the sample is excited by vertically polarized light and the vertically (I_{VV}) and horizontally (I_{VH}) polarized components of the fluorescence emission are detected. The value of anisotropy can be derived as follows:

$$r = \frac{I_{VV} - GI_{VH}}{I_{VV} + 2GI_{VH}} \qquad \textit{(Eq. 1.)}$$

where the first and second subscripts indicate the polarization of the excitation and emission, respectively and factor $G = \frac{I_{HV}}{I_{HH}}$ corrects for the different sensitivities of the detection system to vertically and horizontally polarized light (107).

Sample preparation, measurement and analysis

The steady-state anisotropy of AlexaFluor® 488 succinimidyl ester labeled G-actin (Alexa488NHS-G-actin) was measured to study its interaction with dDAAM. The presence of different compounds, including salt, glycerol and assembly promoting proteins can enhance the assembly of monomeric actin to filaments. Due to the different diffusional properties of G-, and F-actin, polymerization induced by the above agents would result in an undesirable increase in anisotropy. Therefore, in these experiments to avoid artefacts it is of high importance to keep actin in monomeric form. Hence, Alexa488NHS-G-actin (0.2 μM) was preincubated with LatrunculinA (LatA, 4 μM) for 20 min before addition of dDAAM constructs. LatA is a natural toxin produced by certain sponges. This compound binds G-actin with 1:1 stoichiometry near the nucleotide-binding cleft and prevents monomer-filament transition by sequestering monomers (105,108,109). Considering that the dissociation equilibrium constant of the LatA:G-actin complex is K_d = 0.2 μM, 0.19 μM actin (~ 95 % of the total concentration) is in complex with LatA under our experimental conditions. Thus, the amount of LatA-free G-actin (10 nM) is estimated to be well below the critical concentration. This ensures that actin cannot polymerize under these conditions, consequently the increase in anisotropy cannot result from actin assembly. Following LatA treatment,

dDAAM constructs were added to actin at different concentrations and the samples were further incubated for 2 h at 20°C. When profilin was present in the measurements it (0.8 μM) was added to actin directly after the LatA treatment and the samples were further incubated for 30 min at 20°C prior to the addition of dDAAM constructs. Considering the dissociation equilibrium constant of the profilin:G-actin complex (K_d = 0.2 μM (106)), ~ 80 % of the actin was estimated to be bound by profilin under our experimental conditions. The anisotropy measurements were performed using a Horiba Jobin Yvon spectrofluorometer (λ_{ex} = 488 nm, λ_{em} = 516 nm, slits: 5 nm). The dissociation equilibrium constant (K_d) of the dDAAM:G-actin interaction was derived from the dDAAM concentration dependence of the anisotropy of Alexa488NHS-G-actin (r) using the following equation:

$$\frac{r-r_A}{r_{AD}-r_A} = \frac{A_0+D_0+K_d-\sqrt{(A_0+D_0+K_d)^2-4A_0D_0}}{2D_0} \qquad \textit{(Eq. 2.)}$$

where A_0 and D_0 are the total G-actin and dDAAM concentrations, respectively, r_A is the anisotropy of free G-actin and r_{AD} is the anisotropy of G-actin at saturating amount of dDAAM. Alternatively, to study the interaction of dDAAM DAD-CT and profilin:G-actin the anisotropy of Alexa Fluor® 568C_5 maleimide labeled profilin (Alexa568C-profilin) was measured. In these experiments 2 μM of labeled profilin was added to LatA (8 μM) bound actin monomers (4 μM), incubated for 20 min, then supplemented with increasing amount of dDAAM DAD-CT and further incubated for 1 h before the measurement.

4. 3. 2. Pyrenyl polymerization experiments

Kinetics of actin polymerization can be followed by using pyrene (N-(1-pyrene)iodoacetamide) labeled actin (7,110). The fluorescence emission of pyrene increases upon the assembly of the monomers into filaments due to the increase in the quantum efficiency of the actin bound fluorophore. The increase is proportional to the amount of actin filaments formed, thus kinetics of actin assembly can be monitored by measuring the change in the fluorescence emission of pyrene in time. It has to be noted that, although this method is very useful and handy to follow the overall/bulk

polymerization of actin, its disadvantage is that the nucleation and elongation phases of the polymerization are difficult to discern.

Sample preparation, measurement and analysis

In polymerization kinetics measurements the actin concentration was 2 μM that contained 5 % or 2 % pyrenyl labeled actin in the absence or presence of profilin, respectively. The polymerization was initiated by the addition of 1 mM $MgCl_2$ and 50 mM KCl in the absence and presence of different proteins (the exact sample compositions and concentrations are given in corresponding *Figure Legends*). The measurements were performed using a Safas Xenius FLX spectrofluorimeter (λ_{ex} = 365 nm, λ_{em} = 407 nm). For quantitative analysis the bulk polymerization rate at each condition was derived from the slope of the pyrenyl trace at half-maximum polymerization. To analyze the effect of DID on cDAAM mediated actin assembly (*Figure 12*) the relative polymerization rate ($v_{relative}$) was derived as follows:

$$v_{relative} = \frac{v}{v_{cDAAM}} \qquad (Eq.\ 3.)$$

where v is the polymerization rate measured in the presence of different amounts of DID and v_{cDAAM} is the polymerization rate measured in the absence of DID. The DID concentration dependence of the relative polymerization rate was fit by the following equation:

$$v_{relative} = \left(1 - \frac{[DAD{:}DID]}{[DAD_0]}\right) * v_0 + v_{min} \qquad (Eq.\ 4.)$$

where v_0 and v_{min} is the relative polymerization rate in the absence and presence of saturating amount of DID, respectively, $[DAD_0]$ is the total cDAAM concentration and $[DAD{:}DID]$ is the concentration of the DID:cDAAM complex, which was derived from the quadratic binding equation. To analyze the effects of dDAAM constructs on actin assembly (*Figures 13, 18, 19 and 23*) the relative polymerization rates ($v_{relative}$) were derived as follows:

$$v_{relative} = \frac{v}{v_{actin}} \qquad (Eq.\ 5.)$$

where v is the polymerization rate measured in the presence of different amounts of dDAAM and v_{actin} is the rate of actin assembly in the absence of dDAAM. The antagonistic regulation of barbed end dynamics by dDAAM and CP was investigated, as described in (111). Briefly, polymerization of profilin:G-actin was initiated in the presence of different dDAAM constructs. CP was added to the samples at different amounts 120 s after the initiation of pomyerization. The CP concentration dependence of the polymerization rate (v) was derived from the initial slopes of the pyrenyl traces after CP addition. The data was fit by the following equation:

$$v = v_0 - \left(\frac{v_0 - v_{min}}{1 + \frac{IC_{50}}{[CP_0]}}\right) \qquad (Eq.\ 6.)$$

where v_0 and v_{min} is the polymerization rate in the absence and presence of saturating amount of CP, respectively, $[CP_0]$ is the total CP concentration and IC_{50} corresponds to the amount of CP that is required for 50 % inhibition.

4. 4. Total internal reflection fluorescence microscopy

Total internal reflection fluorescence microscopy (TIRFM) uses the unique features of the evanescent field generated upon total internal reflection. According to the Snellius-Descartes' law of refraction, if light propagates from an optically denser (cover glass) medium towards an optically less dense medium (aqueous sample) at an angle larger than the critical angle, light is totally internally reflected back from the boundary of the two media (*Figure 9*). However, Maxwell's equations predict the existence of an electromagnetic field that penetrates into the optically less dense medium. The electromagnetic field decays exponentially from the boundary and fades away within a short distance of ~ 100 nm. Therefore, the evanescent field excites fluorophores only within a thin slice of the sample near the cover glass, consequently fluorescence emission is detected only from this region of the sample giving the opportunity to eliminate the background fluorescence and improve axial resolution (112). Due to the unique excitation mode, TIRFM allows to observe individual actin filaments bound to the functionalized glass, therefore the nucleation and elongation phases of actin polymerization can be discerned and analyzed separately (113). For

quantitative analysis the number of actin filaments and the elongation rate can be derived (*Figure 10*).

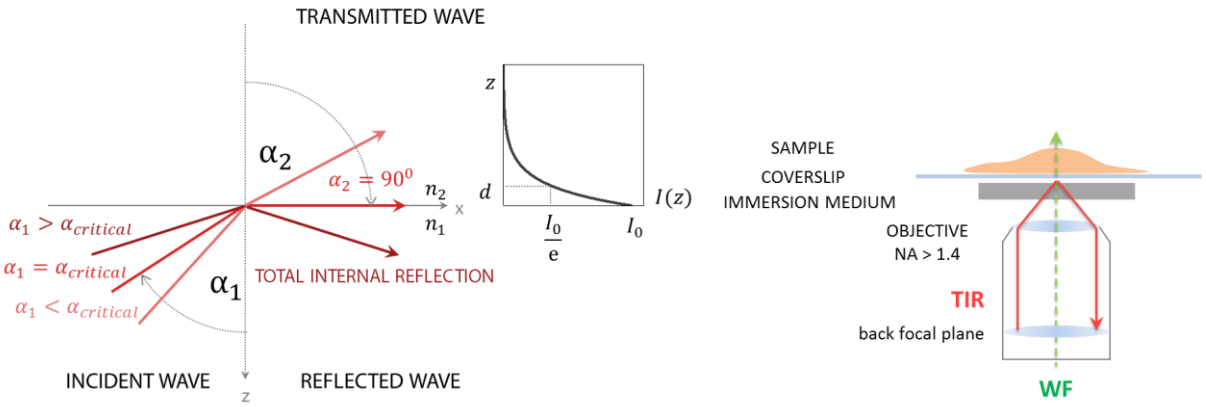

Figure 9. Principles of TIRFM microscopy. (114)

4. 4. 1. Actin assembly experiments

Actin polymerization (0.5 μM Mg^{2+}-G-actin containing 10 % Alexa488NHS-G-actin) was followed by TIRFM in the absence and presence of profilin (2 μM) and dDAAM constructs (the exact protein concentrations are given in the corresponding *Figure Legends*). Glass flow cells (~ 100 μL) were incubated with 1 volume of N-ethylmaleimide (NEM) labeled skeletal muscle myosin S1 for 1 min to functionalize glass surface. NEM-labeled myosin can bind filamentous actin but it lacks motor activity, therefore actin filaments can be captured and hold by NEM-myosin close to the glass surface in the evanescent field (113). After functionalization, flow cells were washed extensively with 2 volumes of myosin buffer (4 mM Tris-HCl pH7.8, 1 mM DTT, 0.2 mM ATP, 0.1 mM $CaCl_2$, 500 mM KCl, 1 mM $MgCl_2$, 0.2 mM EGTA) to remove unbound myosin. Subsequently, flow cells were treated by 2 volumes of 0.1 % (w/v) bovine serum albumin (BSA) to passivate the glass surface free from myosin. Finally, flow cells were equilibrated with 2 volumes of TIRFM buffer (0.5 % (w/v) methylcellulose, 10 % (w/v) BSA, 10 mM 1,4-diazabicyclo-[2,2,2]octane (DABCO), 10 mM DTT in F buffer (4 mM Tris-HCl, pH7.8, 1 mM DTT, 0.2 mM ATP, 0.1 mM $CaCl_2$, 50 mM KCl, 1 mM $MgCl_2$, 0.2 mM EGTA)) before adding the protein mixture. Images were captured every 10 s with an Olympus IX81 microscope equipped with a laser-based (491 nm and 568 nm) TIRFM module using an APON TIRF 60x NA1.45 oil immersion objective and a CCD camera (Hamamatsu Orca-ER-1394). Image analysis was performed by Fiji. Images were background corrected before analysis. Filament

number was derived by using a Fiji plugin from a 66×66 μm region of the image, the plugin was provided by our collaborator (József Mihály, Hungarian Academy of Sciences, Biological Research Centre, Szeged, Hungary). Time-lapse images were analyzed either by the MultipleKymograph plugin of Fiji or by manually tracking filament growth to derive the elongation rate of actin filaments (*Figure 10*). Filament length was converted to subunits using 370 subunits per micron filament (115).

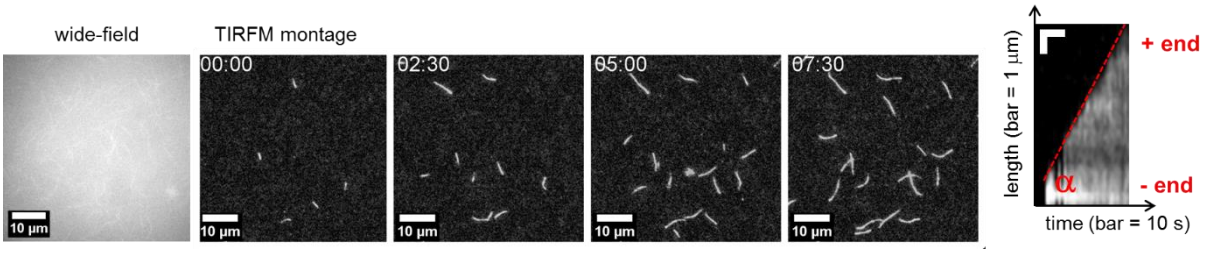

Figure 10. Observation of actin assembly by wide-field and TIRF microscopy.

Left panel: Observations of assembly kinetics of actin filaments by using conventional wide-field fluorescence and TIRFM microscopy. *Right panel*: principles of kymograph analysis. (114)

The spontaneous elongation rate of actin filaments (v_0) was related to the critical concentration of actin assembly ($c_c \sim 0.1\ \mu M$, (3,4)), to the association rate constant of actin monomer incorporation to filament barbed ends (k_+) and to the total actin concentration ($[G_0]$) by the following equation:

$$v_0 = k_+([G_0] - cc) \quad (Eq.\ 7.)$$

4. 4. 2. Actin filament-microtubule co-alignment

Preassembled actin filaments (0.4 μM containing 10 % Alexa568NHS-G-actin) and microtubules (0.4 μM containing 10 % Hylite Fluor™ 488-tubulin) were stabilized by phalloidin (1 : 1 molar ratio) and taxol (1 : 2 molar ratio), respectively. Mixtures of phalloidin:F-actin and taxol:microtubules were incubated with dDAAM constructs (1 μM) in BRB-K buffer (80 mM PIPES pH6.9, 1 mM $MgCl_2$, 1 mM EGTA, 50 mM KCl) at room temperature for 30 minutes. Samples were diluted in BRB-K* buffer (BRB-K supplemented with 0.2 % (w/v) methylcellulose, 0.5 % (w/v) BSA, 50 mM DABCO and 100 mM DTT), applied onto poly-L-lysine-treated (Sigma-Aldrich) coverslips and visualized by TIRFM microscopy. Images were captured with an Olympus IX81 microscope equipped with a laser-based (491 nm and 568 nm) TIRFM module using

an APON TIRF 60x NA1.45 oil immersion objective and a CCD camera (Hamamatsu Orca-ER-1394). Image analysis was performed by Fiji. Images were background corrected before analysis. Microtubule-F-actin co-localization was quantified as described in (41) by using a home-written plugin provided by our collaborator (József Mihály, Hungarian Academy of Sciences, Biological Research Centre, Szeged, Hungary).

4. 5. Sedimentation experiments

Structural organization of cytoskeletal polymers, as well as their interactions with associated proteins can be analyzed by the combination of sedimentation and SDS-PAGE techniques. High-speed sedimentation assays can be used to study the polymer side-binding activities of associated proteins (*Figure 11, upper panel*). As an example, when samples containing actin filaments and an associated protein are centrifuged at high speed (~ 100.000 g), the protein fraction that binds/physically linked to the polymers sediments with F-actin and appears in the pellet, while the unbound fraction remains in the supernatant. Under the experimental conditions, the filament end concentration is relatively low (< nM), while the filament side concentration is in the micromolar range. Thus, the analysis of the protein content of the Coomassie-stained SDS-PAGE gels of the pellets can reveal the binding of a protein to the side of the polymers. Low-speed sedimentation assays can be used to study the cytoskeletal polymer bundling/cross-linking and polymer co-alignment activities of associated proteins (*Figure 11, middle and lower panel*). The sedimentation properties of individual polymers and polymers organized into higher-order structures (e.g. bundled/cross-linked or co-aligned networks) differ. Upon centrifugation at relatively low-speed (4000 - 14.000 g) bundled/cross-linked and co-aligned polymers can sediment and appear in the pellet, while individual polymers remain in the supernatant.

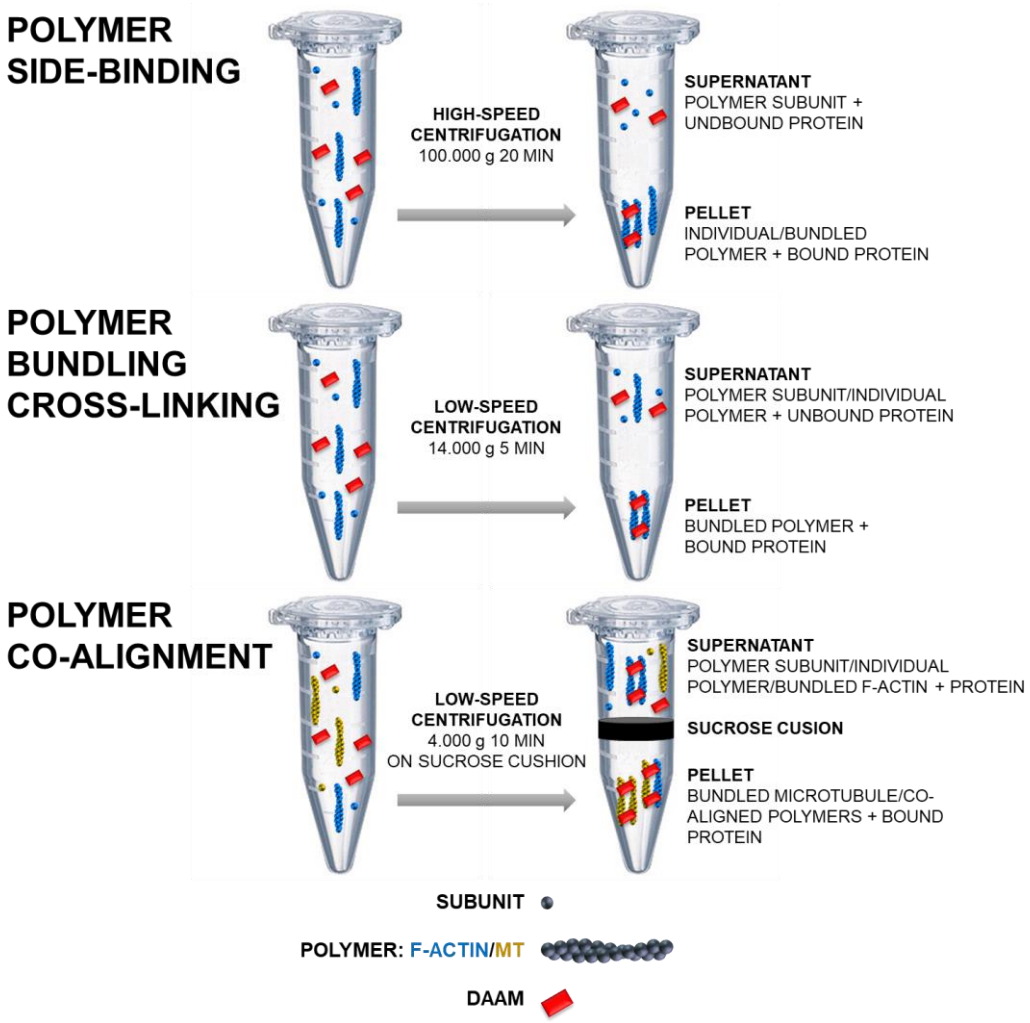

Figure 11. Schematic representation of strategies used in sedimentation experiments to investigate polymer binding, bundling/crosslinking and co-alignment activities of dDAAM.

4. 5. 1. High-speed sedimentation assay

High-speed centrifugation experiments were performed to investigate the binding of the C-terminal constructs of dDAAM to the sides of actin filaments. Preassembled actin filaments (2 μM) were mixed with dDAAM fragments in polymerizing conditions (in the presence of 50 mM KCl and 1 mM $MgCl_2$) and incubated overnight. Samples were ultracentrifuged (100.000 g, 30 min, 20°C), supernatants and pellets were separated and analyzed by SDS-PAGE. The band intensities were corrected for the molecular weights of the proteins and the ratios of the dDAAM and actin band intensities measured in the pellets (D) were plotted as the function of the total dDAAM concentration $[D_0]$. The data were analyzed by using *Equation 8* (45):

$$[A_0]D^2 - ([A_0] + [D_0] + K_D)D + D_0 = 0 \quad (Eq.\ 8.)$$

where $[A_0]$ is the total actin concentration and K_D is the dissociation equilibrium constant of the dDAAM:F-actin interaction. In control experiments we found that the C-terminal constructs of dDAAM appear in the pellet even in the absence of F-actin, however at significantly lower amount than in the presence of it (*Figure 26*). Therefore, for the quantitative analysis the amount of self-pelleting dDAAM protein was subtracted from the amount of dDAAM sedimented in the presence of actin.

4. 5. 2. Actin filament and microtubule bundling/crosslinking assay

To study the polymer bundling/crosslinking activity of dDAAM constructs, either preassembled actin filaments or taxol-stabilized microtubules (1 μM) in F buffer and BRB buffer, respectively, were incubated in the absence or presence of different dDAAM constructs for 1 h at 20°C. Subsequently, samples were centrifuged (14.000 g, 5 min, 20°C). The supernatants and pellets were carefully separated and the supernatants were processed for SDS-PAGE analysis. The relative amount of F-actin/microtubule in the supernatant was derived as the ratio of the amount of F-actin/microtubule in the presence of different dDAAM constructs to the amount of F-actin/microtubule in the absence of any other protein and plotted as the function of dDAAM concentration.

4. 5. 3. Actin filament-microtubule co-alignment assay

A low-speed centrifugation assay was developed to study the F-actin:microtubule co-alignment activity of dDAAM. Phalloidin-stabilized F-actin (2 μM) and taxol-stabilized microtubules (2 μM) were mixed and incubated with dDAAM constructs (9 μM) in BRB-K at room temperature for 40 min. Samples (25 μL) were loaded onto a 30 % sucrose cushion and centrifuged (4000 g, 10 min, 20^{0}C). Control experiments revealed that under these conditions individual polymers, as well as F-actin bundles do not sediment, only larger filament complexes (MT bundles, F-actin:MT co-polymers) appear in the pellet. The pellets and supernatants were carefully separated and analyzed by SDS-PAGE. In control experiments based on high-speed centrifugation (100.000 g, 30 min, 20°C) both F-actin and MTs appeared in the pellet, which confirmed that both proteins exist in polymeric form under the applied

experimental conditions, and the lack of sedimentation of the polymers is not due to depolymerization.

4. 6. SDS-PAGE analysis

For quantitative analysis of the sedimentation experiments, the protein content of the supernatants and/or pellets was derived from Coomassie-stained gels (Syngene bioimaging system). Quantification of Coomassie blue intensities were performed within the linear range of exposure identified by a calibration curve. The intensity values were corrected for the molecular weight of each protein.

4. 7. Statistical analysis

Data presented are derived from at least two independent experiments. Exact replicate numbers are given in *Figure Legends*. Values are displayed as mean ± standard deviation. Microscopy data were analyzed statistically by using two-sample T-test or Z-test considering the number of data and the variance (Excel, Microsoft). By convention $p > 0.05$ was considered as statistically not significant, $*p \leq 0.05$, $**p < 0.01$, $***p < 0.001$, $****p < 0.0001$. The significance levels are given in the text and on the corresponding figures.

5. RESULTS AND DISCUSSION

5. 1. The interaction of dDAAM FH1-FH2 with actin is regulated by the DID-DAD module

Formins of the DRF family, such as Dia1, FHOD1 and FRL2 exist in cells in an inactive form. Since the N-terminal DID and the C-terminal DAD domains form an intramolecular lock, which inhibits the interaction of their FH2 domain with actin (76,116,117). The activation of DRF formins occurs upon binding of an RhoGTPase to the GBD domain, which contributes to the release of the DID:DAD interaction, which results in the exposure of the FH2 domain to actin. This mode of autoregulation has been described for several DRFs but structural details are only known for Dia1 to date (75,77). Sequence analysis reveals that dDAAM also possesses N-, and C-terminal sequence elements, which are characteristic to the DID and DAD regulatory regions (*Figure 8*). Previous *in vivo* investigations of dDAAM showed that deletion either of the DID or DAD domains results in a constitutively active form of the protein in flies (81,87).

To investigate the role of DID and DAD in the actin activities of DAAM FH1-FH2 *in vitro* pyrenyl polymerization assays were performed. Two constructs were used; FH1-FH2 that lacks the C-terminal DAD-CT and cDAAM that possesses the DAD-CT regions (*Figure 8*). First, the effect of isolated DID on spontaneous actin assembly was studied (*Figure 12, A*). This control measurement showed that isolated DID is not able to influence spontaneous actin polymerization. The experiments were repeated both in the absence or presence of FH1-FH2 and cDAAM. The results revealed that DID fails to affect FH1-FH2-mediated actin assembly (*Figure 12, A*). In contrast, the cDAAM-mediated actin polymerization is inhibited by DID in a concentration-dependent manner (*Figure 12, A*). In the presence of saturating amount of DID the polymerization kinetics was equivalent to that of spontaneous actin assembly. Since the only difference between FH1-FH2 and cDAAM can be found at the C-terminal region, we concluded that DID affects the actin polymerization activity of dDAAM by interacting with the C-terminus. For quantification, the relative polymerization rates were derived and plotted as a function of DID concentration (*Figure 12, B*). The dissociation equilibrium constant was found to be ~ 30 nM, indicating a high-affinity interaction between DID and the DAD region of cDAAM (*Figure 12, B*). These findings suggest that the actin activities of *Drosophila* DAAM FH1-FH2 are autoregulated by its

N-terminal DID and C-terminal DAD domains *in vitro*, thus dDAAM is a *bona fide* DRF formin. The above results also indicate that this mode of autoregulation is conserved between flies and humans (49).

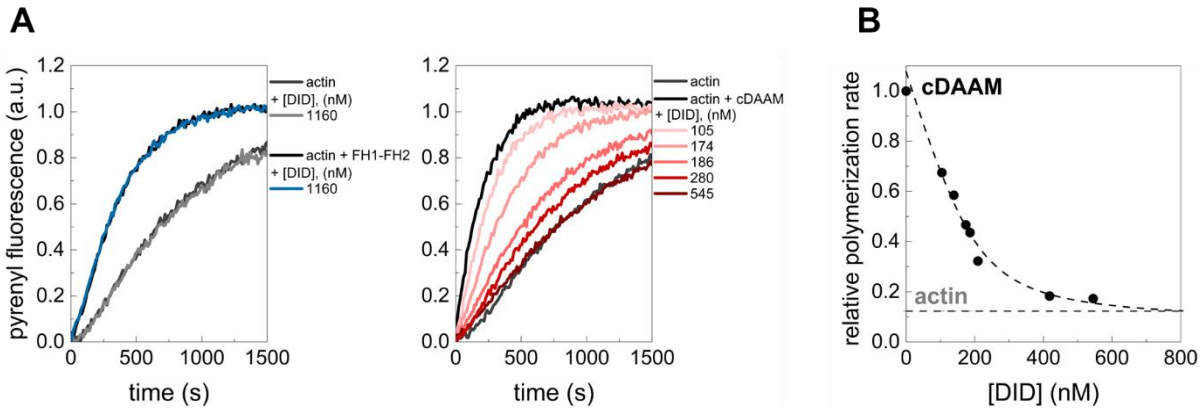

Figure 12. The interaction of dDAAM FH1-FH2 with actin is regulated through the DID:DAD interaction.

(A) Representative polymerization kinetics of actin in the absence and presence of DID, FH1-FH2 and cDAAM, as indicated. [actin] = 2 μM (containing 5 % pyrenyl actin), [FH1-FH2] = 5 μM, [cDAAM] = 0.51 μM. (B) The relative polymerization rate of cDAAM-catalyzed actin assembly as a function of DID concentration. Black dashed line corresponds to the fit of the data using *Eq. 4*. The fit gave half-inhibition of cDAAM by DID at 30.5 ± 14.31 nM. The relative rate of spontaneous actin assembly is indicated by grey dashed line.

5. 2. cDAAM is more efficient in promoting actin assembly than FH1-FH2

The defining feature of formins is the presence of the highly conserved Formin homology (FH1-FH2) domains. The basic unit for catalyzing actin nucleation is the FH2 domain, while the proline-rich FH1 domain interacts with profilin and recruits profilin:G-actin for elongation (32,54,56,79). Interestingly, recently it has been demonstrated using purified proteins, that besides autoregulation the C-terminus of some formins can influence the activities of the FH2 domain *in vitro* (90-93). This activity of the C-terminus of formins can be relevant in the biological context as supported by the observations of our collaborator; they demonstrated that the FH1-FH2 of dDAAM is more efficient in the presence of the C-terminal region in axonal filopodia formation in *Drosophila* primary neurons (118).

To better understand the underlying mechanism and to elaborate on the role of dDAAM DAD-CT in FH1-FH2-mediated actin assembly, first we compared the polymerization promoting efficiencies of the FH1-FH2 region in the absence and

presence of DAD-CT (corresponding constructs are FH1-FH2 and cDAAM, respectively (*Figure 8*)) in pyrenyl polymerization experiments (*Figure 13*). The results showed that both constructs accelerate actin assembly (*Figure 13, A*). However, quantitative analysis revealed that cDAAM accelerates polymerization ~ 36fold more efficiently than FH1-FH2 (*Figure 13, B*). The effect was independent from the presence of profilin (*Figure 13*). These findings suggest that the DAD-CT of dDAAM – besides autoregulation – can tune the actin assembly activity of the active dDAAM FH1-FH2 region.

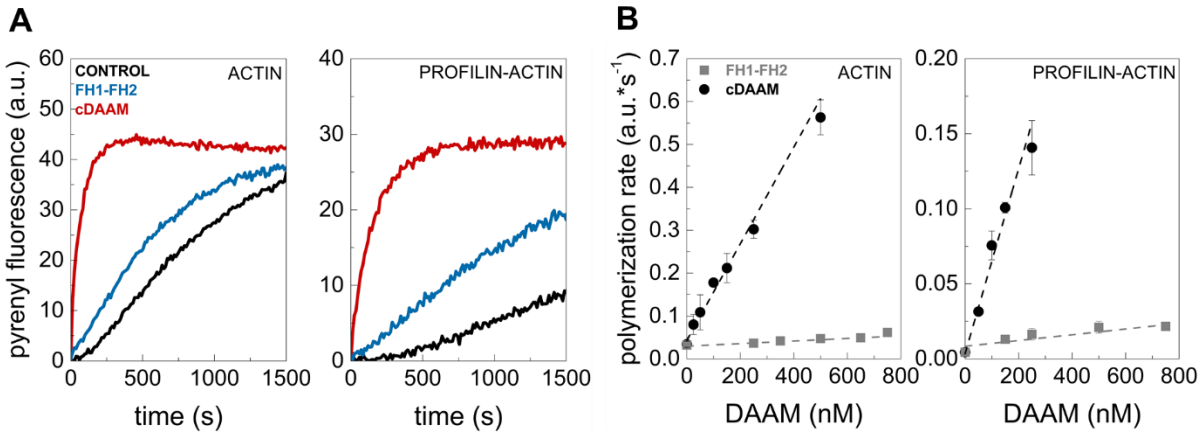

Figure 13. cDAAM is more efficient in catalyzing actin assembly than FH1-FH2.

(A) Representative pyrenyl traces of spontaneous and FH1-FH2-, or cDAAM-catalyzed assembly of free G-actin and profilin:G-actin, as indicated. Final concentrations: [actin] = 2 μM (containing 5 % and 2 % of pyrenyl actin in the absence and presence of profilin, respectively), [profilin] = 6 μM, [FH1-FH2] = 200 nM, [cDAAM] = 200 nM. (B) FH1-FH2 and cDAAM concentration dependence of the relative polymerization rate (*Eq. 5.*) of free G-actin and profilin:G-actin, as indicated. Error bars: standard deviations, n = 3 – 5.

The isolated FH2 domain of some formins (e.g. Bni1p, Dia1) binds G-actin with low affinity in the absence of the C-terminal regions (91,119). The different polymerization efficiencies of dDAAM FH1-FH2 and cDAAM that we detected in pyrenyl polymerization experiments can arise from their different actin binding affinities. To test this possibility, the interactions of FH1-FH2 and cDAAM with G-actin were compared in steady-state fluorescence anisotropy measurements. The titration of fluorescently labeled actin (Alexa488NHS-G-actin) and its complexes with profilin by the constructs resulted in a concentration-dependent increase in anisotropy, implying that both constructs bind actin (*Figure 14*). The actin affinities were found to

be in the few tens of nM range for both constructs, independently from presence of profilin (*Table 4*).

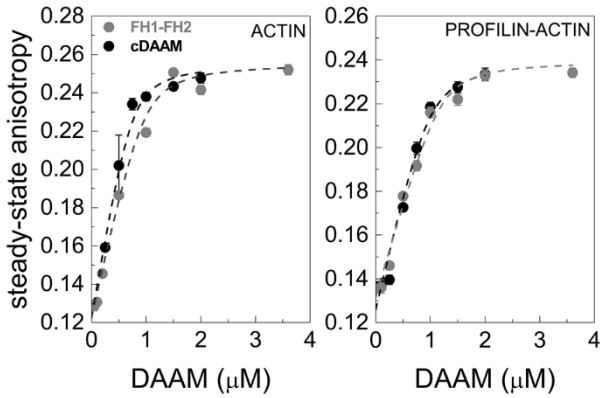

Figure 14. Interaction of FH1-FH2 and cDAAM with actin monomers, as revealed by steady-state anisotropy experiments.

Steady-state anisotropy of Alexa488NHS-G-actin in the absence and presence of profilin as the function of dDAAM concentration, as indicated. Dashed lines in the corresponding colors show the fits to the data according to *Eq. 2*. Dissociation equilibrium constants are summarized in *Table 4*. Error bars: standard deviations, n = 2 – 3. Final concentrations: [actin] = 0.2 μM, [LatA] = 4 μM, [profilin] = 0.8 μM, [NaCl] = 5 mM.

construct	$K_d \pm SD$ (μM)	
	G-actin^{FL}	profilin:G-actin^{FL}
FH1-FH2	0.061 ± 0.02	0.056 ± 0.02
cDAAM	0.052 ± 0.02	0.068 ± 0.02

Table 4. Dissociation equilibrium constants (K_d) of the dDAAM:actin interactions. FL: fluorescently labeled protein.

The results of anisotropy measurements suggest that the different polymerization efficiencies of the DAD-CT lacking and possessing constructs do not arise from their different binding affinities. Our data also suggest that, unlike other formins, the FH2 of dDAAM show significant actin affinity even in the absence of the C-terminal regions.

5. 3. cDAAM catalyzes actin assembly more efficiently than FH1-FH2

The differences between the FH1-FH2-, and cDAAM-mediated polymerization can be explained by their different nucleation and/or elongation efficiencies. Since these phases of actin assembly are difficult to separate in fluorescence spectroscopic

experiments TIRFM measurements were performed (*Figure 15*). TIRFM allows to observe individual filaments and separately analyze actin nucleation and elongation. In control experiments, we found that significantly less filaments are formed in the presence of profilin as compared to spontaneously nucleated actin filaments (34.35 ± 9.43 and 18.60 ± 6.22, respectively, $p < 0.001$, (*Figure 15, A, B*)). This observation is in good agreement with the well-established nucleation-suppressing activity of profilin (3,7,10). Our analysis revealed that, although the number of actin filaments formed in the presence of either FH1-FH2 or cDAAM is significantly higher than that is characteristic for spontaneous actin assembly, cDAAM is more efficient in filament production than the FH1-FH2 both in the absence and presence of profilin (*Figure 15, B*).

The elongation rate of spontaneously polymerizing actin filaments was found to be 4.30 ± 0.61 subunit×s^{-1} and 3.48 ± 0.38 subunit×s^{-1} in the absence and presence of profilin, respectively (*Figure 15, C*). These values are in good agreement with the well-established barbed end association rate constants of ATP-Mg^{2+}-G-actin (free G-actin: k_+ = 10.23 ± 1.5 $\mu M^{-1}\times s^{-1}$, profilin:G-actin: k_+ = 8.29 ± 0.9 $\mu M^{-1}\times s^{-1}$, *Eq. 7.*). FH1-FH2 and cDAAM strongly inhibit the elongation of free G-actin in the absence of profilin ($v_{FH1\text{-}FH2}$ = 0.36 ± 0.15 subunit×s^{-1} ($p < 0.0001$), v_{cDAAM} = 0.37 ± 0.13 subunit×s^{-1} ($p < 0.0001$)). In contrast, in the presence of profilin the elongation rate is similar to that of the spontaneously growing actin filaments ($v_{FH1\text{-}FH2}$ = 3.44 ± 0.34 subunit×s^{-1} ($p = 0.45$), v_{cDAAM} = 3.49 ± 0.44 subunit×s^{-1} ($p = 0.44$). These observations for FH1-FH2 are in agreement with our previous findings (56). dDAAM FH1-FH2 is unique amongst formins in terms of its effects on filament elongation: by almost completely inhibiting elongation in the absence of profilin it behaves as a capping-like protein. Profilin act as a molecular switch in the filament end effects of dDAAM FH1-FH2, although it cannot enhance FH1-FH2-mediated filament growth above the diffusion-limited rate as observed for Dia1 (32).

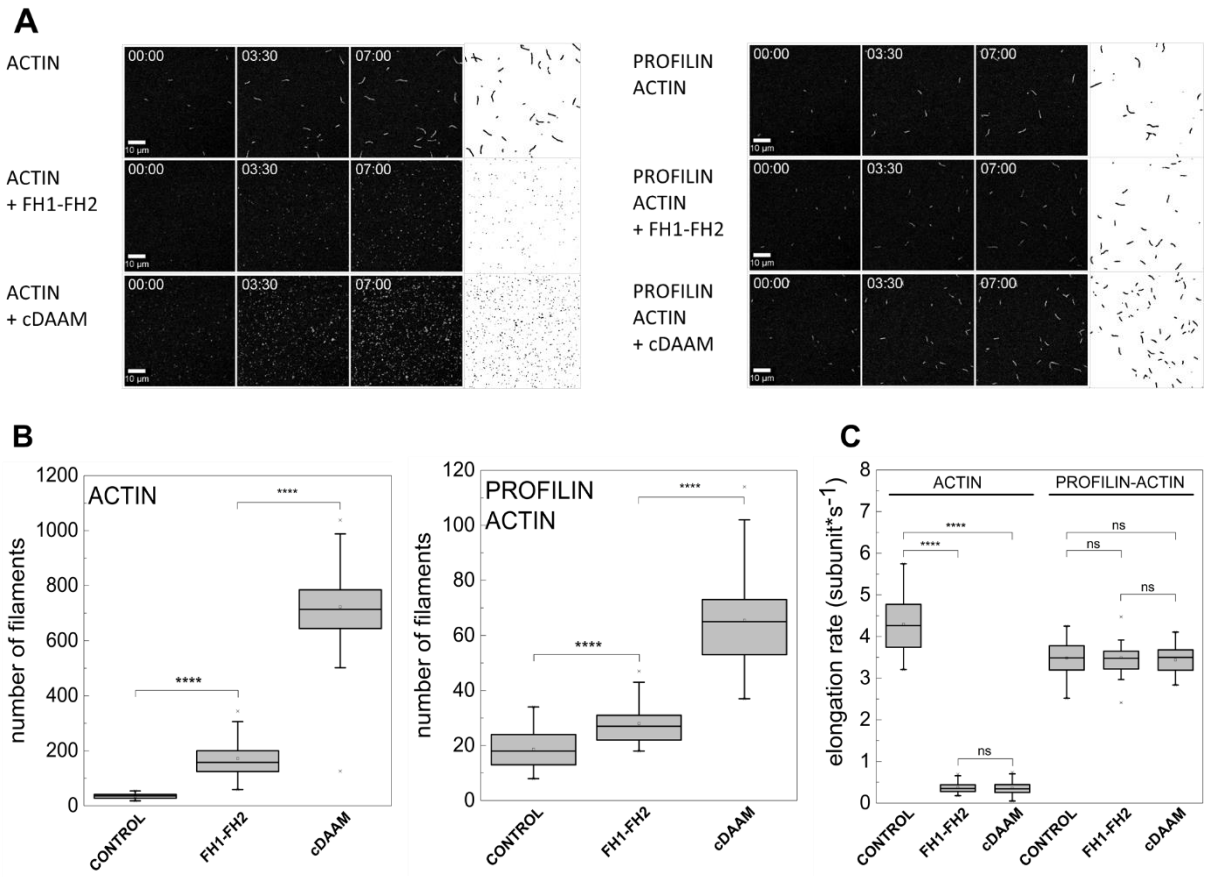

Figure 15. Effects of FH1-FH2 and cDAAM on actin assembly, as revealed by TIRFM measurements.

(A) TIRFM montages of actin assembly and representative skeletonized images showing the field of view of actin assembly in the absence and presence of FH1-FH2 or cDAAM, as indicated. Scale bar = 10 μm, time = min : s. Final concentrations: [actin] = 0.5 μM, [profilin] = 2 μM, [FH1-FH2] = 100 nM, [cDAAM] = 100 nM. (B) The number of actin filaments nucleated spontaneously or in the presence of FH1-FH2 and cDAAM derived from skeletonized images. Final concentrations as in panel (A), n = 20 – 62. (C) The elongation rate of individual actin filaments polymerized from free G-actin and profilin:G-actin in the absence and presence of FH1-FH2 or cDAAM. Final concentrations as in panel (A), n = 30 – 89.

In conclusion, the different actin polymerization promoting efficiency of FH1-FH2 and cDAAM is not the consequence of their different effects on filament elongation. Our observations clearly demonstrate that the more efficient actin assembly promoting activity of cDAAM is due to its more potent nucleating efficiency as compared to FH1-FH2. This suggests that the presence of DAD-CT influences the nucleation promoting activity of FH1-FH2.

5. 4. dDAAM DAD-CT interacts with G-actin, independently from the FH2 domain

Recent work reported that isolated C-terminal regions of some formins (INF2, FMNL3, Dia1 and Capuccino) can bind directly to monomeric actin (90-93). To investigate whether dDAAM DAD-CT shares this property a recombinant DAD-CT fragment was produced (*Figure 8*). The G-actin and profilin:G-actin binding ability of DAD-CT was tested in steady-state anisotropy measurements by using Alexa488NHS-G-actin (*Figure 17*). We found that in the presence of DAD-CT the anisotropy values increase in a concentration-dependent manner, suggesting that this region can interact with actin even in the absence of FH2. The binding was relatively weak, the corresponding affinity was found to be in the few μM range and was not affected significantly by the actin-bound profilin (*Table 5*). Importantly, with increasing salt concentrations (from 5 mM to 50 mM NaCl) the anisotropy values gradually decreased, suggesting that the binding of DAD-CT is strongly salt-dependent (*Figure 17, Table 5*).

To further elaborate on which region of DAD-CT is important for G-actin binding, two other constructs were produced; the DAD domain lacking the very C-terminal amino acids (DAD) and a mutated version of the DAD-CT construct (DAD-CT^{R-A}), in which the arginine residues found in the CT region are replaced by alanine (*Figure 8, 16*).

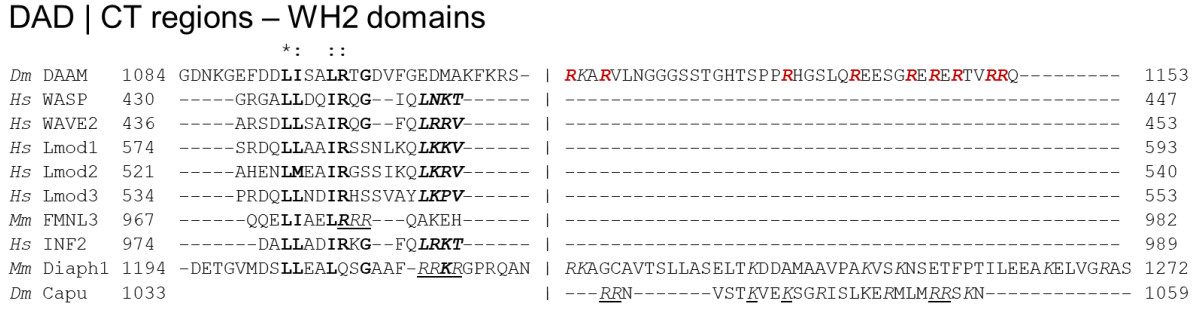

Figure 16. Sequence characteristics of the C-terminal regions of formins and their comparison with WH2 domains.

The hydrophobic amino acid triplet and the LKKT/V motif is shown by bold and bold italics, respectively. Positively charged Arg and Lys residues in the CT region are shown in italics. The Arg residues replaced by Ala in the DAAM DAD-CT^{R-A} construct are highlighted by red. Residues that were shown to be important for actin interaction in mDia1, FMNL3 and Capuccino are underlined (91,92,99). UniProt accession numbers are as follows: *Dm* DAAM Q8IRY0, *Hs* WASP P42768, *Hs* WAVE2 Q9Y6W5, *Hs* Lmod1 P29536, *Hs* Lmod2 Q6P5Q4, *Hs* Lmod3 Q0VAK6, *Mm* FMNL3 Q6ZPF4, *Hs* INF2 Q27J81. *Dm*: *Drosophila melanogaster*, *Hs*: *Homo sapiens*, *Mm*: *Mus musculus*.

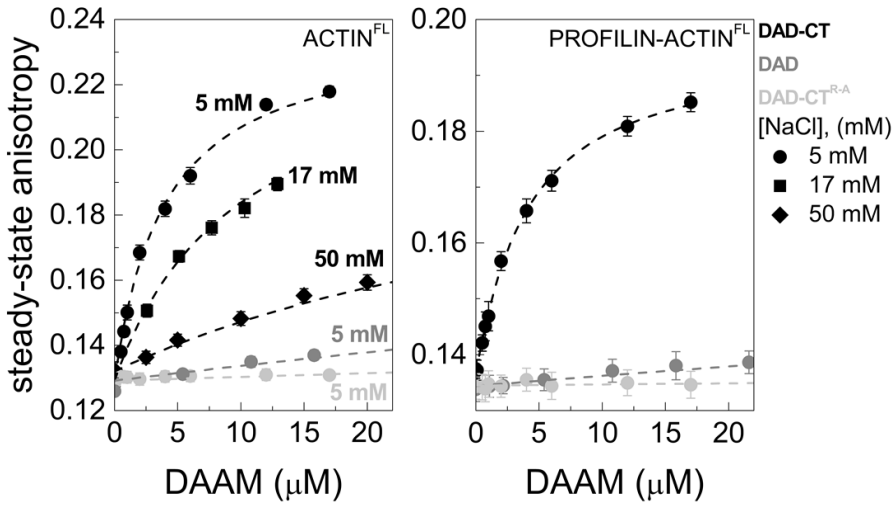

Figure 17. Interaction of the C-terminal regions of DAAM with monomeric actin.

(A) Steady-state anisotropy of Alexa488NHS-G-actin in the absence and presence of profilin as the function of DAD-CT, DAD and DAD-CTR-A concentration, as indicated. Dashed lines in the corresponding colors show the fits to the data according to *Eq. 2*. Error bars: standard deviations, n = 2 – 4. Final concentrations: [actin] = 0.2 μM, [LatA] = 4 μM, [profilin] = 0.8 μM, [NaCl] = 5 mM (circles), 17 mM (squares), 50 mM (diamonds). FL: fluorescently labeled protein. Dissociation equilibrium constants are summarized in *Table 5*.

construct	$K_d \pm$ SD (μM)	
	G-actin^{FL}	profilin:G-actin^{FL}
DAD-CT	3.87 ± 0.19	3.54 ± 0.22
	9.71 ± 0.51 (17 mM NaCl)	nd
	44.43 ± 2.85 (50 mM NaCl)	nd
DAD	> 100	> 100
DAD-CT^{R-A}	> 500	> 500

Table 5. Dissociation equilibrium constants (K_d) of the dDAAM:actin interactions. FL: fluorescently labeled protein.

DAD showed an extremely weak interaction in anisotropy measurements even at low salt conditions (K_d > 100 μM, (*Figure 17, Table 5*)). In case of DAD-CT^{R-A} there was no detectable anisotropy change in the concentration range that we could test in the experiments, suggesting an even weaker binding or no interaction with G-actin (*Figure 17, Table 5*).

In conclusion, the DAD-CT of dDAAM can bind to monomeric actin both in the absence and presence of profilin, even in the absence of the core actin-binding FH2 domain. Our data also indicate that the main actin-interacting element is the CT region. The strong salt dependence of the interaction suggests that the binding is manifested through mostly electrostatic interactions.

5. 5. dDAAM DAD-CT does not influence actin dynamics in the absence of the FH2 domain

The binding of the isolated C-terminal regions of formins to monomeric actin can have functional consequences. As examples, the isolated WH2-like DAD domain of INF2 inhibits actin polymerization by sequestering actin monomers, as well as severs actin filaments (90). In contrast, the C-terminus of FMNL3 and Dia1 in dimeric form possesses nucleation activity, even in the absence of FH2 (91,92). While the isolated tail domain of Capuccino has no influence on actin dynamics (93). To reveal the biochemical activities of isolated dDAAM DAD-CT we studied its effect on actin polymerization in the absence and presence of profilin in fluorescence spectroscopy and TIRFM measurements. The results revealed that DAD-CT does not have any influence on actin assembly – neither on filament number nor on filament growth rate – at lower amounts (*Figure 18*). At higher concentrations (> ~ 40 – 50 μM) the protein slightly inhibits actin assembly kinetics (*Figure 18, A, D*) that might result from its weak sequestration activity. Similar effect was observed for the tail domain of Capuccino (93). In agreement with the very weak actin binding of DAD and DAD-CT$^{R\text{-}A}$ they have no influence actin dynamics in these experiments (*Figure 18, A, D*).

In conclusion, although isolated DAD-CT is able to bind to monomeric actin it has no significant influence on the dynamics of actin assembly in the absence of the FH2 domain, even in its dimeric form that is maintained by the GST-tag. This indicates that dDAAM DAD-CT possesses an FH2-dependent activity in actin dynamics. In agreement with the result of steady-state anisotropy measurements the CT region seems to have larger contribution to the actin activities of DAD-CT than the DAD domain.

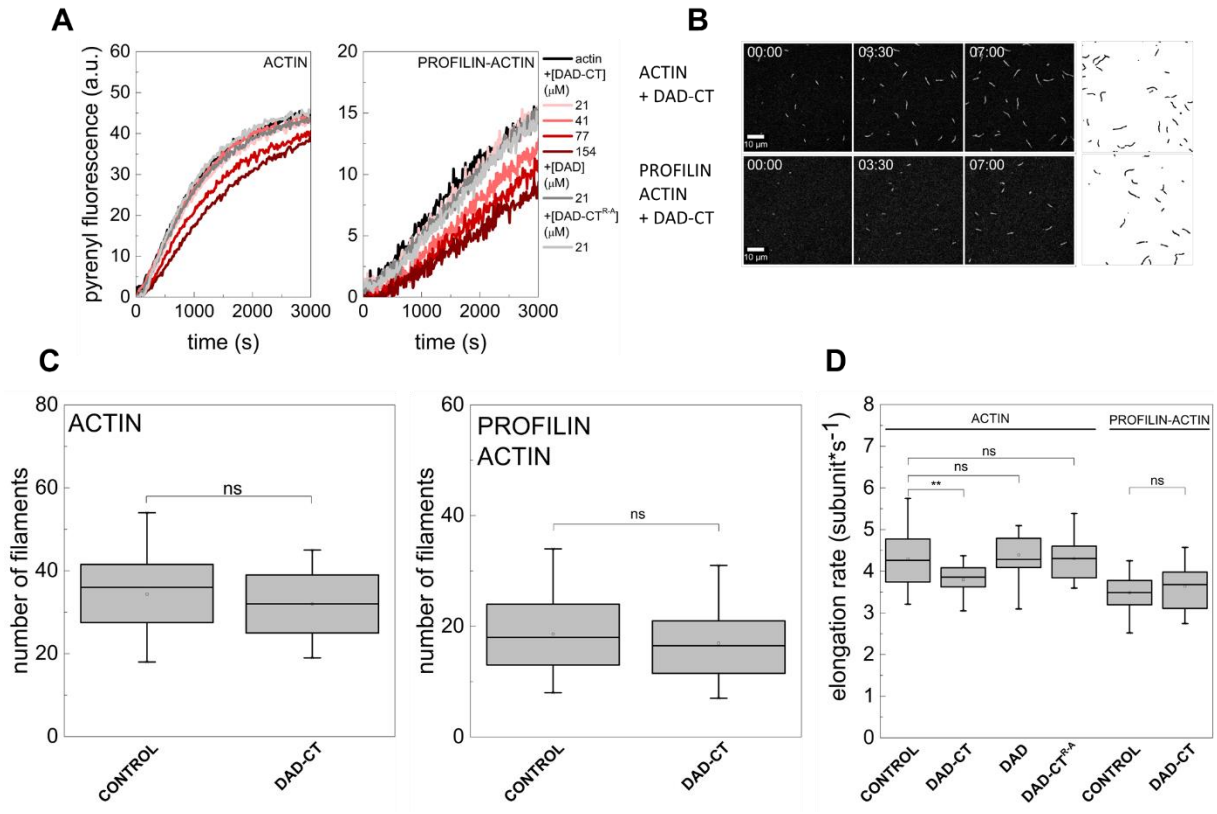

Figure 18. The influence of C-terminal constructs of dDAAM on actin dynamics.

(A) Representative polymerization kinetics of free G-actin and profilin:G-actin in the absence and presence of the C-terminal regions of dDAAM, as indicated. Final concentrations: [actin] = 2 μM (containing 5 % and 2 % of pyrenyl actin in the absence and presence of profilin, respectively), [profilin] = 6 μM. (B) TIRFM montages of actin assembly and representative skeletonized images showing the field of view of actin assembly in the absence and presence of DAD-CT, as indicated (for spontaneous actin assembly see *Figure 15*). Scale bar = 10 μm, time = min : s. Final concentrations: [actin] = 0.5 μM, [profilin] = 2 μM, [DAD-CT] = 42 μM. (C) The number of actin filaments nucleated spontaneously or in the presence of DAD-CT derived from skeletonized images. Final concentrations as in panel (B), n = 16 – 20. (D) The elongation rate of individual actin filaments polymerized from free G-actin and profilin:G-actin in the absence and presence of DAD-CT (42 μM), DAD (42 μM) or DAD-CT^{R-A} (42 μM). Final concentrations as in panel (B), n = 24 – 79.

5. 6. The nucleation promoting activity of dDAAM relies on a functional C-terminus

FH1-FH2 lacks the entire DAD-CT region, therefore it is not straightforward to investigate the individual contributions of DAD and CT to the activity of FH2 when comparing FH1-FH2 with cDAAM. To investigate the contribution of each C-terminal element – DAD and CT – to the functionality of FH2, two modified versions of cDAAM

were generated. In these constructs either the CT region was truncated (cDAAMΔCT) or the arginine amino acids were changed to alanine in the CT region (cDAAM^{R-A}) (*Figure 8*). The constructs behaved similarly both qualitatively and quantitatively in pyrenyl polymerization and TIRFM assays, supporting that the two modifications are equivalent (*Figure 19, 20*). Both cDAAMΔCT and cDAAM^{R-A} accelerate actin assembly, they are ~ 6fold more potent than FH1-FH2, but ~ 6fold less potent than the native cDAAM (*Figure 19, B*). TIRFM experiments showed that this intermediate polymerization promoting effect originates from the more potent nucleation ability of these constructs as compared to FH1-FH2, since they influenced filament elongation quantitatively similarly to FH1-FH2 and cDAAM (*Figure 20*). These results indicate that although DAD enhances the nucleation activity of FH1-FH2 but a functional CT is essential to reconstruct the proper functionality – in terms of actin nucleation – of dDAAM. We also observed that the separate contribution of the C-terminal regions to the nucleation promoting activity of FH1-FH2 was identical, which suggest non-cooperative, additive effects between DAD and CT.

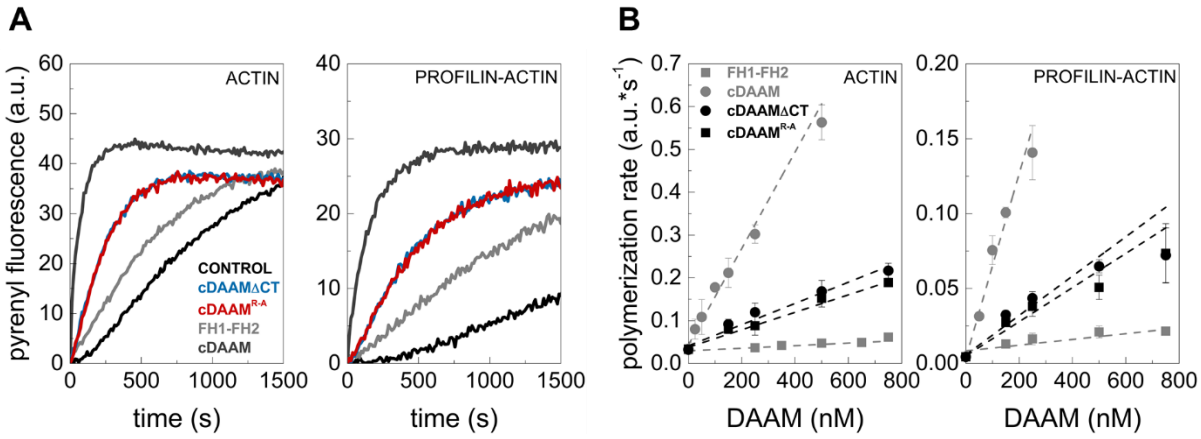

Figure 19. The effects of DAAM DAD and CT regions on actin assembly in the presence of the native FH2 domain, as revealed by fluorescence spectroscopy experiments.

(A) Representative pyrenyl traces of spontaneous and cDAAM^{R-A} or cDAAMΔCT catalyzed assembly of free G-actin and profilin:G-actin, as indicated. The data for FH1-FH2 and cDAAM from (*Figure 13, A*) are shown here as controls. Final concentrations: [actin] = 2 μM (containing 5 % and 2 % of pyrenyl actin in the absence and presence of profilin, respectively), [profilin] = 6 μM, [cDAAM^{R-A}] = 200 nM, [cDAAMΔCT] = 200 nM. (B) cDAAM^{R-A} or cDAAMΔCT concentration dependence of the relative polymerization rate of free G-actin and profilin:G-actin, as indicated. Error bars: standard deviations, n = 3 – 4. Data obtained for FH1-FH2 and cDAAM from (*Figure 13, B*) are shown.

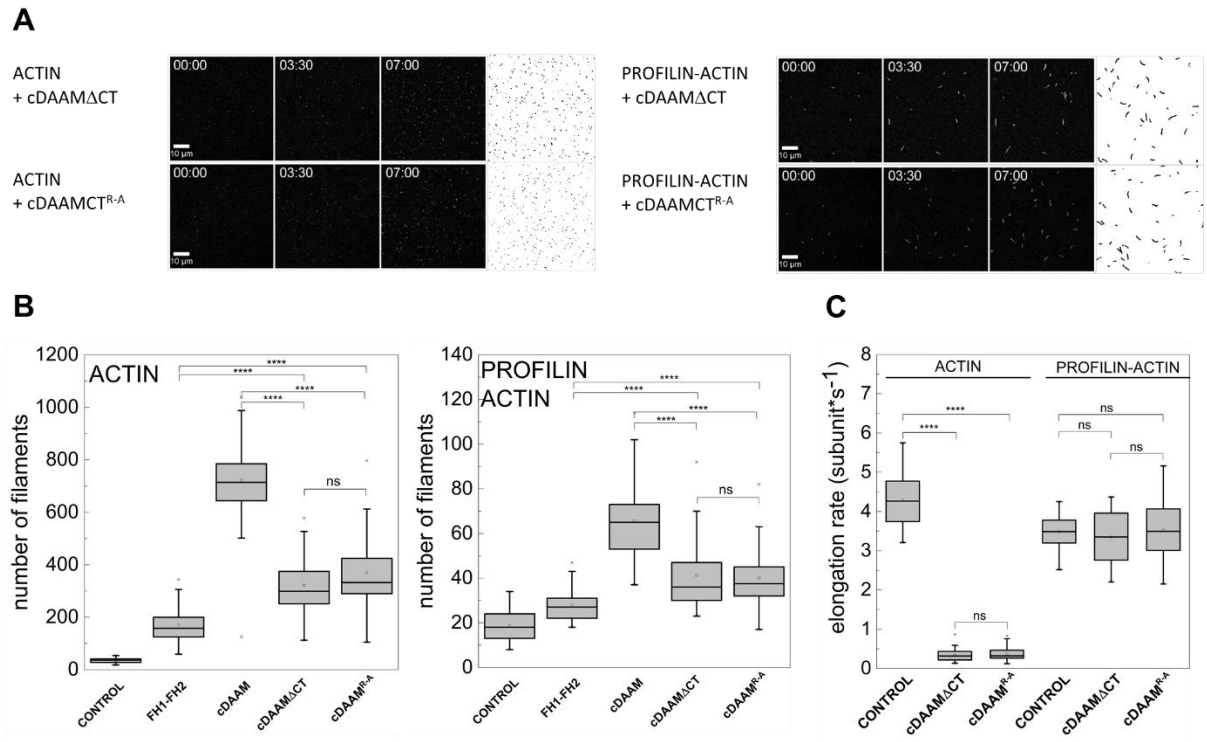

Figure 20. The effects of DAAM DAD and CT regions on actin assembly in the presence of the native FH2 domain, as revealed by TIRFM experiments.

(A) TIRFM montages of actin assembly and representative skeletonized images showing the field of view of actin assembly in the absence and presence of cDAAM^{R-A} or cDAAMΔCT, as indicated (for spontaneous actin assembly see (*Figure 15, A*)). Scale bar = 10 μm, time = min : s. Final concentrations: [actin] = 0.5 μM, [profilin] = 2 μM, [cDAAM^{R-A}] = 100 nM, [cDAAMΔCT] = 100 nM. (B) The number of actin filaments nucleated spontaneously or in the presence of cDAAM^{R-A} or cDAAMΔCT derived from skeletonized images. Final concentrations as in panel (A), n = 20 – 54. (C) The elongation rate of individual actin filaments polymerized from free G-actin and profilin:G-actin in the absence and presence of cDAAM^{R-A} or cDAAMΔCT. Final concentrations as in panel (A), n = 39 – 79.

5. 7. dDAAM DAD-CT cannot compensate for the loss of function mutation-induced defects in the core activities of the FH2 domain

The above observations indicate that although the isolated DAD-CT of dDAAM can interact with actin, it can influence efficiently the actin activities of the protein only in the presence of the native FH2. To further assess the role of the C-terminus of dDAAM in actin dynamics, we produced two mutant versions of the protein. The FH2 domain of formins possesses an isoleucine residue that is conserved from yeast to humans (*Figure 8, 21*). The residue is found in the αD helix of the knob region and was shown to be essential for FH2-mediated actin polymerization (45-47,91,92). The

corresponding residue in *Drosophila* DAAM is Ile^{732}. Based on this, two mutated constructs were generated in which the Ile^{732} residue was changed to alanine; one lacks the C-terminal regions (FH1-FH2^{I732A}), while the other possesses the DAD-CT (cDAAM^{I732A}) (*Figure 8*).

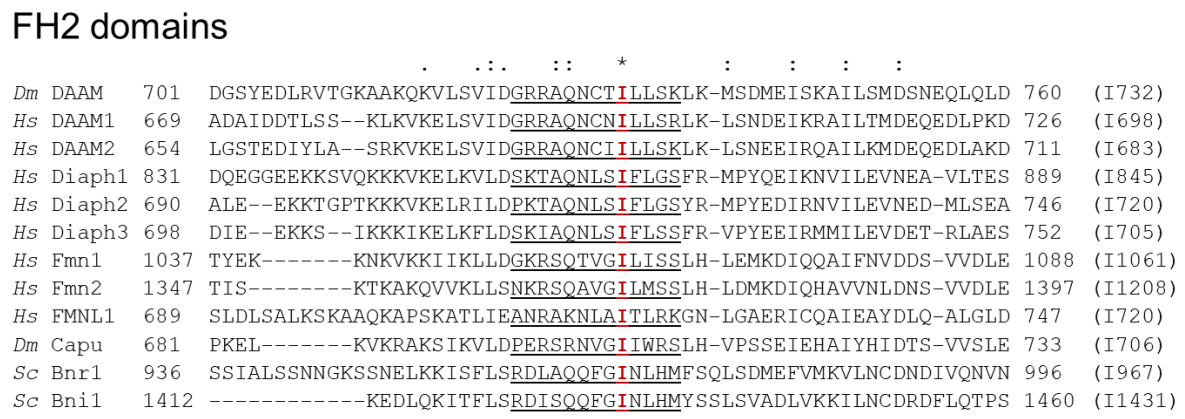

Figure 21. Sequence alignment of FH2 domains from different formins.

The conserved isoleucine in the FH2 domain is highlighted by red, its position in each formin is given in parenthesis at the end of the sequences. The αD helix of the knob region is underlined. UniProt accession numbers are as follows: *Dm* DAAM Q8IRY0, *Hs* DAAM1 Q9Y4D1, *Hs* DAAM2 Q86T65, *Hs* Diaph1 O60610, *Hs* Diaph2 O60879, *Hs* Diaph3 Q9NSV4, *Hs* Fmn1 Q68DA7, *Hs* Fmn2 Q9NZ56, *Hs* FMNL1 O95466, *Dm* Capu Q24120, *Sc* Bnr1 P40450, *Sc* Bni1 P41832. *Dm*: *Drosophila melanogaster*, *Hs*: *Homo sapiens*, *Sc*: *Saccharomyces cerevisiae*.

First, the G-actin binding ability of these mutated constructs were investigated in steady-state anisotropy measurements. The results revealed that cDAAM^{I732A} is able to bind both G-actin and profilin:G-actin with approximately the same affinity in the tens of nM range (*Figure 22, Table 6*). Nevertheless, the FH1-FH2^{I732A} construct binds monomeric actin with significantly lower affinity in the μM range (*Figure 22, Table 6*). These data suggest that mutation of the conserved Ile^{732} severely compromises actin binding by FH2. However, we observed that cDAAM^{I732A} can bind actin with similar affinity as cDAAM, which indicates that the presence of DAD-CT can compensate for the defects in monomer binding induced by the Ile^{732A} mutation (*Figure 22*).

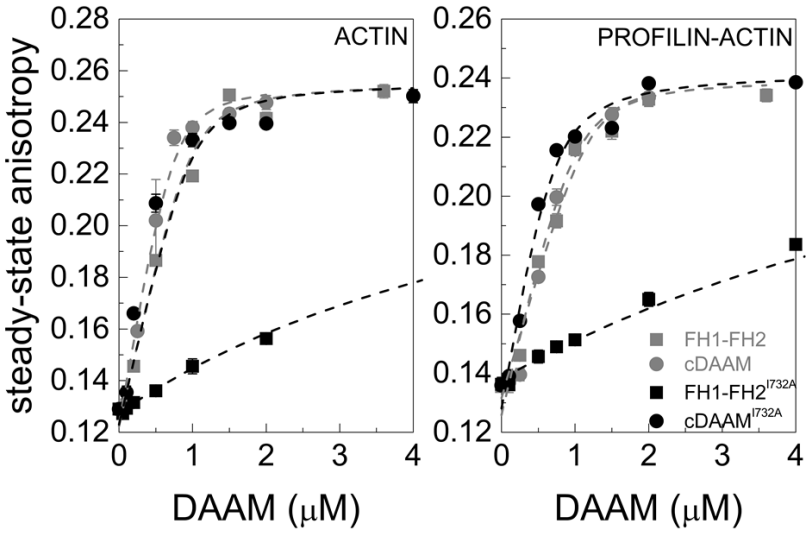

Figure 22. Interaction of FH1-FH2^{I732A} and cDAAM^{I732A} with actin, as revealed by steady-state anisotropy.

Steady-state anisotropy of Alexa488NHS-G-actin in the absence and presence of profilin as the function of dDAAM concentration, as indicated. The data for FH1-FH2 and cDAAM from (*Figure 14, A*) are shown here as controls. Dashed lines in the corresponding colors show the fits to the data according to *Eq. 2*. Dissociation equilibrium constants are summarized in *Table 6*. Error bars: standard deviations, n = 2 – 3. Final concentrations: [actin] = 0.2 μM, [LatA] = 4 μM, [profilin] = 0.8 μM, [NaCl] = 5 mM.

construct	$K_d \pm SD$ (μM)	
	G-actin^{FL}	profilin:G-actin^{FL}
FH1-FH2^{I732A}	6.78 ± 0.96	4.41 ± 0.76
cDAAM^{I732A}	0.064 ± 0.02	0.093 ± 0.04

Table 6. Dissociation equilibrium constants (K_d) of the dDAAM:actin interactions. FL: fluorescently labelled protein.

To further test the effect of the mutation in FH2 on actin assembly pyrenyl polymerization assays were performed. These investigations revealed that FH1-FH2^{I732A} inhibits actin polymerization from free G-actin, while the assembly of profilin:G-actin is not affected significantly in the concentration range that we could test in the experiments (*Figure 23*). cDAAM^{I732A} inhibited actin assembly from both free G-actin and profilin:G-actin more efficiently than FH1-FH2 ^{I732A} (*Figure 23*). First, it has to be noted that, importantly, the inhibition of polymerization is the opposite that we observed for the native FH2-containing constructs (*Figure 13*). This indicates that the

I732A mutation impairs not only the monomer binding ability, but also the proper actin assembly activities of dDAAM FH2, which is consistent with previous data (47).

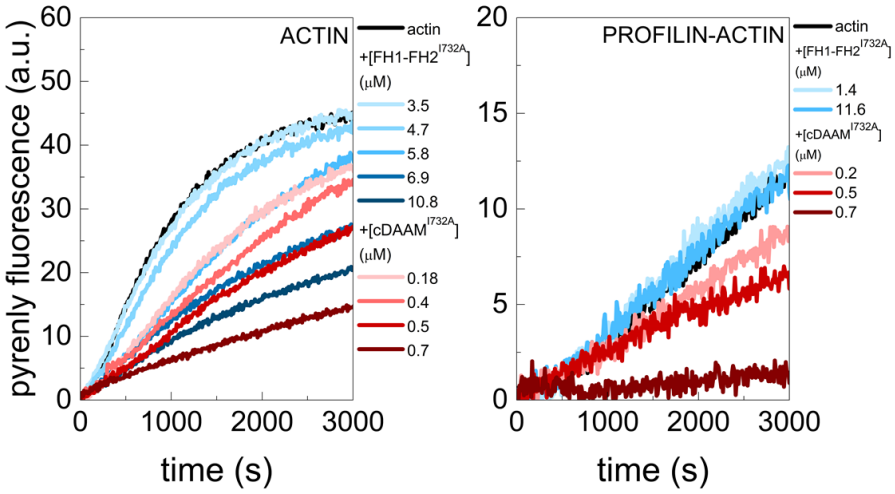

Figure 23. Effects of FH1-FH2^{I732A} and cDAAM^{I732A} on actin assembly as revealed by fluorescence spectroscopy experiments.

Representative polymerization kinetics of free G-actin and profilin:G-actin in the absence and presence of different regions of dDAAM, as indicated. Final concentrations: [actin] = 2 μM (containing 5 % and 2 % of pyrenyl actin in the absence and presence of profilin, respectively), [profilin] = 6 μM.

To investigate the mechanisms underlying the polymerization inhibition by FH1-FH2 ^{I732A} and cDAAM^{I732A} we analyzed their effects on actin dynamics in TIRFM experiments (*Figure 24*). In contrast to the wild type FH2 domain-containing constructs, filament number was not changed significantly in the presence of the mutant constructs (*Figure 24, A, B*). This indicates that despite of being able to interact with actin, as revealed by anisotropy measurements (*Figure 22*), the I732A mutation abolishes the nucleation ability of dDAAM. Our anisotropy data also suggest that the presence of the DAD-CT region is able to counteract the actin binding defects of the FH2 domain induced by I732A (*Figure 22*), however it cannot restore the proper functionality of the mutated FH2 domain in actin nucleation (*Figure 24, A, B*). The analysis of the effects on filament elongation revealed that FH1-FH2^{I732A} only moderately affects filament growth from free G-actin in the concentration range, in which the wild type construct almost completely inhibits elongation ($v_{FH1\text{-}FH2}{}^{I732A}$ = 4.09 ± 0.42 subunit×s^{-1} (p = 0.03), (*Figure 24, C*)). Even higher amount (20 μM FH1-FH2^{I732A}) resulted only in ~ 55 % inhibition (*Figure 24, C*). In agreement with the pyrenyl polymerization experiments, FH1-FH2^{I732A} does not affect significantly filament growth from profilin:G-actin at low concentrations ($v_{FH1\text{-}FH2}{}^{I732A}$ = 3.53 ± 0.45 subunit×s^{-1} (p = 0.30), (*Figure 24, C*)), while

it moderately inhibits elongation when it is added at higher amounts ($v_{FH1\text{-}FH2}^{I732A}$ = 2.09 ± 0.14 subunit×s^{-1} (p < 0.0001), (*Figure 24, C*)). cDAAM^{I732A} moderately slows filament elongation when it is added at the same amount as cDAAM (v_{cDAAM}^{I732A} = 3.97 ± 0.32 subunit×s^{-1} (p = 0.00014), (*Figure 24, C*)). At relatively high concentrations (2 μM) it markedly slows down the elongation from free G-actin, similarly to the wild-type protein (v_{cDAAM}^{I732A} = 0.15 ± 0.02 subunit×s^{-1} (p < 0.0001), (*Figure 24, C*)). However, unlike cDAAM that maintains elongation in the presence of profilin, cDAAM^{I732A} functions oppositely, it hinders profilin:G-actin association to barbed ends in a concentration dependent manner (*Figure 24, C*).

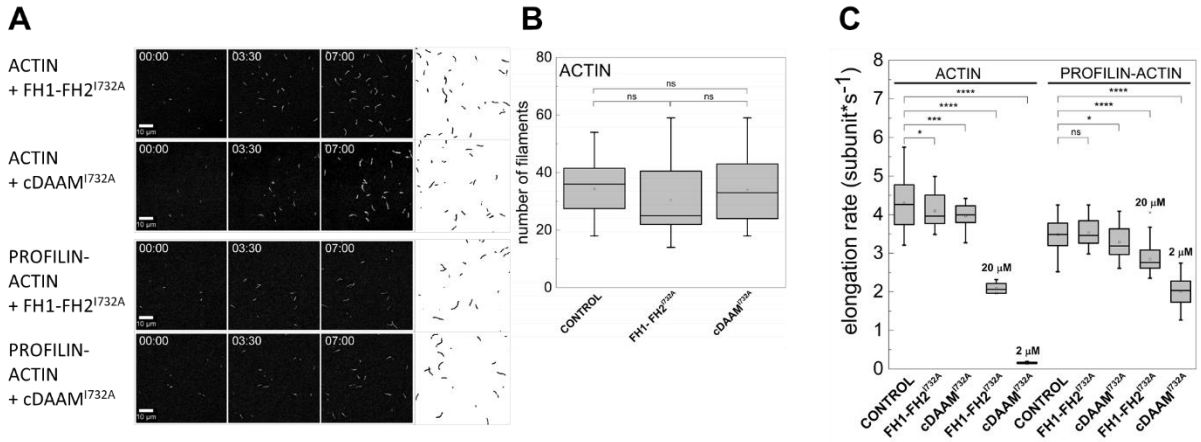

Figure 24: Effects of FH1-FH2^{I732A} and cDAAM^{I732A} on actin assembly, as revealed by TIRFM experiments.

(A) TIRFM montages of actin assembly and representative skeletonized images showing the field of view of actin assembly in the absence and presence of FH1-FH2^{I732A} and cDAAM^{I732A}, as indicated (for spontaneous actin assembly see (*Figure 15, A*). Scale bar = 10 μm, time = min : s. Final concentrations: [actin] = 0.5 μM, [profilin] = 2 μM, [FH1-FH2^{I732A}] = 100 nM, [cDAAM^{I732A}] = 100 nM. (B) The number of actin filaments nucleated spontaneously or in the presence of FH1-FH2^{I732A} and cDAAM^{I732A} derived from skeletonized images. Final concentrations as in panel (A), n = 20 – 50. (C) The elongation rate of individual actin filaments polymerized from free G-actin and profilin:G-actin in the absence and presence of FH1-FH2^{I732A} and cDAAM^{I732A}. Final concentrations as in panel (A). 20 μM and 2 μM indicate the data obtained in the presence of higher concentrations of FH1-FH2^{I732A} and cDAAM^{I732A}, respectively, n = 15 – 79.

In conclusion, our results revealed that, consistently with the importance of the conserved isoleucine residue in actin interaction (120), the mutation impairs both the nucleation ability of the FH2 domain and its interaction with the barbed end of the filaments. The combination of these two effects results in a decreased polymerization rate, detected in the pyrenyl polymerization assays (*Figure 23*). At high concentration,

dDAAM FH2^{I732A} can maintain some interactions with filament ends similarly to other formins (e.g. Dia1 (91)). Even if such high concentration is not physiological, this approach allowed us to address the effects of DAD-CT on the interaction of FH2 with barbed ends. Our data indicates that besides the key Ile^{732} residue, other residues/binding sites in the FH2 domain also contribute to barbed end interactions of dDAAM, albeit with much lower affinities. Comparative structural analysis of dDAAM FH2 with other formins reveals that residues in the knob region near the Ile^{732}, as well as the lasso/post interface can contribute to actin binding (47). Based on our data, the coordination between these different binding sites is crucial for functional barbed end interaction. Importantly, our observations – that the magnitude of the effect of the FH2^{I732A} mutant on filament elongation is more pronounced in the presence of DAD-CT than in the absence of it – suggests that the C-terminal regions are important for filament end interaction.

5. 8. dDAAM antagonizes with capping proteins and DAD-CT contributes to this activity

Classic capping proteins (CP, like CapG) bind filament ends with ~ 10 pM affinity. The high-affinity interaction is characterized by low dissociation rate constant (k_{-} ~ 10^{-4} s^{-1}), therefore they completely and permanently block barbed end dynamics and contribute to limited actin filament elongation both *in vitro* and *in vivo* (25,111,121,122). Some formins – including FRL, Dia1, INF2 and FMNL2 – are known to be able to compete for barbed ends with classic CPs, which was thought to be based on the mutually exclusive interactions of these proteins with filament ends (50,54,111,122,123). Recent microfluidics-based TIRFM studies combined with single-molecule visualization gave novel mechanistic insight into the antagonistic regulation of barbed end dynamics by CPs and formins proposing the ‘decision complex’ mechanism (111,122). According to this mechanism, both proteins can bind simultaneously to filament barbed ends forming a ternary complex, irrespective of the order of their binding. In the ternary complex the affinities of both CPs and formins are mutually reduced, which can be explained by steric clashes between the two proteins, resulting to fast displacement of one protein by the other.

To explore the ability of dDAAM to antagonize with CPs we performed pyrenyl polymerization assays (*Figure 25*). In these assays, actin assembly was initiated and

monitored in the presence of different dDAAM constructs and subsequently (after ~ 120 s) CP was added to the samples. The analysis of the data showed that both cDAAM and FH1-FH2 can compete with CPs, however, quantitative analysis revealed that cDAAM is more efficient in maintaining filament elongation in the presence of CPs than FH1-FH2 (*Table 7*).

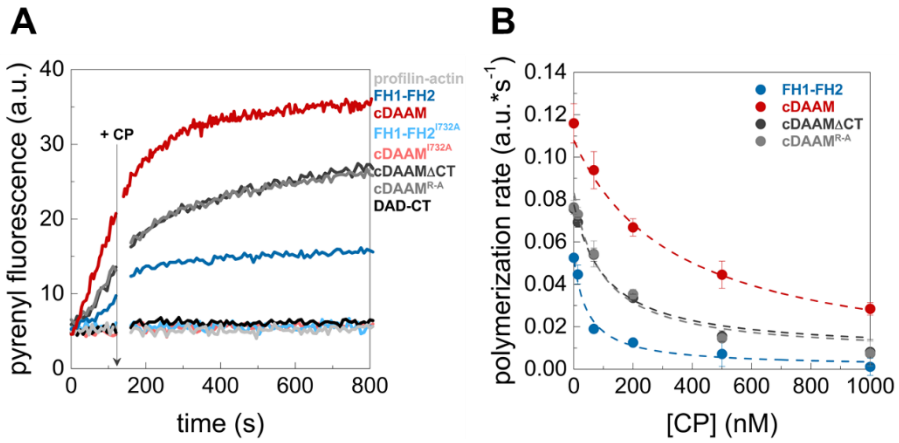

Figure 25. Antagonistic regulation of filament barbed end dynamics by dDAAM and CP.

(A) Polymerization of profilin:G-actin initiated in the absence and presence of dDAAM constructs, as indicated. The addition of CP after 120 s is indicated by arrow. Final concentrations: [actin] = 2 μM, [profilin] = 6 μM, [CP] = 68 nM, [dDAAM] = 200 nM. (B) Polymerization rates before ([CP] = 0 nM) and after addition of CP at different concentrations derived from pyrenyl traces. Dashed lines in the corresponding color show the fit of the data using *Eq. 6.*, IC_{50} values are summarized in *Table 7*. Error bars: standard deviations, n = 2 – 4.

construct	IC_{50} ± SD (nM)
FH1-FH2	47.7 ± 16.97
cDAAM	345.9 ± 27.60
cDAAMΔCT	108.6 ± 19.35
$cDAAM^{R-A}$	93.7 ± 19.06
DAD-CT	ND
$FH1\text{-}FH2^{I732A}$	ND
$cDAAM^{I732A}$	ND

Table 7. IC_{50} values for antagonistic effects of CP and DAAM constructs. ND: not determined.

Our results suggest that – besides its ability to promote FH1-FH2-mediated nucleation – DAD-CT can also contribute to proper filament end interaction of dDAAM FH1-FH2, as already indicated in the above experiments: $cDAAM^{I732A}$ affected filament

end dynamics more efficiently than FH1-FH2^{I732A} (*Figures 23, 24*). To further elaborate on this issue, the ability of C-terminally truncated/mutated cDAAM constructs (cDAAMΔCT and cDAAMCT^{R-A}) to compete with CPs was investigated. We found that truncations/mutations in the CT region partially reduces the efficiency of cDAAM to uncap CPs bound barbed ends, yet these constructs are still more effective than FH1-FH2 (*Figure 25, Table 7*). Neither cDAAM^{I732A} nor FH1-FH2^{I732A} can compete with CPs, when they are added at a same amount as the wild-type construct (*Figure 25*, A). This observation is consistent with well-known role of the conserved isoleucine residue in filament end interaction. Also, isolated DAD-CT fails to antagonize with CPs in the absence of FH2 (*Figure 25*, A). These results suggest that the wild-type FH2 is necessary for the antagonistic action between dDAAM and CPs. However, this activity is tuned by the DAD-CT region, which further supports that – besides monomer binding – the C-terminus of dDAAM is important to strengthen the filament end interaction of FH2. In conclusion, our data reveal a novel role of the C-terminal region as the part of the anti-capping module of formins.

5. 9. dDAAM binds to the side of actin filaments and possesses F-actin bundling activity

Certain formins are able to bind to the side of actin filaments and upon these interactions they can organize individual filaments into bundles (63,124,125). Our previous studies revealed that the FH2 and FH1-FH2 of dDAAM possess these activities (56). Since the C-terminus of dDAAM is an actin-binding region, we tested if it is able to bind actin filaments in high-speed sedimentation experiments (*Figure 26, A, B*). We found that DAD-CT binds to the sides of actin filaments with a dissociation equilibrium constant of 38.9 ± 3.2 μM. This suggests that DAD-CT interacts with actin filaments, however, with lower efficiency as compared to the FH1-FH2 domain (K_d = 2.1 ± 0.5 μM (56)). Truncation in the CT significantly reduces the filament binding ability of the C-terminus (K_d(DAD) > 100 μM), while the R-A mutation diminishes actin filament interaction (*Figure 26, A, B*).

To test whether the actin filament side-binding ability of the C-terminal regions of dDAAM is coupled to F-actin bundling activity low-speed sedimentation experiments were performed (*Figure 26, C*). SDS-PAGE analysis of the supernatants revealed that both FH1-FH2 and cDAAM are able to bundle actin filaments with approximately the

same efficiency. As expected, the I732A mutation of FH2 has no effect on this activity, since its mostly important for filament end interactions and not for side-binding. The isolated DAD-CT bundled actin filaments, however with extremely low efficiency, consistently with its weak binding to actin filaments. Truncation/mutation of the C-terminus of dDAAM (DAD, DAD-CT^{R-A}) abolishes the bundling ability of this region. This in agreement with anisotropy data (*Figure 17*) and further supports that the CT region is dominant in the DAD-CT:actin interaction.

These observations show that, besides interacting with actin monomers isolated DAD-CT can decorate the side of actin filaments, and as a functional consequence it arranges actin filaments into higher-order bundled structures. Our data also suggest that the main side-binding/bundling element of DAAM is the FH2 domain, while the DAD-CT region has minor contribution to this activity.

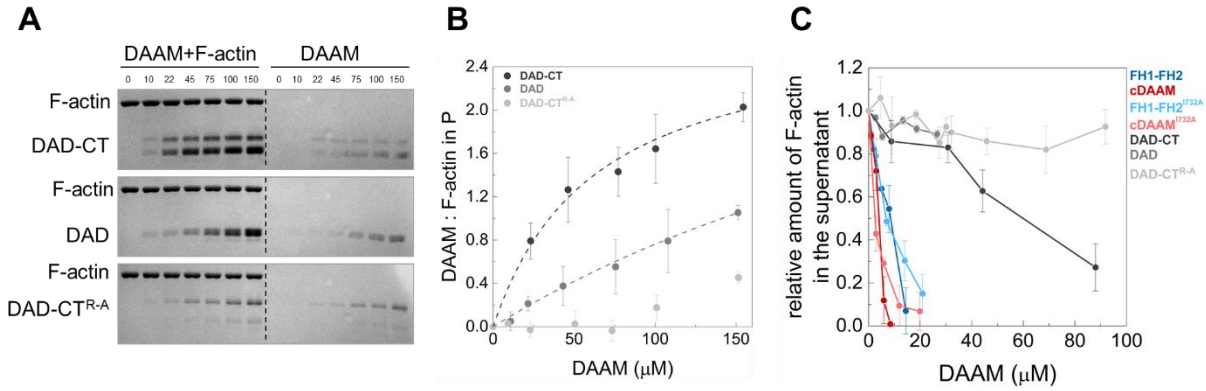

Figure 26. Interaction of dDAAM with actin filaments as revealed by high-, and low-speed sedimentation assays.

(A) Coomassie-stained SDS-PAGE gels from co-sedimentation experiments to study the interactions of the C-terminal regions of dDAAM with F-actin. The amount of each dDAAM construct in the pellet is shown in the presence and absence of F-actin. Numbers indicate the dDAAM concentration in each sample. [F-actin] = 2.5 μM. (B). The dDAAM:F-actin ratio in the pellet derived from the analysis of SDS-PAGE gels, shown in panel (A). Dashed lines correspond to the fit of the data according to *Eq. 8*, the fit gave K_d values of K_d(DAD-CT) = 38.9 ± 3.2 μM and K_d(DAD) > 100 μM. Error bars: standard deviations, n = 2 – 4. (C) Bundling activity of the different regions of dDAAM. The relative amount of actin filaments in the supernatant as the function of dDAAM concentration, determined from the quantification of SDS-PAGE analysis of the samples. Final concentrations: [actin] = 1 μM. Error bars: standard deviations, n = 2 – 3.

5. 10. Sequence characteristics and possible binding modes of DAD-CT on actin

We showed that the DAD-CT region of dDAAM interacts with actin *in vitro*, however, the binding of DAD is very weak, which is markedly enhanced by the CT

region (*Figure 17, 26*). While the binding mode of the FH2 domains of formins on actin is well established, the exact structural features of the interaction of their C-terminal regions with actin is not known. Sequence analysis reveals that the C-terminal regions of formins, including Dia1, INF, FMNL3 possess sequence elements characteristic to the N-terminal region of the short actin-binding Wiskott-Aldrich syndrome homology (WH2) domain (*Figure 16*). WH2 domains are largely intrinsically disordered protein regions (IDR), defined by a central canonical LKKT/V motif that is flanked by variable N-, and C-terminus (21,126-128). The structural features of the binding of WH2 domains from different proteins to actin are well known from high-resolution X-ray structures (*Figure 27, A*). The N-terminal part of the WH2 folds into an amphipathic α-helix that interacts with the hydrophobic cleft of actin, the interaction is mediated by a conserved hydrophobic amino acid triplet LLxxI of WH2 (*Figure 16*). The binding is further strengthened by the downstream LKKT/V motif (*Figure 16*). While their C-terminus extends along the negative surface patch of the actin molecule towards the pointed face, through interactions mainly controlled by electrostatic forces. Apparently, our bioinformatics analysis revealed that the DAD-CT of DAAM contains the conserved LLxxI motif, however the consensus LKKT/V motif that fundamentally strengthens actin interactions of WH2 domains is absent, similarly to Dia1 that binds relatively weakly to actin (*Figure 16*) (91). On the other hand, the CT of dDAAM is a relatively long (~ 40 amino acid) extension and bioinformatics analysis predicts to be intrinsically disordered (*Figure 27, B*), a structural feature that is shared by WH2 domains. On the basis of the sequence and predicted structural similarities we hypothesized that dDAAM DAD-CT adopts a WH2-like binding mode on actin.

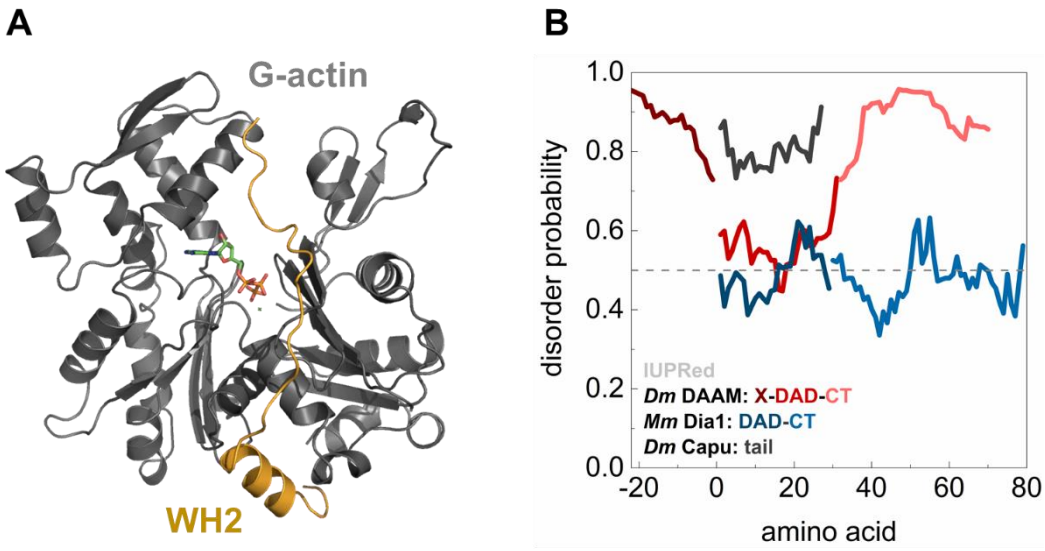

Figure 27. Structural features of WH2 domains and the C-terminal regions of formins.
(A) Ribbon representation of the G-actin:WH2 domain complex. The known X-ray structure of WASP-interacting protein (WIP) was used (PBD2A41 (128)). The figure was made by PyMol. (B) Bioinformatics analysis of the C-terminal regions of different formins. The analysis was made by IUPRed.

To probe this hypothesis, we performed competition experiments based on steady-state anisotropy (*Figure 28*). In our previous measurements we found that profilin does not affect significantly the binding of dDAAM DAD-CT to actin and its actin activities, either (*Figure 17, 18*). The binding site of profilin on actin monomers is found to be on the hydrophobic cleft between subdomain 1 and 3 at the barbed face (*Figure 28, C*) (9). In the anisotropy experiments presented above we used fluorescently labeled actin in complex with profilin. To further investigate the interaction of DAD-CT with monomeric actin in the presence of profilin we repeated the measurements by using Alexa Fluor® C_5 568 maleimide-labeled profilin (Alexa568C-profilin) in complex with actin (*Figure 28, A*). This strategy allows to obtain information about the rotational diffusion of profilin in the presence of both G-actin and dDAAM. A concentration-dependent increase in the anisotropy of Alexa568C-profilin was observed upon titration with DAD-CT. The value of the dissociation equilibrium constant derived from this measurement was similar to that obtained in experiments using unlabeled profilin and labeled actin (K_d = 4.71 ± 0.53 μM and *Figure 17, Table 5*). Considering competitive binding one would have expected the dissociation of profilin from actin by DAD-CT, which would be expected to cause a decrease in the anisotropy of the fluorescently labeled profilin. The opposite tendency that we detected suggests that profilin and

DAD-CT can bind simultaneously to monomeric actin and form a ternary complex. This result predicts that the binding site of the two proteins on actin largely differ.

In subsequent experiments we studied the actin binding ability of DAD-CT in the presence of the WH2 domains of Sarcomere Length Short (SALS) protein (*Figure 28, B, D*). These measurements were performed by Réka Pintér, a PhD student in our group. As we reported previously, the binding strength of SALS-WH2 is tighter than that of DAD-CT (K_d(SALS-WH2) = 0.34 ± 0.2 μM (105) and K_d(DAD-CT) = 3.87 ± 0.19 μM, (*Figure 17, Table 5*)). Their complexes with fluorescent actin monomers (Alexa488NHS) are characterized by different anisotropy values ($r_{DAD\text{-}CT:G\text{-}actin}$ ~ 0.20, $r_{SALS\text{-}WH2:G\text{-}actin}$ ~ 0.15), most likely due to their different sizes ($MW_{DAD\text{-}CT}$ = 34.8 kDa, $MW_{SALS\text{-}WH2}$ = 21.1 kDa). Upon titrating the DAD-CT:G-actin complex with SALS-WH2, we observed that the values of anisotropy decrease from r ~ 0.20 in a SALS-WH2 concentration dependent manner (*Figure 28, B*). In the presence of high amount of SALS-WH2 the measured value was characteristic to the SALS-WH2:G-actin complex (r ~ 0.15, *Figure 28, B*). These results suggest that the binding of SALS-WH2 interferes with that of DAD-CT, indicating that the main binding sites of these proteins overlap.

Altogether our data support that the weak actin binding of dDAAM DAD may be due to the interaction of the WH2-like amino acid triplet LLxxI with the hydrophobic cleft of actin, but the complex is fundamentally strengthened by the CT region that may mediate the connections between the negative stretch of G-actin towards the pointed end in a similar manner as the C-terminal extension of WH2 domains.

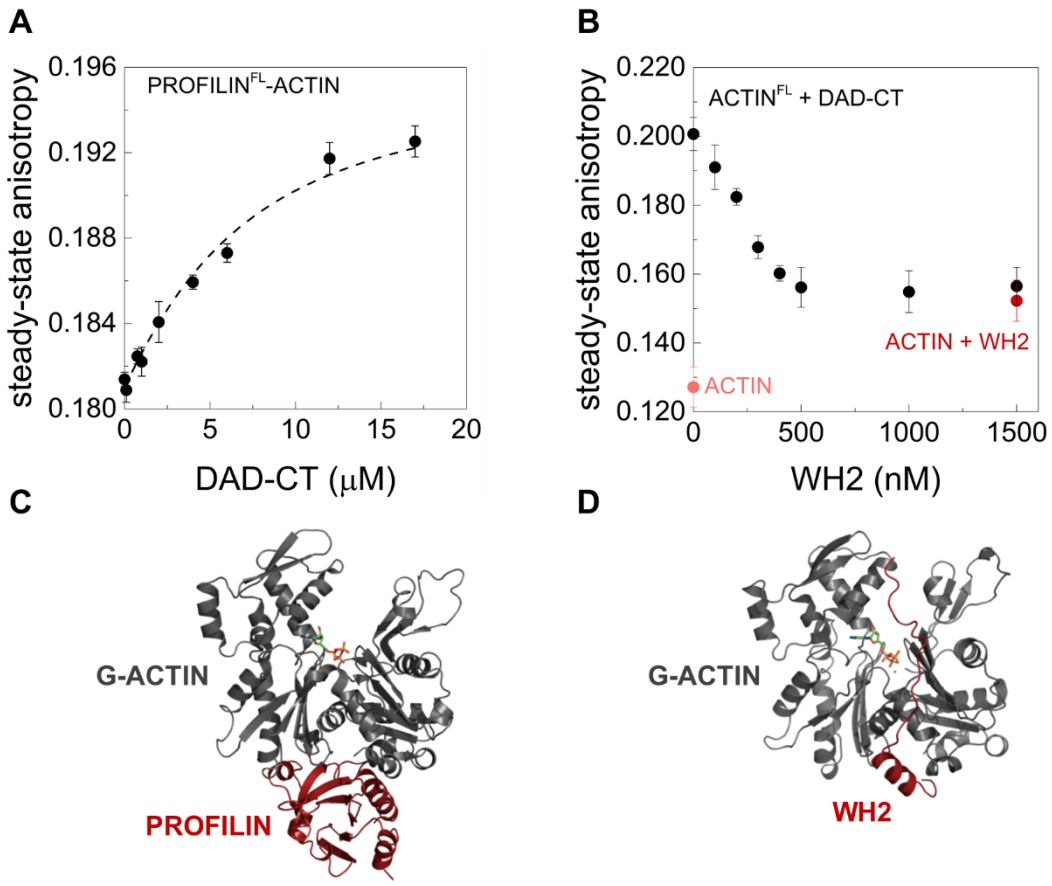

Figure 28. DAAM DAD-CT does not compete with profilin for G-actin binding, in contrast, SALS-WH2 and DAD-CT bind G-actin in a competitive fashion.

(A) Steady-state anisotropy of Alexa568C-profilin in the presence of G-actin as the function of DAD-CT concentration, as indicated. Dashed line in the corresponding color shows the fit to the data according to *Eq. 2*. Dissociation equilibrium constant was found to be K_d = 4.71 ± 0.53 μM. Error bars: standard deviations, n = 2 – 3. Final concentrations: [actin] = 4 μM, [LatA] = 8 μM, [profilin] = 2 μM, [NaCl] = 5 mM. FL: fluorescently labelled protein. (B) Steady-state anisotropy of Alexa488NHS labelled G-actin in complex with DAD-CT as a function of SALS-WH2 concentration. As controls, the steady-state anisotropy of G-actin in the absence of any binding proteins and G-actin saturated with SALS-WH2 (1.5 μM) are shown. Final concentrations: [actin] = 0.2 μM, [LatA] = 4 μM, [DAD-CT] = 20 μM, [NaCl] = 5 mM. FL: fluorescently labelled protein. (C) Ribbon representation of the G-actin:profilin complex (PDB 1HLU). (D) Ribbon representation of the G-actin:WH2 domain complex (PDB 2A41). Panel (C) and (D) were made by PyMol.

5. 11. dDAAM interacts with microtubules and organizes these polymers into bundled/cross-linked networks

Formins have been shown to be able to interact not only with actin but with microtubules, as well. They participate in MT stabilization and in their organization in diverse cellular processes (94). *In vivo* results demonstrated that the main microtubule-

interacting partner is the FH2 domain, but the C-terminus has also been shown to be able to bind to microtubules (40,96-99). The investigations of our collaborator in *Drosophila* primary neurons revealed that dDAAM co-localizes not only to actin-based neuronal structures (~ 47 % of the protein), but a significant fraction of the protein (~ 37 %) also accumulates along microtubules in axonal growth cones and it regulates both the morphology and dynamics of the microtubule cytoskeleton (129). Subsequent *in vitro* investigations revealed that the recombinantly produced FH1-FH2 and DAD-CT regions of dDAAM bind along the sides of taxol-stabilized microtubules and prevent them from cold-induced depolymerization (129).

We performed additional *in vitro* experiments to test the functional consequences of dDAAM:microtubule interaction (*Figure 29-31*). In low-speed sedimentation experiments we found that besides microtubule-side binding cDAAM is able to induce the formation of bundled/cross-linked microtubule arrays (*Figure 29*). Interestingly, FH1-FH2 lacking the C-terminal regions does not possess this activity (*Figure 29*), albeit it was able form actin filament bundles, as revealed by control experiments (*Figure 29, B*). Isolated DAD-CT also fails to bundle/crosslink microtubules in the absence of FH1-FH2 (*Figure 29, B*). These observations indicate that, despite their microtubule side-binding ability, isolated FH1-FH2 and DAD-CT regions alone are not sufficient to bundle/crosslink these polymers. The efficient bundling/crosslinking requires the simultaneous binding of both of these regions of dDAAM to microtubules, and our data suggest that this activity of dDAAM relies on cooperative interactions. Furthermore, our results indicate that the mechanism of actin filament and microtubule bundling/crosslinking by formins may differ.

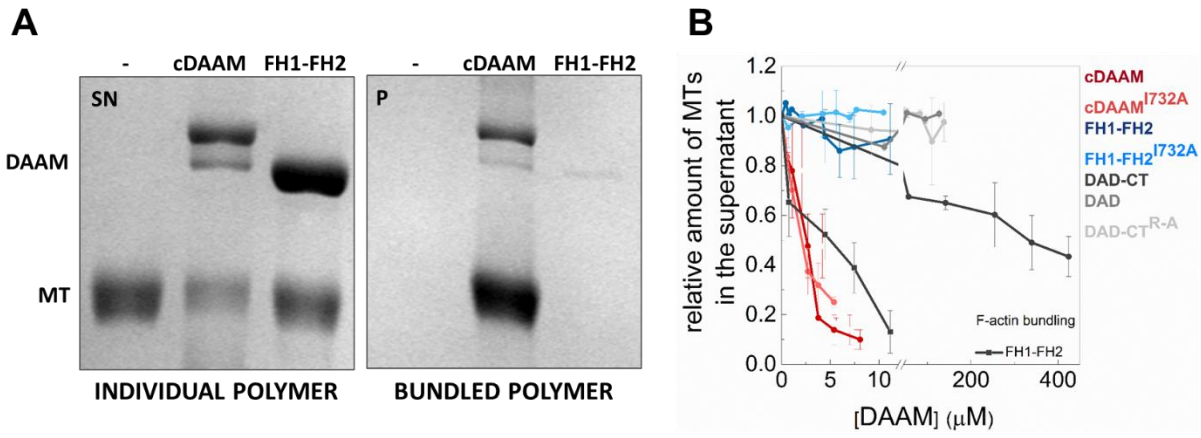

Figure 29. Bundling/cross-linking of microtubules by dDAAM as revealed by low-speed sedimentation experiments.

(A) Representative Coomassie-stained SDS-PAGE gels from low-speed centrifugation experiments showing the amount of MTs in in the supernatants (SN) and the pellets (P), in the presence of cDAAM, FH1-FH2 and DAD-CT as indicated. (B) The relative amount of microtubules in the supernatant (SN) as the function of dDAAM concentration, determined from the quantification of SDS-PAGE analysis of the samples. Final concentrations: [MT] = 1 μM. Error bars: standard deviations, n = 2 – 3.

5. 12. dDAAM simultaneously interacts with actin filaments and microtubules and co-aligns these polymers

As introduced in the *2.2 section*, recent evidences identify the members of the formin protein family as functional coordinators of actin-microtubule dynamics in diverse cellular processes. Regarding the neuronal cytoskeleton, our collaborator's work revealed that, besides associating to either the actin or the microtubule cytoskeleton, a significant portion (~ 22 %) of the dDAAM protein localizes to places where to two cytoskeletal polymers overlap in *Drosophila* primary neurons (129). This raises the intriguing possibility that dDAAM has the ability to physically interact with the two polymers simultaneously. To test this possibility we developed a low-speed sedimentation protocol that offers conditions, which allow to separate the F-actin:MTs complexes from other polymer species (e.g. individual polymers or bundled/cross-linked polymers). To achieve such conditions the centrifugation is performed through a 30 % sucrose gradient at relatively low speed (4000 g). Control experiments showed that under these conditions individual or bundled/cross-linked actin filaments (e.g. by FH1-FH2 or cDAAM) remain in the supernatant (*Figure 30, A*), while larger protein complexes (e.g. bundled/cross-linked microtubules by cDAAM) can be selectively sedimented and appear in the pellet (*Figure 30, B*). Intrinsic to this strategy, actin filaments can sediment and appear in the pellet only if they are physically linked to microtubules. Our results revealed that a significant fraction of actin filaments appeared in the pellet with microtubules in the presence of cDAAM, implying a simultaneous interaction between cDAAM and the two polymers (*Figure 30, C*). In contrast, actin filaments do not sediment in the presence of microtubules and FH1-FH2, DAD-CT, DAD or DAD-CT^{R-A} (*Figure 30, C, D*).

These observations suggest that both the FH2 and CT regions are needed for the physical co-alignment of actin filaments and microtubules, however neither is sufficient alone, indicating a cooperative nature of this activity.

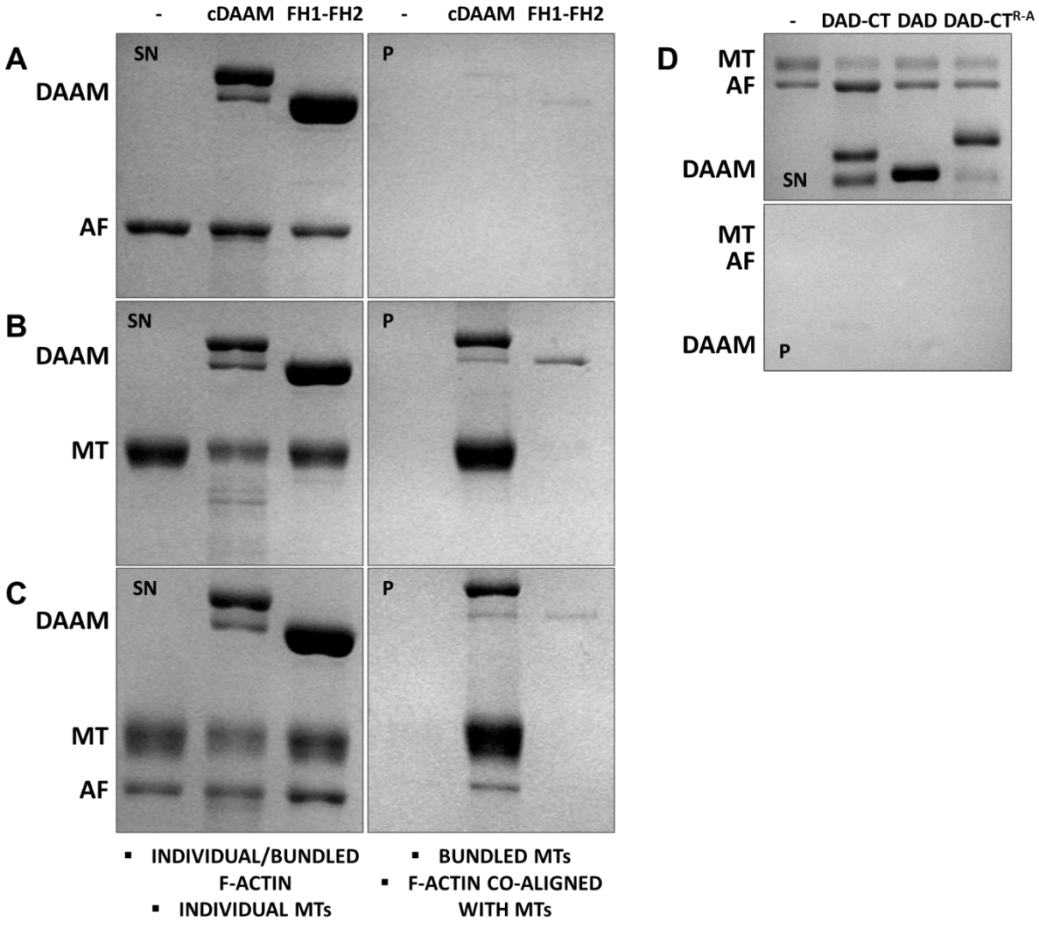

Figure 30. Simultaneous interaction of dDAAM with actin filaments and microtubules as revealed by low-speed sedimentation experiments.

(A-C) Representative Coomassie-stained SDS-PAGE gels from low-speed centrifugation experiments showing the amount of MTs and F-actin in the supernatants (SN) and the pellets (P), in the presence of cDAAM, FH1-FH2, as indicated. (D) Representative Coomassie-stained SDS-PAGE gels from low-speed centrifugation experiments showing the amount of MTs and F-actin in the supernatants (SN) and the pellets (P) in the presence of the C-terminal constructs of dDAAM, as indicated. Final concentrations: [F-actin] = 2 μM, [MT] = 2 μM, [dDAAM] = 9 μM.

To further support the above observations, fluorescently labeled actin filaments (Alexa568NHS) and microtubules (HIlyte488) were visualized in dual color TIRFM in the absence and presence of dDAAM (*Figure 31, A*). In control samples, containing only F-actin and microtubules and lacking dDAAM a ~ 13 % overlap was detected between the two polymers, which can be attributed the random co-organization of the polymers (*Figure 31, B*). When FH1-FH2 was added to the samples the fraction of the co-aligned polymers was not significantly increased as compared to the control (~ 12 %, $p > 0.05$, *Figure 31, B*). In the presence of cDAAM the area of overlapping regions

significantly increased to ~ 40 % (p = 0.0015, *Figure 31, B*). This result further supports that cDAAM has the capacity to co-align F-actin and microtubules *in vitro*, which corroborates our results from sedimentation experiments.

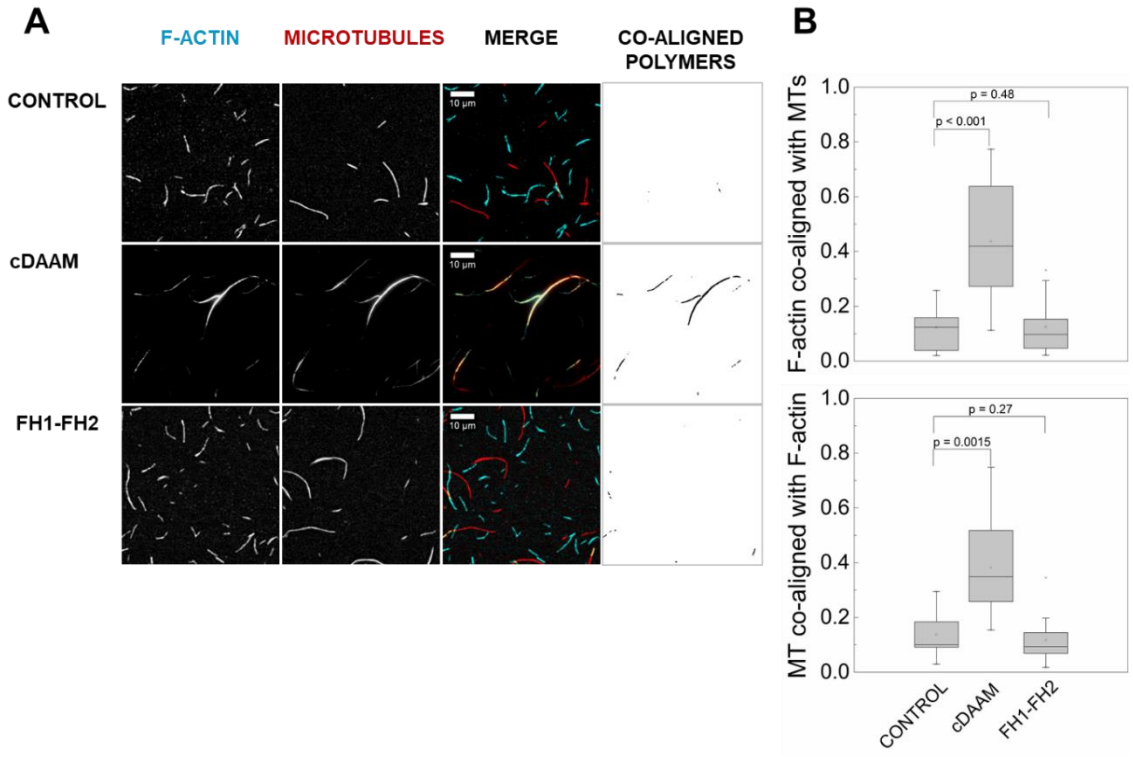

Figure 31. Simultaneous interaction of dDAAM with actin filaments and microtubules, as revealed by TIRFM experiments.

(A) Representative TIRF micrographs showing the simultaneous visualization of fluorescently labeled F-actin (cyan) and MTs (red) in the absence or presence of cDAAM and FH1-FH2, as indicated. Yellow regions on the merged images highlight the overlapping F-actin and MT regions. Binary images show the overlapping polymer area. (B) Ratio of the co-aligned F-actin and MT area in the absence or presence of cDAAM and FH1-FH2 derived from fluorescence micrographs, n = 19 - 22.

6. CONCLUSIONS AND WORKING MODELS

6. 1. Mechanistic view of the enhancement of FH2-mediated actin assembly by the C-terminus of formins

In this work the interaction of dDAAM DAD-CT with actin and its functional consequences were described. Attempts were also made to investigate the possible structural features of the dDAAM DAD-CT:G-actin interaction. Our main findings are that dDAAM DAD-CT makes the FH1-FH2 region a more potent nucleator, it also contributes to the strengthening of interactions of FH1-FH2 with filament ends. How can we relate and interpret the structural and functional behavior of DAD-CT? Analysis of the role of the N-terminally located FH1 domain of FMNL3 in the antagonism of FH2 with Capping proteins revealed that FH1 increases the ability of FH2 to maintain filament elongation in the presence of CPs. Since FH1 is not able to directly interact with actin, this observation led to the proposal that FH1 increases the stability of the FH2 dimer, which makes it a more efficient elongator (48,91). One possible explanation of our findings is that DAD-CT adopts a similar mode of action, it can make the FH2 dimer a more efficient nucleator by stabilizing its structure. In this way, DAD-CT would contribute indirectly – independently from its own actin binding ability – to the core activities of FH2.

Considering that isolated dDAAM DAD-CT can bind monomeric actin independently from the FH2 domain (*Figure 17*) an alternative proposal can be envisaged. We suggest that DAD-CT contribute to the enhanced nucleation activity of FH2 by its direct interactions with actin. We performed alignments of known X-ray structures of actin, WH2 domains and formins to investigate the possible actin binding modes of DAD-CT in the FH1-FH2-DAD-CT dimer (*Figure 32*). Structural data predicts that each of the DAD-CT regions in the FH1-FH2-DAD-CT dimer can establish contacts with an actin monomer, in addition to the monomers bound by the FH2 dimer (*Figure 32*). Considering these, DAD-CT can directly interact with actin in their complexes with FH1-FH2-DAD-CT, which can lead to the stabilization of nucleation intermediates, thus enhanced nucleation. We propose the ‘monomer stabilization model’ to explain the contribution of the C-terminus of formins to FH2-mediated nucleation (*Figure 33*). According to this model, the actin monomers that are captured by the FH1-FH2 dimer are subsequently bound and stabilized by DAD-CT in their complexes with dDAAM. In

this scenario, the concerted binding of actin by FH1-FH2 and DAD-CT domains in the dDAAM dimer would result in the stabilization of four actin subunits by dDAAM, which would completely overcome the structural and kinetic barrier of actin assembly imposed by the nucleation phase.

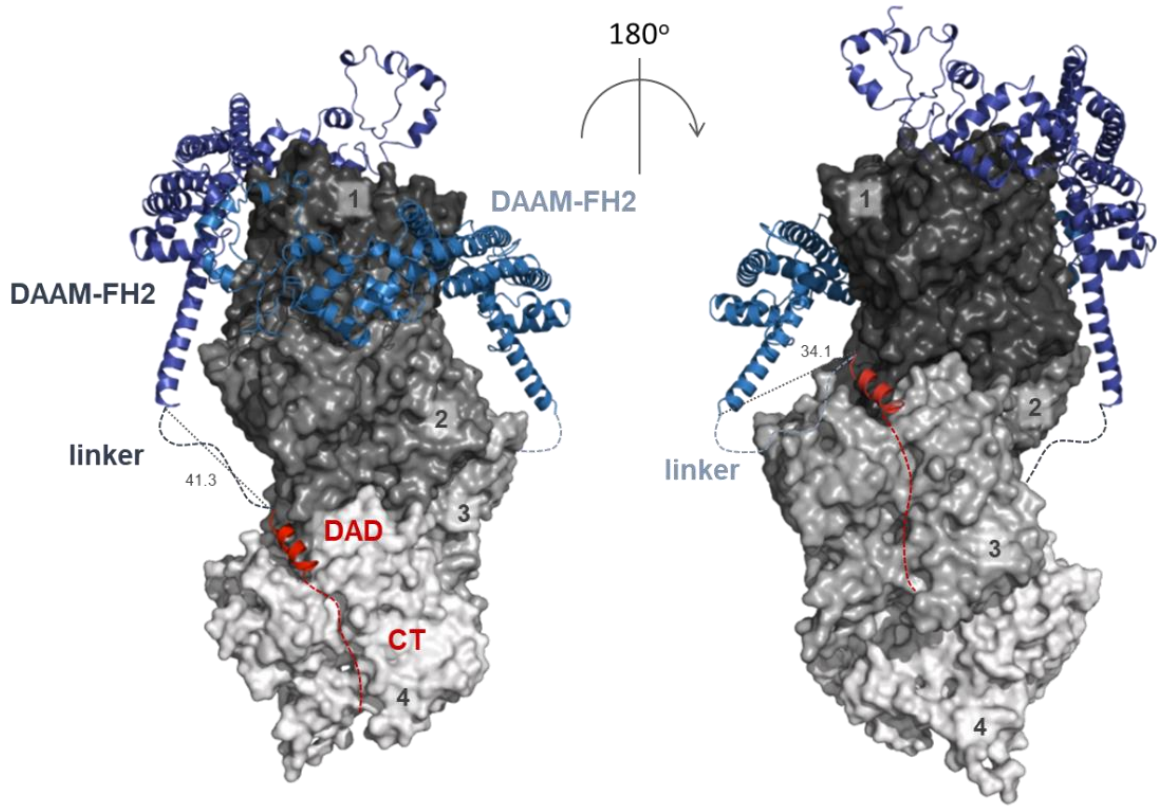

Figure 32. Structural model of the interactions of FH2 and C-terminal domains of dDAAM with actin.

The model was generated using X-ray structures of complexes of FH2:G-actin and WH2:G-actin. Four actin subunits (gray, indicated by numbers) are shown according to their arrangement in the Oda's model (5). The FH2 dimer of dDAAM (blue) and the DAD region of mouse Dia1 (red) are represented as ribbons. Red dashed lines indicate the possible orientation of the disordered CTs of dDAAM. Blue dashed lines indicate the ~ 20 amino acid linkers connecting the FH2 and DAD of DAAM. Distances are given in Å. The model was generated with PyMOL based on the alignment of the following structures: FMNLFH2-TMR-actin (PDB4EAH (48), human Daam1-FH2 (PDB2Z6E (130), mouse Dia1-DAD (PDB2BAP (75), WIP-WH2 (PDB2A41 (128).

A recent model proposes that the FH1-FH2-C-terminus of formins forms a tripartite machinery, in which the C-terminus serves as a monomer recruitment motif that captures monomers and subsequently assembles to the FH1-FH2-bound dimer (*Figure 33* (91)). The 'monomer recruitment' model implies that the DAD-CT bound actin monomers incorporate at pointed ends, which would be inhibited by profiling. Yet,

we do not detect inhibition of the activities of DAD-CT by profilin (*Figure 17, 28*). On the other hand, one has to consider that the actin affinity of the C-terminus of dDAAM and other formins is relatively weak in the absence of the FH2 domain (*Table 8*). Efficient monomer recruitment would require reasonable actin binding strength. Considering this, the 'monomer recruitment' model implicates that the affinity of the C-terminus of formins in the FH1-FH2-C-terminus is substantially strengthened. This might occur by FH2-mediated structural changes in the C-terminal regions, or the FH2 domain by bringing actin subunits into the close proximity of DAD-CT could increase the apparent affinity of the C-terminus. In this scenario, the low-affinity C-terminal regions of formins may be involved in the stabilization of actin monomers captured by the FH2 dimer, while high-affinity C-terminal domains can mediate monomer recruitment.

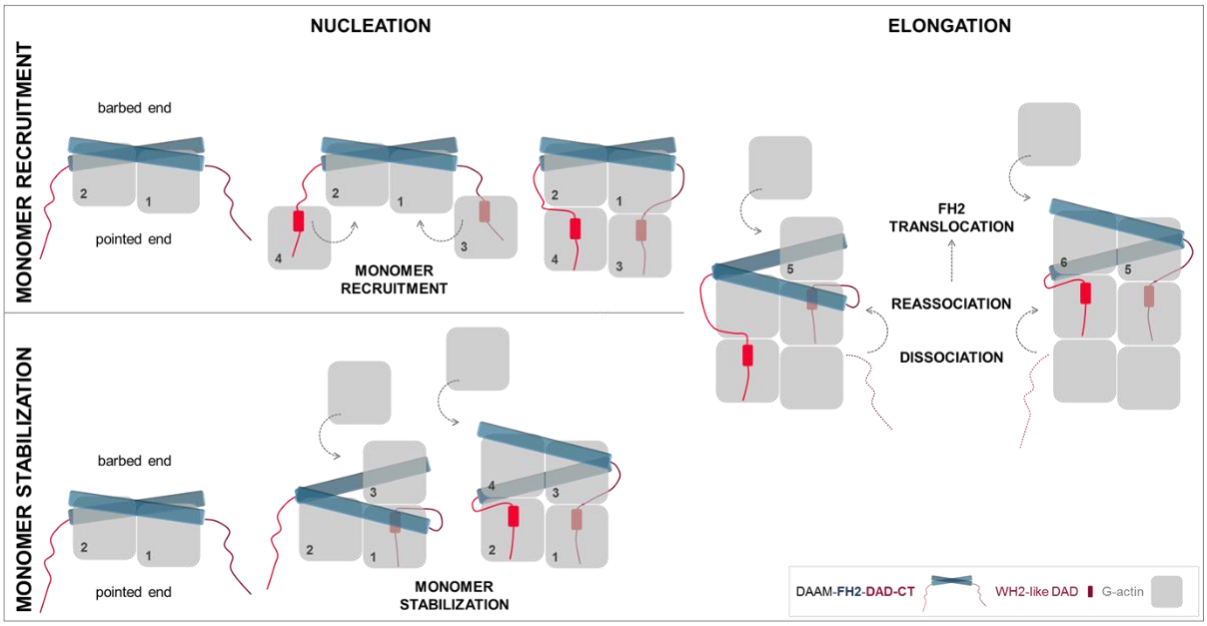

Figure 33. Alternative model of the concerted monomer recruitment and filament end interaction by the FH2 and C-terminal regions of formins.

Schematic representation of the 'monomer recruitment' (91) and 'monomer stabilization' models, as alternative scenarios to explain actin nucleation and elongation mediated by FH1-FH2-DAD-C-terminus.

formin	main actin interacting module[1]	G-actin binding affinity	nucleation activity in isolated form/ contribution to FH2-mediated nucleation	affecting G-actin interaction	other effects in actin dynamics

***Mm* INF2** (90)	**WH2-like/DAD sequence**	K_D ~ 0.06 μM 50 mM KCl	no/yes	profilin interferes	monomer sequestration, filament severing
***Mm* FMNL3** (92)	**WH2**-DAD-CT	K_D ~ 2-3 μM 50 mM KCl	yes/yes	INF2 C-term interferes mDia1 C-term does not interfere	inhibits elongation (~ nM)
***Mm* Dia1** (91)	**DAD**-CT	K_D ~ 100 μM 200 mM NaCl	yes/yes	profilin does not interfere	accelerates elongation (~ μM)
***Dm* Capu** (93)	**tail**	K_D ~ 20 μM 50 mM NaCl	no/yes	WH2, RPEL1 interfere profilin does not significantly interfere	inhibits elongation (> 10 μM)
***Dm* DAAM** (in this study)	DAD-**CT**	K_D = 44.4 ± 2.85 μM 50 mM NaCl	no/yes	profilin does not interfere WH2 interferes	inhibits elongation (> 40-50 μM)

Table 8. Comparative summary of the properties of the C-terminal elements of different formins.

[1]The main actin interacting element of the C-terminal regions are highlighted in bold.

Besides nucleation DAD-CT also supports the interaction of FH2 with the filament ends, as well as its anti-capping efficiency (*Figure 23, 25*). This is manifested possibly through interactions of the DAD-CT with the sub-terminal actin subunits, consistently with the proposed structural model (*Figure 32*). In the presence of the C-terminal regions, the stair stepping of formins requires the dissociation and re-association of both FH2 and DAD-CT, which can influence the processive mode of filament end tracking, as suggested by our data and other work.

6. 2. Mechanisms of the coordinated regulation of the actin-microtubule cytoskeleton by dDAAM

Besides its actin interactions, in this work we identified novel interactions and activities of dDAAM: it can bundle/crosslink microtubules and simultaneously interacts with both actin filaments and microtubules and co-align the two cytoskeletal polymers. Interestingly, the main actin interacting FH2 domain is not sufficient for microtubule bundling/crosslinking and actin-microtubule co-alignment, these activities essentially require the presence of the C-terminus (*Figure 29-31*). Thus, our data reveal a novel interaction of the DAD-CT region of dDAAM. Our collaborator revealed that these

interactions and activities have biological relevance in *Drosophila* primary neurons (129). In growth cones dDAAM co-localizes with both the actin and the microtubule cytoskeleton, and a significant fraction of the protein (~ 22 %) co-aligns with both polymer networks. As a functional relevance of these interactions, dDAAM is crucial for proper growth cone filopodia formation and dynamics. Albeit more work has to be done to truly understand the molecular choreography underlying the actin-microtubule cytoskeleton-related neuronal functions of dDAAM, based on our *in vitro* data we propose a working hypothesis of the role of dDAAM in growth cone filopodia formation (*Figure 34*). At the actin-rich peripheral zones, the entangled actin array of lamellipodial protrusions is maintained by coordinated action of the Arp2/3 complex machinery and Capping proteins, which determine the force production and mechanical properties of the network (20). Capping proteins by binding to the filament ends inhibit their elongation. At sites of filopodia formation dDAAM is activated by binding to RhoGTPases, which in turn relieves the autoinhibitory interaction between DID and DAD and exposes the FH1-FH2 module to actin. dDAAM by competing with Capping proteins can maintain directed and sustained profilin:actin incorporation at filament ends, which results in net filopodial lengthening. On the other hand, dDAAM can bundle filopodial actin filaments that may contribute to the mechanical integrity of the array. Due to its ability to simultaneously interact with both actin filaments and microtubules, dDAAM can co-align the two to polymer networks, which may help for the microtubules to emanate into the actin-rich peripheral zone.

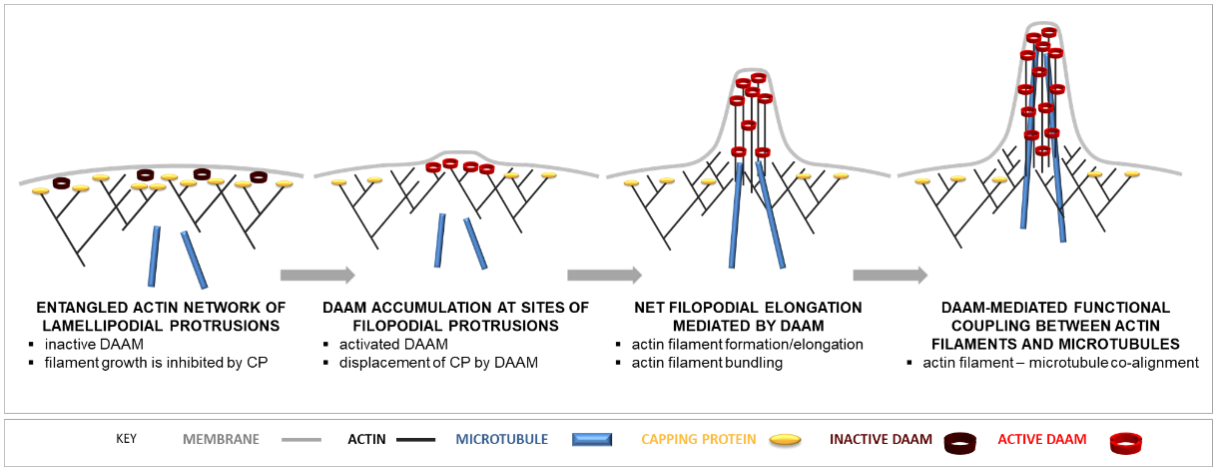

Figure 34. Working model of the dDAAM-mediated filopodia formation in neurons.

7. SUMMARY

In my PhD work I was interested in the role of *Drosophila* Dishevelled-associated activator of morphogenesis (dDAAM) formin in cytoskeleton dynamics regulation. DAAM is essential in diverse biological processes and was found to be an important component of the regulatory machinery of actin and microtubule remodeling in neurons. Previously, our group described the actin activities of the FH1-FH2 of dDAAM. Recent studies suggested that the C-terminal regions of formins can also influence actin dynamics. Also, *in vivo* data demonstrated that dDAAM can interact with the neuronal microtubule cytoskeleton.

To better understand the molecular mechanism underlying the biological functions of DAAM in the nervous system, I analyzed the interactions of different regions of dDAAM with actin and microtubules. My results are summarized below:

- dDAAM is a *bona fide* DRF, it is autoregulated through its N-terminal DID and C-terminal DAD domains.
- The DAD-CT containing cDAAM fragment is more efficient in catalyzing actin assembly as compared to FH1-FH2, due to its more potent actin nucleation activity.
- The DAD-CT containing cDAAM fragment is more efficient in maintaining filament end dynamics in the presence of Capping proteins as compared to FH1-FH2, which points towards a novel role of the C-terminus, as part of the filament elongation machinery and the anti-capping module of formins.
- The isolated dDAAM DAD-CT can bind actin monomers and filaments, independently from the FH2 domain, and the interaction is mainly mediated by electrostatic forces.
- The binding of dDAAM DAD-CT to monomeric actin is not influenced significantly by profilin, in contrast WH2 domain proteins can disrupt the interaction.
- Despite of the ability of dDAAM DAD-CT to bind actin, it fails to influence actin dynamics in the absence of FH2, thus this region possesses FH2-dependent activities.
- dDAAM can assemble actin filaments into bundled structures, the FH1-FH2 is necessary and sufficient for this activity.

- dDAAM can organize microtubules into higher order bundled structures, which requires the simultaneous binding of both FH2 and the DAD-CT regions to microtubules, presumably via cooperative interactions.
- dDAAM is able to bind actin filaments and microtubules simultaneously and co-align the two polymer systems, which relies on both the FH2 and DAD-CT regions.

Altogether, my data provide novel insight into the mechanistic view of the regulation of the actin and co-regulation of the actin-microtubule cytoskeleton by dDAAM, as well as broadens of our understanding of the regulation of these polymers by each region of formins.

ACKNOWLEDGEMENTS

First of all, I would like to thank my supervisor, Dr. Beáta Bugyi for all her hard work, support and for teaching me how to do science. Thank you for all the patience and persistence allowing me to be able to accomplish and finish my PhD.

I thank Prof. Dr. Nyitrai Miklós for giving me the opportunity to work at the Department of Biophysics and for guiding me through the years.

I would like to thank Dr. József Mihály (Hungarian Academy of Sciences, Biological Research Centre, Szeged) and the members of his group (Szilárd Szikora, István Földi, Ede Migh) for producing and providing us the plasmids of the DAAM proteins.

I thank Mónika Ágnes Tóth for providing me with the purified and fluorescently labelled profilin.

I thank Réka Pintér for her contribution to my thesis by performing the steady-state anisotropy measurements with SALS-WH2.

I thank Tamás Huber for his initial contribution to the optimization of the purification protocol of DAAM proteins.

REFERENCES

1. Straub, F. B. (ed) (1942) *Actin*, S. Karger Basel, New York
2. Sept, D., and McCammon, J. A. (2001) Thermodynamics and kinetics of actin filament nucleation. *Biophys J* **81**, 667-674
3. Bugyi, B., and Carlier, M. F. (2010) Control of actin filament treadmilling in cell motility. *Annu Rev Biophys* **39**, 449-470
4. Pollard, T. D. (2007) Regulation of actin filament assembly by Arp2/3 complex and formins. *Annu Rev Biophys Biomol Struct* **36**, 451-477
5. Oda, T., Iwasa, M., Aihara, T., Maeda, Y., and Narita, A. (2009) The nature of the globular- to fibrous-actin transition. *Nature* **457**, 441-445
6. Pantaloni, D., Hill, T. L., Carlier, M. F., and Korn, E. D. (1985) A model for actin polymerization and the kinetic effects of ATP hydrolysis. *Proc Natl Acad Sci U S A* **82**, 7207-7211
7. Pollard, T. D., and Cooper, J. A. (1984) Quantitative analysis of the effect of Acanthamoeba profilin on actin filament nucleation and elongation. *Biochemistry* **23**, 6631-6641
8. Schuler, H. (2001) ATPase activity and conformational changes in the regulation of actin. *Biochim Biophys Acta* **1549**, 137-147
9. Schutt, C. E., Myslik, J. C., Rozycki, M. D., Goonesekere, N. C., and Lindberg, U. (1993) The structure of crystalline profilin-beta-actin. *Nature* **365**, 810-816
10. Pollard, T. D. (2016) Actin and Actin-Binding Proteins. *Cold Spring Harb Perspect Biol* **8**
11. Eriksson, J. E., Dechat, T., Grin, B., Helfand, B., Mendez, M., Pallari, H. M., and Goldman, R. D. (2009) Introducing intermediate filaments: from discovery to disease. *J Clin Invest* **119**, 1763-1771
12. Omary, M. B. (2009) "IF-pathies": a broad spectrum of intermediate filament-associated diseases. *J Clin Invest* **119**, 1756-1762
13. Herrmann, H., Strelkov, S. V., Burkhard, P., and Aebi, U. (2009) Intermediate filaments: primary determinants of cell architecture and plasticity. *J Clin Invest* **119**, 1772-1783
14. Cooper, G. M. (ed) (2000) *Cell: A Molecular Approach*
15. Akhmanova, A., and Steinmetz, M. O. (2015) Control of microtubule organization and dynamics: two ends in the limelight. *Nat Rev Mol Cell Biol* **16**, 711-726
16. Chakraborti, S., Natarajan, K., Curiel, J., Janke, C., and Liu, J. (2016) The emerging role of the tubulin code: From the tubulin molecule to neuronal function and disease. *Cytoskeleton (Hoboken)* **73**, 521-550
17. Mitchison, T., and Kirschner, M. (1984) Dynamic instability of microtubule growth. *Nature* **312**, 237-242
18. Coles, C. H., and Bradke, F. (2015) Coordinating neuronal actin-microtubule dynamics. *Curr Biol* **25**, R677-691
19. Hild, G., Bugyi, B., and Nyitrai, M. (2010) Conformational dynamics of actin: effectors and implications for biological function. *Cytoskeleton (Hoboken)* **67**, 609-629
20. Blanchoin, L., Boujemaa-Paterski, R., Sykes, C., and Plastino, J. (2014) Actin dynamics, architecture, and mechanics in cell motility. *Physiol Rev* **94**, 235-263
21. Dominguez, R. (2016) The WH2 Domain and Actin Nucleation: Necessary but Insufficient. *Trends Biochem Sci* **41**, 478-490
22. Fowler, V. M., and Dominguez, R. (2017) Tropomodulins and Leiomodins: Actin Pointed End Caps and Nucleators in Muscles. *Biophys J* **112**, 1742-1760
23. Renault, L., Bugyi, B., and Carlier, M. F. (2008) Spire and Cordon-bleu: multifunctional regulators of actin dynamics. *Trends Cell Biol* **18**, 494-504
24. Hild, G., Kalmar, L., Kardos, R., Nyitrai, M., and Bugyi, B. (2014) The other side of the coin: functional and structural versatility of ADF/cofilins. *Eur J Cell Biol* **93**, 238-251

25. Wear, M. A., Yamashita, A., Kim, K., Maeda, Y., and Cooper, J. A. (2003) How capping protein binds the barbed end of the actin filament. *Curr Biol* **13**, 1531-1537
26. Nag, S., Larsson, M., Robinson, R. C., and Burtnick, L. D. (2013) Gelsolin: the tail of a molecular gymnast. *Cytoskeleton (Hoboken)* **70**, 360-384
27. Akhmanova, A., and Hoogenraad, C. C. (2015) Microtubule minus-end-targeting proteins. *Curr Biol* **25**, R162-171
28. Hitchcock-DeGregori, S. E., and Barua, B. (2017) Tropomyosin Structure, Function, and Interactions: A Dynamic Regulator. *Subcell Biochem* **82**, 253-284
29. Machesky, L. M., Atkinson, S. J., Ampe, C., Vandekerckhove, J., and Pollard, T. D. (1994) Purification of a cortical complex containing two unconventional actins from Acanthamoeba by affinity chromatography on profilin-agarose. *J Cell Biol* **127**, 107-115
30. Vinzenz, M., Nemethova, M., Schur, F., Mueller, J., Narita, A., Urban, E., Winkler, C., Schmeiser, C., Koestler, S. A., Rottner, K., Resch, G. P., Maeda, Y., and Small, J. V. (2012) Actin branching in the initiation and maintenance of lamellipodia. *J Cell Sci* **125**, 2775-2785
31. Kollman, J. M., Merdes, A., Mourey, L., and Agard, D. A. (2011) Microtubule nucleation by gamma-tubulin complexes. *Nat Rev Mol Cell Biol* **12**, 709-721
32. Kovar, D. R., Harris, E. S., Mahaffy, R., Higgs, H. N., and Pollard, T. D. (2006) Control of the assembly of ATP- and ADP-actin by formins and profilin. *Cell* **124**, 423-435
33. Kapitein, L. C., and Hoogenraad, C. C. (2015) Building the Neuronal Microtubule Cytoskeleton. *Neuron* **87**, 492-506
34. Prokop, A., Beaven, R., Qu, Y., and Sanchez-Soriano, N. (2013) Using fly genetics to dissect the cytoskeletal machinery of neurons during axonal growth and maintenance. *J Cell Sci* **126**, 2331-2341
35. Bugyi, B., Le Clainche, C., Romet-Lemonne, G., and Carlier, M. F. (2008) How do in vitro reconstituted actin-based motility assays provide insight into in vivo behavior? *FEBS Lett* **582**, 2086-2092
36. Goncalves-Pimentel, C., Gombos, R., Mihaly, J., Sanchez-Soriano, N., and Prokop, A. (2011) Dissecting regulatory networks of filopodia formation in a Drosophila growth cone model. *PLoS One* **6**, e18340
37. Xu, K., Zhong, G., and Zhuang, X. (2012) Actin, spectrin, and associated proteins form a periodic cytoskeletal structure in axons. *Science* **339**, 452-456
38. Ahmad, F. J., Hughey, J., Wittmann, T., Hyman, A., Greaser, M., and Baas, P. W. (2000) Motor proteins regulate force interactions between microtubules and microfilaments in the axon. *Nat Cell Biol* **2**, 276-280
39. Mitchison, T., and Kirschner, M. (1988) Cytoskeletal dynamics and nerve growth. *Neuron* **1**, 761-772
40. Chesarone, M. A., DuPage, A. G., and Goode, B. L. (2010) Unleashing formins to remodel the actin and microtubule cytoskeletons. *Nat Rev Mol Cell Biol* **11**, 62-74
41. Elie, A., Prezel, E., Guerin, C., Denarier, E., Ramirez-Rios, S., Serre, L., Andrieux, A., Fourest-Lieuvin, A., Blanchoin, L., and Arnal, I. (2015) Tau co-organizes dynamic microtubule and actin networks. *Sci Rep* **5**, 9964
42. Castrillon, D. H., and Wasserman, S. A. (1994) Diaphanous is required for cytokinesis in Drosophila and shares domains of similarity with the products of the limb deformity gene. *Development* **120**, 3367-3377
43. Zuniga, A., Michos, O., Spitz, F., Haramis, A. P., Panman, L., Galli, A., Vintersten, K., Klasen, C., Mansfield, W., Kuc, S., Duboule, D., Dono, R., and Zeller, R. (2004) Mouse limb deformity mutations disrupt a global control region within the large regulatory landscape required for Gremlin expression. *Genes Dev* **18**, 1553-1564
44. Schonichen, A., and Geyer, M. (2010) Fifteen formins for an actin filament: a molecular view on the regulation of human formins. *Biochim Biophys Acta* **1803**, 152-163

45. Shimada, A., Nyitrai, M., Vetter, I. R., Kuhlmann, D., Bugyi, B., Narumiya, S., Geeves, M. A., and Wittinghofer, A. (2004) The core FH2 domain of diaphanous-related formins is an elongated actin binding protein that inhibits polymerization. *Mol Cell* **13**, 511-522
46. Xu, Y., Moseley, J. B., Sagot, I., Poy, F., Pellman, D., Goode, B. L., and Eck, M. J. (2004) Crystal structures of a Formin Homology-2 domain reveal a tethered dimer architecture. *Cell* **116**, 711-723
47. Lu, J., Meng, W., Poy, F., Maiti, S., Goode, B. L., and Eck, M. J. (2007) Structure of the FH2 domain of Daam1: implications for formin regulation of actin assembly. *J Mol Biol* **369**, 1258-1269
48. Thompson, M. E., Heimsath, E. G., Gauvin, T. J., Higgs, H. N., and Kull, F. J. (2013) FMNL3 FH2-actin structure gives insight into formin-mediated actin nucleation and elongation. *Nat Struct Mol Biol* **20**, 111-118
49. Liu, W., Sato, A., Khadka, D., Bharti, R., Diaz, H., Runnels, L. W., and Habas, R. (2008) Mechanism of activation of the Formin protein Daam1. *Proc Natl Acad Sci U S A* **105**, 210-215
50. Ramabhadran, V., Gurel, P. S., and Higgs, H. N. (2012) Mutations to the formin homology 2 domain of INF2 protein have unexpected effects on actin polymerization and severing. *J Biol Chem* **287**, 34234-34245
51. Higashida, C., Suetsugu, S., Tsuji, T., Monypenny, J., Narumiya, S., and Watanabe, N. (2008) G-actin regulates rapid induction of actin nucleation by mDia1 to restore cellular actin polymers. *J Cell Sci* **121**, 3403-3412
52. Iskratsch, T., Lange, S., Dwyer, J., Kho, A. L., dos Remedios, C., and Ehler, E. (2010) Formin follows function: a muscle-specific isoform of FHOD3 is regulated by CK2 phosphorylation and promotes myofibril maintenance. *J Cell Biol* **191**, 1159-1172
53. Taniguchi, K., Takeya, R., Suetsugu, S., Kan, O. M., Narusawa, M., Shiose, A., Tominaga, R., and Sumimoto, H. (2009) Mammalian formin fhod3 regulates actin assembly and sarcomere organization in striated muscles. *J Biol Chem* **284**, 29873-29881
54. Romero, S., Le Clainche, C., Didry, D., Egile, C., Pantaloni, D., and Carlier, M. F. (2004) Formin is a processive motor that requires profilin to accelerate actin assembly and associated ATP hydrolysis. *Cell* **119**, 419-429
55. Kovar, D. R., and Pollard, T. D. (2004) Insertional assembly of actin filament barbed ends in association with formins produces piconewton forces. *Proc Natl Acad Sci U S A* **101**, 14725-14730
56. Barko, S., Bugyi, B., Carlier, M. F., Gombos, R., Matusek, T., Mihaly, J., and Nyitrai, M. (2010) Characterization of the biochemical properties and biological function of the formin homology domains of Drosophila DAAM. *J Biol Chem* **285**, 13154-13169
57. Kovar, D. R., Kuhn, J. R., Tichy, A. L., and Pollard, T. D. (2003) The fission yeast cytokinesis formin Cdc12p is a barbed end actin filament capping protein gated by profilin. *J Cell Biol* **161**, 875-887
58. Higashida, C., Miyoshi, T., Fujita, A., Oceguera-Yanez, F., Monypenny, J., Andou, Y., Narumiya, S., and Watanabe, N. (2004) Actin polymerization-driven molecular movement of mDia1 in living cells. *Science* **303**, 2007-2010
59. Watanabe, N., and Higashida, C. (2004) Formins: processive cappers of growing actin filaments. *Exp Cell Res* **301**, 16-22
60. Pollard, T. D. (2011) Cell biology. Formin tip tracking. *Science* **331**, 39-41
61. Gauvin, T. J., Young, L. E., and Higgs, H. N. (2015) The formin FMNL3 assembles plasma membrane protrusions that participate in cell-cell adhesion. *Mol Biol Cell* **26**, 467-477
62. Young, L. E., Heimsath, E. G., and Higgs, H. N. (2015) Cell type-dependent mechanisms for formin-mediated assembly of filopodia. *Mol Biol Cell* **26**, 4646-4659
63. Harris, E. S., Rouiller, I., Hanein, D., and Higgs, H. N. (2006) Mechanistic differences in actin bundling activity of two mammalian formins, FRL1 and mDia2. *J Biol Chem* **281**, 14383-14392

64. Pollard, T. D., Earnshaw, W. C., Lippincott-Schwartz, J., and Johnson, G. T. (2017) *Cell Biology*, Elsevier
65. Mahoney, N. M., Janmey, P. A., and Almo, S. C. (1997) Structure of the profilin-poly-L-proline complex involved in morphogenesis and cytoskeletal regulation. *Nat Struct Biol* **4**, 953-960
66. Mahoney, N. M., Rozwarski, D. A., Fedorov, E., Fedorov, A. A., and Almo, S. C. (1999) Profilin binds proline-rich ligands in two distinct amide backbone orientations. *Nat Struct Biol* **6**, 666-671
67. Petrella, E. C., Machesky, L. M., Kaiser, D. A., and Pollard, T. D. (1996) Structural requirements and thermodynamics of the interaction of proline peptides with profilin. *Biochemistry* **35**, 16535-16543
68. Ezezika, O. C., Younger, N. S., Lu, J., Kaiser, D. A., Corbin, Z. A., Nolen, B. J., Kovar, D. R., and Pollard, T. D. (2009) Incompatibility with formin Cdc12p prevents human profilin from substituting for fission yeast profilin: insights from crystal structures of fission yeast profilin. *J Biol Chem* **284**, 2088-2097
69. Kursula, P., Kursula, I., Massimi, M., Song, Y. H., Downer, J., Stanley, W. A., Witke, W., and Wilmanns, M. (2008) High-resolution structural analysis of mammalian profilin 2a complex formation with two physiological ligands: the formin homology 1 domain of mDia1 and the proline-rich domain of VASP. *J Mol Biol* **375**, 270-290
70. Vavylonis, D., Kovar, D. R., O'Shaughnessy, B., and Pollard, T. D. (2006) Model of formin-associated actin filament elongation. *Mol Cell* **21**, 455-466
71. Paul, A. S., and Pollard, T. D. (2008) The role of the FH1 domain and profilin in formin-mediated actin-filament elongation and nucleation. *Curr Biol* **18**, 9-19
72. Kuhn, S., and Geyer, M. (2014) Formins as effector proteins of Rho GTPases. *Small GTPases* **5**, e29513
73. Alberts, A. S. (2001) Identification of a carboxyl-terminal diaphanous-related formin homology protein autoregulatory domain. *J Biol Chem* **276**, 2824-2830
74. Watanabe, N., Kato, T., Fujita, A., Ishizaki, T., and Narumiya, S. (1999) Cooperation between mDia1 and ROCK in Rho-induced actin reorganization. *Nat Cell Biol* **1**, 136-143
75. Lammers, M., Rose, R., Scrima, A., and Wittinghofer, A. (2005) The regulation of mDia1 by autoinhibition and its release by Rho*GTP. *Embo J* **24**, 4176-4187
76. Li, F., and Higgs, H. N. (2005) Dissecting requirements for auto-inhibition of actin nucleation by the formin, mDia1. *J Biol Chem* **280**, 6986-6992
77. Nezami, A. G., Poy, F., and Eck, M. J. (2006) Structure of the autoinhibitory switch in formin mDia1. *Structure* **14**, 257-263
78. Higgs, H. N. (2005) Formin proteins: a domain-based approach. *Trends Biochem Sci* **30**, 342-353
79. Goode, B. L., and Eck, M. J. (2007) Mechanism and function of formins in the control of actin assembly. *Annu Rev Biochem* **76**, 593-627
80. Habas, R., Kato, Y., and He, X. (2001) Wnt/Frizzled activation of Rho regulates vertebrate gastrulation and requires a novel Formin homology protein Daam1. *Cell* **107**, 843-854
81. Matusek, T., Djiane, A., Jankovics, F., Brunner, D., Mlodzik, M., and Mihaly, J. (2006) The Drosophila formin DAAM regulates the tracheal cuticle pattern through organizing the actin cytoskeleton. *Development* **133**, 957-966
82. Prokop, A., Sanchez-Soriano, N., Goncalves-Pimentel, C., Molnar, I., Kalmar, T., and Mihaly, J. (2011) DAAM family members leading a novel path into formin research. *Commun Integr Biol* **4**, 538-542
83. Molnar, I., Migh, E., Szikora, S., Kalmar, T., Vegh, A. G., Deak, F., Barko, S., Bugyi, B., Orfanos, Z., Kovacs, J., Juhasz, G., Varo, G., Nyitrai, M., Sparrow, J., and Mihaly, J. (2014) DAAM is required for thin filament formation and Sarcomerogenesis during muscle development in Drosophila. *PLoS Genet* **10**, e1004166

84. Bao, B., Zhang, L., Hu, H., Yin, S., and Liang, Z. (2012) Deletion of a single-copy DAAM1 gene in congenital heart defect: a case report. *BMC Med Genet* **13**, 63
85. Kida, Y., Shiraishi, T., and Ogura, T. (2004) Identification of chick and mouse Daam1 and Daam2 genes and their expression patterns in the central nervous system. *Brain Res Dev Brain Res* **153**, 143-150
86. Sanchez-Soriano, N., Tear, G., Whitington, P., and Prokop, A. (2007) Drosophila as a genetic and cellular model for studies on axonal growth. *Neural Dev* **2**, 9
87. Matusek, T., Gombos, R., Szecsenyi, A., Sanchez-Soriano, N., Czibula, A., Pataki, C., Gedai, A., Prokop, A., Rasko, I., and Mihaly, J. (2008) Formin proteins of the DAAM subfamily play a role during axon growth. *J Neurosci* **28**, 13310-13319
88. Jaiswal, R., Breitsprecher, D., Collins, A., Correa, I. R., Jr., Xu, M. Q., and Goode, B. L. (2013) The formin Daam1 and fascin directly collaborate to promote filopodia formation. *Curr Biol* **23**, 1373-1379
89. Sato, A., Khadka, D. K., Liu, W., Bharti, R., Runnels, L. W., Dawid, I. B., and Habas, R. (2006) Profilin is an effector for Daam1 in non-canonical Wnt signaling and is required for vertebrate gastrulation. *Development* **133**, 4219-4231
90. Chhabra, E. S., and Higgs, H. N. (2006) INF2 Is a WASP homology 2 motif-containing formin that severs actin filaments and accelerates both polymerization and depolymerization. *J Biol Chem* **281**, 26754-26767
91. Gould, C. J., Maiti, S., Michelot, A., Graziano, B. R., Blanchoin, L., and Goode, B. L. (2011) The formin DAD domain plays dual roles in autoinhibition and actin nucleation. *Curr Biol* **21**, 384-390
92. Heimsath, E. G., Jr., and Higgs, H. N. (2012) The C terminus of formin FMNL3 accelerates actin polymerization and contains a WH2 domain-like sequence that binds both monomers and filament barbed ends. *J Biol Chem* **287**, 3087-3098
93. Vizcarra, C. L., Bor, B., and Quinlan, M. E. (2014) The role of formin tails in actin nucleation, processive elongation, and filament bundling. *J Biol Chem* **289**, 30602-30613
94. Bartolini, F., and Gundersen, G. G. (2010) Formins and microtubules. *Biochim Biophys Acta* **1803**, 164-173
95. Bartolini, F., Moseley, J. B., Schmoranzer, J., Cassimeris, L., Goode, B. L., and Gundersen, G. G. (2008) The formin mDia2 stabilizes microtubules independently of its actin nucleation activity. *J Cell Biol* **181**, 523-536
96. Gaillard, J., Ramabhadran, V., Neumanne, E., Gurel, P., Blanchoin, L., Vantard, M., and Higgs, H. N. (2011) Differential interactions of the formins INF2, mDia1, and mDia2 with microtubules. *Mol Biol Cell* **22**, 4575-4587
97. Young, K. G., Thurston, S. F., Copeland, S., Smallwood, C., and Copeland, J. W. (2008) INF1 is a novel microtubule-associated formin. *Mol Biol Cell* **19**, 5168-5180
98. Zhou, F., Leder, P., and Martin, S. S. (2006) Formin-1 protein associates with microtubules through a peptide domain encoded by exon-2. *Exp Cell Res* **312**, 1119-1126
99. Roth-Johnson, E. A., Vizcarra, C. L., Bois, J. S., and Quinlan, M. E. (2014) Interaction between microtubules and the Drosophila formin Cappuccino and its effect on actin assembly. *J Biol Chem* **289**, 4395-4404
100. Palazzo, A. F., Cook, T. A., Alberts, A. S., and Gundersen, G. G. (2001) mDia mediates Rho-regulated formation and orientation of stable microtubules. *Nat Cell Biol* **3**, 723-729
101. Feuer, G., Molnar, F., and et al. (1948) Studies on the composition and polymerization of actin. *Hung Acta Physiol* **1**, 150-163
102. Spudich, J. A., and Watt, S. (1971) The regulation of rabbit skeletal muscle contraction. I. Biochemical studies of the interaction of the tropomyosin-troponin complex with actin and the proteolytic fragments of myosin. *J Biol Chem* **246**, 4866-4871

103. Bugyi, B., Didry, D., and Carlier, M. F. (2010) How tropomyosin regulates lamellipodial actin-based motility: a combined biochemical and reconstituted motility approach. *Embo J* **29**, 14-26
104. Bugyi, B., Papp, G., Hild, G., Lorinczy, D., Nevalainen, E. M., Lappalainen, P., Somogyi, B., and Nyitrai, M. (2006) Formins regulate actin filament flexibility through long range allosteric interactions. *J Biol Chem* **281**, 10727-10736
105. Toth, M. A., Majoros, A. K., Vig, A. T., Migh, E., Nyitrai, M., Mihaly, J., and Bugyi, B. (2016) Biochemical Activities of the Wiskott-Aldrich Syndrome Homology Region 2 Domains of Sarcomere Length Short (SALS) Protein. *J Biol Chem* **291**, 667-680
106. Perelroizen, I., Marchand, J. B., Blanchoin, L., Didry, D., and Carlier, M. F. (1994) Interaction of profilin with G-actin and poly(L-proline). *Biochemistry* **33**, 8472-8478
107. Lakowicz, J. R. (2006) *Principles of Fluorescence Spectroscopy*, 3rd edition ed., Springer US
108. Bosch, M., Le, K. H., Bugyi, B., Correia, J. J., Renault, L., and Carlier, M. F. (2007) Analysis of the function of Spire in actin assembly and its synergy with formin and profilin. *Mol Cell* **28**, 555-568
109. Coue, M., Brenner, S. L., Spector, I., and Korn, E. D. (1987) Inhibition of actin polymerization by latrunculin A. *FEBS Lett* **213**, 316-318
110. Cooper, J. A., Walker, S. B., and Pollard, T. D. (1983) Pyrene actin: documentation of the validity of a sensitive assay for actin polymerization. *J Muscle Res Cell Motil* **4**, 253-262
111. Bombardier, J. P., Eskin, J. A., Jaiswal, R., Correa, I. R., Jr., Xu, M. Q., Goode, B. L., and Gelles, J. (2015) Single-molecule visualization of a formin-capping protein 'decision complex' at the actin filament barbed end. *Nat Commun* **6**, 8707
112. Axelrod, D. (1981) Cell-substrate contacts illuminated by total internal reflection fluorescence. *J Cell Biol* **89**, 141-145
113. Amann, K. J., and Pollard, T. D. (2001) Direct real-time observation of actin filament branching mediated by Arp2/3 complex using total internal reflection fluorescence microscopy. *Proc Natl Acad Sci U S A* **98**, 15009-15013
114. Bugyi, B. M., J. Nagy, P. Szöllősi, J. Vámosi, Gy. Vereb, Gy. (2017) Fénymikroszkópiák a sejtszintű fehérjekutatásban in *1001 arcú fehérjék*. pp
115. Hanson, J., and Lowy, J. (1964) The Structure Of Actin Filaments And The Origin Of The Axial Periodicity In The I-Substance Of Vertebrate Striated Muscle. *Proc R Soc Lond B Biol Sci* **160**, 449-460
116. Schonichen, A., Alexander, M., Gasteier, J. E., Cuesta, F. E., Fackler, O. T., and Geyer, M. (2006) Biochemical characterization of the diaphanous autoregulatory interaction in the formin homology protein FHOD1. *J Biol Chem* **281**, 5084-5093
117. Vaillant, D. C., Copeland, S. J., Davis, C., Thurston, S. F., Abdennur, N., and Copeland, J. W. (2008) Interaction of the N- and C-terminal autoregulatory domains of FRL2 does not inhibit FRL2 activity. *J Biol Chem* **283**, 33750-33762
118. Vig, A. T., Foldi, I., Szikora, S., Migh, E., Gombos, R., Toth, M. A., Huber, T., Pinter, R., Talian, G. C., Mihaly, J., and Bugyi, B. (2017) The activities of the c-terminal regions of the formin protein disheveled-associated activator of morphogenesis (daam) in actin dynamics. *J Biol Chem*
119. Pring, M., Evangelista, M., Boone, C., Yang, C., and Zigmond, S. H. (2003) Mechanism of formin-induced nucleation of actin filaments. *Biochemistry* **42**, 486-496
120. Otomo, T., Tomchick, D. R., Otomo, C., Panchal, S. C., Machius, M., and Rosen, M. K. (2005) Structural basis of actin filament nucleation and processive capping by a formin homology 2 domain. *Nature* **433**, 488-494
121. Kuhn, J. R., and Pollard, T. D. (2007) Single molecule kinetic analysis of actin filament capping. Polyphosphoinositides do not dissociate capping proteins. *J Biol Chem* **282**, 28014-28024
122. Shekhar, S., Kerleau, M., Kuhn, S., Pernier, J., Romet-Lemonne, G., Jegou, A., and Carlier, M. F. (2015) Formin and capping protein together embrace the actin filament in a menage a trois. *Nat Commun* **6**, 8730

123. Harris, E. S., Li, F., and Higgs, H. N. (2004) The mouse formin, FRLalpha, slows actin filament barbed end elongation, competes with capping protein, accelerates polymerization from monomers, and severs filaments. *J Biol Chem* **279**, 20076-20087
124. Esue, O., Harris, E. S., Higgs, H. N., and Wirtz, D. (2008) The filamentous actin cross-linking/bundling activity of mammalian formins. *J Mol Biol* **384**, 324-334
125. Machaidze, G., Sokoll, A., Shimada, A., Lustig, A., Mazur, A., Wittinghofer, A., Aebi, U., and Mannherz, H. G. (2010) Actin filament bundling and different nucleating effects of mouse Diaphanous-related formin FH2 domains on actin/ADF and actin/cofilin complexes. *J Mol Biol* **403**, 529-545
126. Didry, D., Cantrelle, F. X., Husson, C., Roblin, P., Moorthy, A. M., Perez, J., Le Clainche, C., Hertzog, M., Guittet, E., Carlier, M. F., van Heijenoort, C., and Renault, L. (2009) How a single residue in individual beta-thymosin/WH2 domains controls their functions in actin assembly. *Embo J* **31**, 1000-1013
127. Renault, L., Deville, C., and van Heijenoort, C. (2013) Structural features and interfacial properties of WH2, beta-thymosin domains and other intrinsically disordered domains in the regulation of actin cytoskeleton dynamics. *Cytoskeleton (Hoboken)* **70**, 686-705
128. Chereau, D., Kerff, F., Graceffa, P., Grabarek, Z., Langsetmo, K., and Dominguez, R. (2005) Actin-bound structures of Wiskott-Aldrich syndrome protein (WASP)-homology domain 2 and the implications for filament assembly. *Proc Natl Acad Sci U S A* **102**, 16644-16649
129. Szikora, S., Foldi, I., Toth, K., Migh, E., Vig, A., Bugyi, B., Maleth, J., Hegyi, P., Kaltenecker, P., Sanchez-Soriano, N., and Mihaly, J. (2017) The formin DAAM is required for coordination of the actin and microtubule cytoskeleton in axonal growth cones. *J Cell Sci*
130. Yamashita, M., Higashi, T., Suetsugu, S., Sato, Y., Ikeda, T., Shirakawa, R., Kita, T., Takenawa, T., Horiuchi, H., Fukai, S., and Nureki, O. (2007) Crystal structure of human DAAM1 formin homology 2 domain. *Genes Cells* **12**, 1255-1265

PUBLICATIONS

Publications related to my PhD work

1. **Andrea Teréz Vig**, István Földi, Szilárd Szikora, Ede Migh, Rita Gombos, Mónika Ágnes Tóth, Tamás Huber, Réka Pintér, Gábor Csaba Talián, József Mihály, Beáta Bugyi: The activities of the C-terminal regions of the formin protein dishevelled-associated activator of morphogenesis (DAAM) in actin dynamics. ***JOURNAL OF BIOLOGICAL CHEMISTRY* 292:**(33) pp. 13566-13583. (2017)
   IF: 4.125
   Ranking: Biochemistry D1, Cell Biology: Q1, Molecular Biology: Q1

2. Szilárd Szikora, István Földi, Krisztina Tóth, Ede Migh E, **Andrea Teréz Vig**, Beáta Bugyi, József Maléth, Péter Hegyi, Péter Kaltenecker P., Natalia Sanchez-Soriano, József Mihály J: The formin DAAM is required for coordination of the actin and microtubule cytoskeleton in axonal growth cones. ***JOURNAL OF CELL SCIENCE* 130:**(15) pp. 2506-2519. (2017)
   IF: 4.431
   Ranking: Cell Biology: Q1
   Citations: Independent: 2/Total: 3

Other publications

1. Mónika Ágnes Tóth, Andrea Majoros, **Andrea Vig**, Ede, Migh, Miklós Nyitrai, József Mihály Beáta Bugyi: Biochemical Activities of the Wiskott-Aldrich Syndrome Homology Region 2 Domains of Sarcomere Length Short: WH2 domains in sarcomeric actin regulation. ***JOURNAL OF BIOLOGICAL CHEMISTRY* 291:** pp. 667-680. (2016) (2016)
   IF: 4.573
   Ranking: Biochemistry D1, Cell Biology: Q1, Molecular Biology: Q1
   Citations: Independent: 4/Total: 7

2. Nikolett Kis-Bicskei, **Andrea Vig**, Miklós Nyitrai, Beáta Bugyi, Csaba Gábor Talián: Purification of Tropomyosin Br-3 and NM1 and Characterization of Their Interactions with Actin. ***CYTOSKELETON* 70:**(11) pp. 755-765. (2013)
   IF: 2.865
   Ranking: Cell Biology: Q1, Structural Biology: Q1
   Citations: Independent: 10/Total: 12

3. **Vig, A.,** Ohmacht, R., Jámbor, E., Bugyi, B., Nyitrai, M. and Hild, G.: The effect of toxins on inorganic phosphate release during actin polymerization. ***EUROPEAN BIOPHYSICS JOURNAL* 40:**(5) pp. 619-626. (2011)
   IF: 2.139
   Ranking: Biophysics: Q2, Medicine: Q1

Citations: Independent: 2/Total: 3

4. Ujfalusi, Z., **Vig, A.,** Hild, G., Nyitrai, M.: Effect of Tropomyosin on Formin-Bound Actin Filaments. ***BIOPHYSICAL JOURNAL*** **96:**(1) pp. 162-168. (2009)
   IF 4.39
   Ranking: Biophysics: D1
   Citations: Independent: 10/Total: 15

5. **Vig, A.,** Dudás, R., Kupi , T., Orbán, J., Hild, G., Lőrinczy D., Nyitrai, M.: Effect of phalloidin on filaments polymerized from heart muscle ADP-actin monomers. ***JOURNAL OF THERMAL ANALYSIS AND CALORIMETRY*** **95:**(3) pp. 7219-725. (2009)
   IF: 1.587
   Ranking: Physical and theoretical Chemistry: Q3, Condensed matter physics: Q2
   Citations: Independent: 2/Total: 6

6. Dudás R., Kupi T., **Vig A.**, Orbán J., Lőrinczy D.: Effect of Phalloidin on the Skeletal Muscle ADP-Actin Filaments. ***JOURNAL OF THERMAL ANALYSIS AND CALORIMETRY*** **95:**(3) pp. 709-712. (2009)
   IF: 1.587
   Ranking: Physical and theoretical Chemistry: Q3, Condensed matter physics: Q2
   Citations: Independent: 1/Total: 4

7. Kardos, R., **Vig, A.,** Orbán, J., Hild, G., Nyitrai, M., Lőrinczy D.: The effect of Jasplakinolide on the Thermodynamic properties of ADP.BeFx bound Actin Filaments. ***THERMOCHIMICA ACTA*** **463:**(1-2) pp. 77-80. (2007)
   IF: 1.562
   Ranking: Physical and theoretical Chemistry: Q2, Condensed matter physics: Q2, Instrumentation: Q1
   Citations: Independent: 1/Total: 2

Impact factor: 27.259
Citations (total/independent): 50/31

Conference talks related to my PhD work

1. **Andrea Vig**, Péter Gaszler, Mónika Ágnes Tóth, Beáta Bugyi: The CT region of DAAM has a supporting role in FH2-mediated actin dynamics regulation, 2016.05.27-29. 5th Interdisciplinary Doctoral Conference, Pécs

2. **Andrea Vig**, Andrea Majoros, Tamás Huber, Ede Migh, József Mihály, Miklós Nyitrai and Beáta Bugyi: DAAM formin's C-terminal end in the actin-formin interaction, Membrán Transzport Konferencia 2015.05.19-22. Sümeg

Other conference talks

1. **Andrea Vig**, Beáta Bugyi: Tropomyosin Isoform Specific Regulation Of Nucleation Factors, Summer school on Actin Dynamics, 2011.09.17-23. Regensburg, Germany
2. **Andrea Vig**, Tamás Huber, Miklós Nyitrai and Beáta Bugyi: Isoform-specific regulation of the actin cytoskeleton, III. Interdiszciplináris Konferencia, 2014.04.15-17, 2014, Pécs

Conference posters related to my PhD work

1. Pintér Réka, Fórizs Judit Viktória, Huber Tamás, **Vig Andrea Teréz**, Bugyi Beáta (2017): *A Disheveled-Associated Activator of Morphogenesis (DAAM) formin szerepe az aktin dinamikájában.* (2017. 08. 22–25. A Magyar Biofizikai társaság XXVI. Kongresszusa, Szeged)

2. Fórizs Judit Viktória, Pintér Réka, **Vig Andrea Teréz**, Huber Tamás, Bugyi Beáta (2017): *A DAAM (Disheveled-Associated Activator of Morphogenesis) formin szerepe az aktin-mikrotubulus dinamika koordinációjában*. (2017. 08. 22–25. A Magyar Biofizikai társaság XXVI. Kongresszusa, Szeged)

3. Szilárd Szikora, István Földi, Krisztina Tóth, **Andrea Vig**, Ede Migh, Beáta Bugyi, József Mihály (2017): *The formin DAAM coordinates the actin and the microtubule cytoskeleton during axonal development*. (2017. 03. 31–04. 02. Hungarian Molecular Life Sciences, Eger)

4. István Földi, Szilárd Szikora, Krisztina Tóth, **Andrea Vig**, Beáta Bugyi, József Mihály (2017): *Characterization of the interaction between a Drosophila formin DAAM and microtubules*. (2017. 03. 31–04. 02. Hungarian Molecular Life Sciences, Eger)

5. Péter Gaszler, Judit Viktória Fórizs, Tamás Huber, **Andrea Teréz Vig**, Beáta Bugyi (2017): *Coordination of actin-microtubule dynamics by Disheveled-Associated Activator of Morphogenesis (DAAM) formin*. (2017. 03. 31–04. 02. Hungarian Molecular Life Sciences, Eger)

6. Péter Gaszler, Judit Viktória Fórizs, **Andrea Teréz Vig**, Beáta Bugyi (2016): *Coordination of actin-microtubule dynamics by DAAM formin.* (2016. 08. 28–31. Annual Conference of the Hungarian Biochemical Society, Szeged)

7. Péter Gaszler, **Andrea Vig**, Judit Viktória Fórizs, Mónika Ágnes Tóth, István Földi, József Mihály, Beáta Bugyi (2016): *The CT region of DAAM has a supporting role in FH2-mediated actin dynamics regulation.* (2016. 08. 28–31. Annual Conference of the Hungarian Biochemical Society, Szeged)

8. **Andrea Vig**, Péter Gaszler, Mónika Ágnes Tóth, István Földi, József Mihály, Beáta Bugyi (2016): *The CT region of DAAM has a supporting role in FH2-mediated actin dynamics regulation*. (2016. 06. 20–23. European Cytoskeletal Forum, Cambridge)

9. **Vig Andrea**, Majoros Andrea, Huber Tamás, Migh Ede, Mihály József, Nyitrai Miklós és Bugyi Beáta (2015): *A DAAM formin C-terminális régióinak szerepe az aktin-formin kölcsönhatás integritásában*, (2015. 05.19-22. Membrán Transzport Konferencia, Sümeg)

Other conference posters

1. Fórizs Judit Viktória, Pintér Réka, Huber Tamás, **Vig Andrea Teréz**, Tóth Mónika Ágnes, Bugyi Beáta (2017): *Flightless I fehérje szerepe az aktin sejtváz szerveződésében*. (2017. 08. 22–25. A Magyar Biofizikai társaság XXVI. Kongresszusa, Szeged)

2. Péter Gaszler, Judit Viktória Fórizs, **Andrea Teréz Vig**, Tamás Huber, Beáta Bugyi (2017): *The activities of the Disheveled-Associated Activator of Morphogenesis (DAAM) formin in actin dynamics*. (2017. 03. 31–04. 02. Hungarian Molecular Life Sciences, Eger)

3. Mónika Ágnes Tóth, Péter Gaszler, Judit Viktória Fórizs, **Andrea Teréz Vig**, Ede Migh, József Mihály, Beáta Bugyi (2016): *Biochemical activities of the Wiskott-Aldrich syndrome homology region 2 domains of Sarcomere Length Short protein*. (2016. 08. 28–31. Annual Conference of the Hungarian Biochemical Society, Szeged)

4. Mónika Ágnes Tóth, Péter Gaszler, **Andrea Teréz Vig**, Ede Migh, József Mihály, Beáta Bugyi (2016): *Biochemical activities of the Wiskott-Aldrich syndrome homology region 2 domains of Sarcomere Length Short protein.* (2016. 06. 20–23. European Cytoskeletal Forum, Cambridge)

5. **Andrea Vig**, Tamás Huber, Miklós Nyitrai and Beáta Bugyi (2014): *Distinct Polymerization Properties of Actin Isoforms due to various Assembly Factors*, (2014.05.15-20. Regional Biophysics Conference, Smolenice, Slovakia)

6. **Vig Andrea**, Huber Tamás, Nyitrai Miklós és Bugyi Beáta (2013): *Aktin izoformák funkcionális sajátságai, (*Magyar Biofizikai Társaság XXIV. Kongresszusa 2013.08.27-30, Veszprém)

7. **Andrea Vig**, Tamás Huber and Beáta Bugyi (2012): *Tropomyosin isoform-specific regulation of actin assembly,* „From molecules to life and back" FEBS3+Meeting (2012. 06.12-16., Opatija, Croatia)

8. Tamás Huber, **Andrea Vig**, Miklós Nyitrai and Beáta Bugyi (2012): *Tropomyosins regulate actin assembly factors in an isoform dependent manner*, (The 27th European Cytoskeletal Forum Meeting 2012.11.2-3 Pécs,)

9. **Andrea Vig**, Tamás Huber and Beáta Bugyi (2011): *Tropomyosin isoform specific regulation of nucleation factors* (2012-08.20-22. EBSA_Satellite Conference Intracellular Fluorescence Spectroscopy, Pécs)

10. Mónika Á. Tóth, Ágnes Kokas, Katalin Türmer, **Andrea Vig**, Tamás Huber, Gábor Hild, Miklós Nyitrai, Beáta Bugyi (2011): *Tropomyosin isoform specific regulation of nucleation factors* (2011.05.17-20. Membrán - transzport Konferencia, Sümeg 2011)

11. **Vig Andrea**, Ohmacht Róbert, Jámbor Éva, Nyitrai Miklós és Hild Gábor (2010): *Toxinok hatása az inorganikus foszfát felszabadulására az aktin filamentumok képződésekor* (Membrán - transzport Konferencia,2010.05.18-21. Sümeg)

12. **Vig Andrea**, Kupi Tünde, Hild Gábor és Nyitrai Miklós (2009): *Toxinok hatása az inorganikus foszfát felszabadulására az aktin filamentumok képződésekor* (2009. 08. 23–26. A Magyar Biofizikai társaság XXIII. Kongresszusa, Pécs)

13. **Andrea Vig**, Tünde Kupi, Gábor Hild and Miklós Nyitrai (2009): *The Effect of Toxins on the Inorganic Phosphate Release During the Actin Filament Formation* (2009. 07. 11—15. 7th EBSA European Biophysics Congress Genoa, Italy)

14. **Andrea Vig**, Réka Dudás, Tünde Kupi, József Orbán, Gábor Hild, Dénes Lőrinczy and Miklós Nyitrai (2008): *The effect of phalloidin on cardiac ADP-actin filaments.* (XV. International Conference on Biological Calorimetry. Pécs, 2008)

15. Tünde Kupi, Réka Dudás, **Andrea Vig**, József Orbán, Miklós Nyitrai, Gábor Hild and Dénes Lőrinczy (2008): *Effect of AMP PNP as a nucleotide analogue on actin filaments.* (XV. International Conference on Biological Calorimetry. Pécs, 2008)

16. Zoltán Ujfalusi, **Andrea Vig**, Tünde Kupi, Réka Dudás, Gábor Hild and Miklós Nyitrai (2008): *The effect of tropomyosin on formin-bound actin filaments.* FEBS Workshop "Mechanics and Dynamics of the Cytoskeleton". Potsdam, 2008)

17. Roland Kardos, **Andrea Vig**, Réka Dudás, Tünde Kupi, Elisa Nevalainen, Pekka Lappalainen, Miklós Nyitrai and Gábor Hild (2008): *The effect of actin-binding proteins on the dynamic properties of monomeric actin.* FEBS Workshop "Mechanics and Dynamics of the Cytoskeleton". (Potsdam, 2008)

18. Lívia Czimbalek, Szilvia Barkó, **Andrea Vig**, Réka Dudás, Tünde Kupi, Gábor Hild and Miklós Nyitrai (2008): *Characterisation of the nuclear actin in the human oesophagus tumour cells (HEp-2).* FEBS Workshop "Mechanics and Dynamics of the Cytoskeleton". (Potsdam, 2008)

19. Sz. Barkó, **A. Vig**, R. Dudás, T. Kupi, M. Nyitrai (2007): *Characterization the FH2 Domain of the Formin DAAM by Biophysical Methods.* (2007. 09. 23-30. EMBO Young Investigator Programme PhD course, Heidelberg, Germany)

20. R. Kardos, K. Pozsonyi, **A. Vig,** M. Nyitrai, E. Nevalainen, P. Lappalainen, G. Hild (2007): *The effect of the actin binding proteins on the conformation of the ATP binding cleft on actin.* (2007. 08. 21-25. Regional Biophysics Conference, Balatonfüred)

21. **A. Vig**, Z. Ujfalusi, R. Kardos, G. Hild, M. Nyitrai (2007): *The Effect of Tropomyosin on the Stability of Formin-Bound Actin Filaments.* (2007. 08. 15-18. IV. International Conference on Molecular Recognition, Pécs)

22. J. Orbán, **A. Vig**, R. Kardos, B. Somogyi, G. Hild, D. Lőriczy, M. Nyitrai (2007): *The Effect of Phalloidin on the Thermal Properties of the Skeletal ADP.BeFx-F-actin.* (2007. 05. 17-20.Time and Space Resolved Methods in Molecular Biophysics, Hünfeld, Germany)

23. R. Kardos, **A. Vig**, J. Orbán, G. Hild, M. Nyitrai, D. Lőrinczy (2007): *The Effect of Jasplakinolide on the Thermodynamic Properties of BeFx Bound Actin Filaments.* (2007. 03. 28-30. 17. Ulm-Freiberger Kalorimetrietage (Freiberg, Germany)